I recognise that the copyright of this thesis rests with the author, and I undertake not to copy or quote any part of the work without first obtaining written permission from the author.

Name	Student No./Dept.	Date consulted

AN ELECTRON-ATOM CROSSED BEAM

APPARATUS AND ITS FIRST APPLICATIONS

by

Volker Raible

Thesis submitted to the University of Stirling

for the degree of Doctor of Philosophy

Physics Department
University of Stirling
Stirling

1974

ABSTRACT

An electron-atom crossed beam apparatus has
been designed and constructed. The set up uses an
electron impact spectrometer in which electrons with
a well defined energy are crossed with atomic target
beams. The apparatus can be used for optical excitation
measurements as well as for energy loss and elastic
scattering experiments. Observations can be made at fixed
or variable angles. Owing to the availability of independent
detection channels for scattered electrons and photons it
is possible to use the apparatus to make coincidence
measurements.

The instrument has so far been used to study
elastic scattering of electrons from atomic hydrogen and
helium and for energy loss observations with helium.
Further investigations have been made of the resonance
structure in the excitation of first excitation levels
of Ne,Ar,Kr[§] and Xe[§], as well as in the 2S excitation of
atomic hydrogen.[§]

[§] These experiments are described in H. Koschmieder,
    Ph.D. thesis, Physics Department, University of Stirling.

TABLE OF CONTENTS

1. INTRODUCTION

Recent improvements in the design of electron guns, leading to electron monochromators, which, to some extent coincided with theoretical predictions of so-called resonances have again stimulated electron-atom collision experiments. These have led to the discovery of many narrow structures in electron-atom collision cross-sections. These structures are referred to as resonances. In a number of cases resonances have been observed experimentally but can not yet be fully described theoretically.

One particular process is especially interesting, namely electron-atomic hydrogen scattering. This process involves three particles and all the interactions between the three particles are well known, as well as the eigen-functions of the H-atom. Therefore theory can formulate the electron-atomic hydrogen scattering processes exactly. Nevertheless it was not yet possible to obtain exact solutions of these theoretical problems. In recent years many approximations have been developed, resulting in the prediction of resonance structure in the elastic and inelastic channels. These theories can be tested by electron-atomic hydrogen scattering experiments.

The hydrogen problem is of interest to experimentalists as well. The precise knowledge of the elastic scattering reso-nances would supply a useful reference for experiments on other targets. Energy scales could be calibrated absolutely and furthermore it would become possible to do absolute cross-section measurements with much higher accuracy and less experimental difficulties than it has been hitherto. This requires a complete

set of elastic scattering phase-shifts to be deduced from
angular distribution measurements of the elastic resonances
in atomic hydrogen. Unfortunately the experimental situation,
as far as atomic hydrogen scattering is concerned, is totally
different from the theoretical position. Atomic hydrogen is
so far one of the most difficult targets for scattering
experiments.

Apart from the atomic hydrogen case it seems to
be of great interest to get more information about similar
features in other atomic and molecular systems, if only to
stimulate theoretical work.

The growing interest in these types of features
has led to the design of a crossed-beam apparatus which permits
investigations of elastic and inelastic electron-atom scattering
processes at fixed or variable angles. The apparatus has been
set up and used for hydrogen and rare gas scattering experiments.
It is possible to use the apparatus for a number of target gases,
since one aim of the design was to achieve flexibility in the
choice of target source.

1.1 General features of resonant scattering.

Resonances in electron-atom scattering can be
explained by the formation of temporary negative ion states.
The incident electron is retained by the target atom for a
short time, thus forming an ion-state, which then decays.
These ion states, which are analogous to the compound states
in nuclear physics, distort the wave functions of the normal
scattering processes and therefore affect the cross-section.

Resonance processes can be described schematically in the following way

$$A + e\ (E_{res}) \to A^{*-} \to A + e\ (E_{res})$$

in the case of elastic scattering. These processes interfere with the direct process

$$A + e\ (E) \to A + e\ (E)$$

The interference between those two processes has a strong influence on the cross-section. Similar processes can occur in electron impact excitation

$$A + e\ (E_{res}) \to A^{*-} \to A^{*} + e\ (E_{res} - E_n)$$
$$\quad\quad\quad\quad\quad\quad\quad\quad\longrightarrow A + h\nu$$
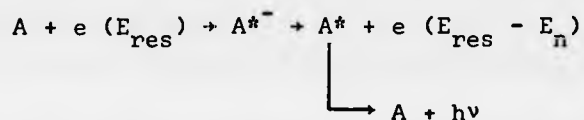
again interfering with the direct process for excitation. The final state of the target can be the groundstate or an excited state. The shape of the resonance can take different forms which depend on the decay mechanisms. Generally resonances show themselves as sharp anomalies in the cross-section.

One distinguishes between two basic forms of resonances - shape resonances (or open-channel or Type II resonances), and Feshbach resonances (or closed-channel or Type I resonances). The difference is in the way in which the electrons are trapped by the target. In the case of a shape resonance the electron passes close to the target atom and is trapped there by a potential barrier. The resonance decays by the electron tunnelling through the potential barrier. The energy width of the resonance is determined by the height of the potential barrier. If the electron has excited the

target and is left with little energy, then it is bound for
a long time and the width of the resonance can be of the order
of a few millivolts as in the case of the 10.22 eV shape
resonance of atomic hydrogen.

Feshbach resonances occur when the incident
electron causes an excited compound state which is energetically
lower than the excited states of the target and is left with
less energy than is required for tunnelling. The electron must
therefore gain energy to escape. Feshbach resonances are thus
very narrow, since they almost correspond to bound states.
(Taylor H.S. et al 1966).

1.2 Some theoretical aspects of low energy electron-atom
     scattering.

Scattering processes are described by cross-sections.
The cross-section for a particular process can be defined as the
apparent area presented by the target atom to the incident
particle. The differential cross-section $\sigma(\theta)$ is used to
describe angular variations of scattering processes and is
defined as the apparent target area $d\sigma$ causing an incident
particle to be scattered into a solid angle $d\Omega$ between
scattering angles θ and $\theta + d\theta$. The scattering angle is
the angle through which the incident particle is deflected
by the target:

$$\sigma(\theta) = \frac{d\sigma}{d\Omega} \qquad\qquad cm^2 \qquad\qquad (1)$$

The total cross section

$$\sigma_{tot} = 2\pi \int_o^{\pi} \sigma(\theta)\sin\theta d\theta \quad cm^2 \qquad\qquad (2)$$

describes the deflection of incident particles through any angle.

Theories of electron scattering by atoms face various difficulties. The equation of motion for the system, consisting of projectile electron and target atom, is a many-body problem and cannot yet be solved exactly. One cannot distinguish between projectile and atomic electrons. Inelastic processes can occur if the electron energy is high enough to induce transitions of the target atom to its excited states.

The time-independent Schrödinger equation for the total system of target atom and projectile electron is

$$[H_1(\vec{r}_1) + H_A(\vec{r}_2,\ldots,\vec{r}_j) + V(\vec{r}_1,\vec{r}_2,\ldots,\vec{r}_j) - E] \cdot$$

$$\Psi(\vec{r}_1,\ldots\vec{r}_j,s_1,\ldots s_j) = 0 \qquad (3)$$

$H_A(\vec{r}_j)$ is the atomic Hamiltonian, $H_1(\vec{r}_1)$ is the Hamiltonian of the incoming electron and $V(\vec{r}_1,\vec{r}_i)$ describes the interaction between incoming electron and the i-th target electron. Distances are measured from the nucleus, assumed to be at rest. s_i is the spin coordinate of the i-th electron. Spin coordinates are included, in order to satisfy the Pauli exclusion principle.

The simplest target system is the hydrogen atom with only one electron. The importance of the hydrogen case is amplified by the fact that, in this scattering process, all the interactions are known and the eigenfunctions of the hydrogen atom are known exactly. It is however, even in the case of hydrogen, still very difficult to get cross-section values of reasonable accuracy by means of the different approximations. An exact solution has not yet been obtained.

For the case of atomic hydrogen, (3) reduces to

$$[\frac{\hbar^2}{2m}(\nabla_1^2 + \nabla_2^2) + \frac{e^2}{r_1} + \frac{e^2}{r_2} - \frac{e^2}{r_{12}} - E]\Psi(\vec{r}_1,\vec{r}_2) = 0 \qquad (4)$$

Index 1 refers to the projectile electron, 2 to the target electron.   E is the total Energy of the System

$$E = E_o + E_k \qquad (5)$$

E_o being the energy of the atom in the ground state, E_k the kinetic energy of the projectile electron.

A standard method of describing the collision between electron and atom was suggested by H.S.W. Massey and C. B. Mohr in 1932.   The wave function is expanded in terms of the unperturbed eigenfunctions of the target atom

$$\Psi(\vec{r}_1, \vec{r}_2) = (\sum_n + \int) \psi_n(\vec{r}_2) F_n(\vec{r}_1) \qquad (6)$$

Discrete states of the atom are taken into account by $\sum_n$ and the continuum states by $\int$.   The eigenfunctions $\psi_n(\vec{r}_2)$ satisfy the Schrödinger equation of the H-atom

$$(\frac{\hbar^2}{2m} \nabla_2^2 + \frac{e^2}{r_2} - E_n) \psi_n(\vec{r}_2) = 0 \qquad (7)$$

and are known exactly.   Equations (6) and (4) result in

$$(\frac{\hbar^2}{2m}(\nabla_1^2 + \nabla_2^2) + \frac{e^2}{r_1} + \frac{e^2}{r_2} - \frac{e^2}{r_{12}} - E)(\sum_n + \int) \psi_n(\vec{r}_2) F_n(\vec{r}_1) = 0 \qquad (8)$$

Putting $k_n^2 = (\frac{2m}{\hbar^2})(E-E_n)$ the E_n represent the energy eigenvalues, and since (7)

$$\left(\frac{\hbar^2}{2m}(\nabla_1^2 + k_n^2) + \frac{e^2}{r_1} - \frac{e^2}{r_{12}}\right)(\sum_n + \int).F_n(\vec{r}_1)\psi_n(\vec{r}_2) = 0 \qquad (9)$$

Multiplying (8) by ψ_n^* and integrating over $\vec{r}_2$ it follows that, since $\int \psi_n^* \psi_m d\vec{r}_2 = 0$ for $n \neq m$

$$(\nabla^2 + k_n^2)F_n(\vec{r}_1) = (\sum_n + \int)U_{nm}F_m(\vec{r}_1) \qquad (10)$$

where

$$U_{nm}(\vec{r}_1) = \frac{2me^2}{\hbar^2} \int \psi_n(\vec{r}_2)(\frac{1}{r_{12}} - \frac{1}{r_1})\psi_m(\vec{r}_2)d\vec{r}_2 \tag{11}$$

$$= \frac{2m}{\hbar^2} V_{nm}$$

(11) represents the averaged interaction potential experienced by the projectile electron. Equation (10) represents a system of coupled differential equations for the expansion coefficients $F_n(\vec{r}_1)$.

The scattering process, neglecting exchange processes, requires a wavefunction with the following asymptotic form

$$\Psi(\vec{r}_1, \vec{r}_2) \underset{r_1 \to \infty}{\sim} \psi_{n=1}(\vec{r}_2)e^{i\vec{k}_o\vec{r}_1} + \sum_{n=1}\psi_n(\vec{r}_2).\frac{f_n(\theta)}{r_1}.e^{i\vec{k}_n\vec{r}_1} \tag{12}$$

which means that, before the collosion, the atom is in the groundstate and the projectile electron is represented by a plane wave. $f_n(\theta)$ is the scattering amplitude. After the scattering occurs, the projectile electron is represented by a spherical wave, whereas the atom may be in an excited state. By comparing (12) and (6), the original expansion,

$$F_n(\vec{r}_1) \sim \frac{f_n(\theta)}{r_1}.e^{i\vec{k}_n\vec{r}_1} \tag{13}$$

Since the differential cross section for the scattering process is defined as

$$\sigma_n(\theta) = |f_n(\theta)|^2,$$

and the total cross section can be obtained by integrating over

all scattering angles

$$\sigma = 2\pi_0 \int^{\pi} |f(\theta)|^2 \sin\theta d\theta,$$

one can describe the scattering process completely.

Another way of solving the Schrödinger equation in order to calculate the scattering amplitudes and hence the cross sections is to expand the wavefunction in terms of Legendre Polynomials:

$$\Psi(\vec{r}) = \frac{1}{r}\Sigma A_\ell (k^2)\mu_\ell(r)P_\ell(\cos\theta)$$

This leads to the following expression for the scattering amplitude

$$f(\theta) = \frac{1}{2ik} \sum_{\ell=0}^{\infty}(2\ell+1)(e^{2i\delta_\ell}-1)P_\ell(\cos\theta) \tag{14}$$

and thus to

$$\sigma(\theta) = |f(\theta)|^2 = \frac{1}{4k^2}\left|\sum_\ell(2\ell+1)(e^{2i\delta_\ell}-1)P_\ell(\cos\theta)\right|^2 \tag{15}$$

δ_ℓ represents the phase shift of a partial wave with orbital angular momentum ℓ. If only elastic scattering occurs, then the δ_ℓ are real. In case of inelastic collisions δ_ℓ has an imaginary part describing absorption by the target and thus excitation. So far both methods are equivalent and exact in describing the solution of the scattering problem.
Equation (10) represents an infinite set of coupled differential equations, coupled by means of the averaged potential which is experienced by the projectile electron during scattering and

described by (11). Since one cannot solve this complete set
numerically one has to truncate the set of states taken into
account. This leads to various approximations as solutions
for the truncated expansion of the wave function.

The first theoretical evidence for resonances in
elastic scattering of electrons by hydrogen was indicated in a
2-state strong coupling approximation by Smith et al (1962).
A very rapid increase in the cross section was caused by anomalous
increases in the ^{1}S and ^{3}P scattering phase shifts. Using close
coupling approximations, that is, more than 2 states, in the
expansion of the wavefunction, Burke and Schey (1962) were
able to resolve this structure in 1962. Further calculations
predicted a set of structures.

Although this approach can be generalized for
all atoms, it is so far only applicable for those atoms whose
eigenfunctions are well enough known. Apart from Hydrogen,
this is only true for Helium. Therefore, there are no
theoretical calculations available which predict resonances
in heavy rare gases, although it is experimentally proven that
they exist.

If one knows the positions of resonances and the
exact partial waves which cause these structures, it is possible
to work out the line profiles which will show up in scattering
experiments. For the case of atomic hydrogen, one can write the
differential cross section for elastic scattering of electrons
in the following form

$$\sigma(\theta) = \frac{1}{4k^2} \left| \Sigma_\ell (2\ell+1)(e^{2i\delta_\ell^+} -1)P_\ell(\cos\theta) \right|^2$$

$$+ \frac{3}{4k^2} \left| \Sigma_\ell (2\ell+1)(e^{2i\delta_\ell^-} -1)P_\ell(\cos\theta) \right|^2 \tag{16}$$

The first part of the partial wave expansion represents singlet terms, the second part triplet terms. The phase shifts δ_ℓ can be split up into phase shifts due to potential scattering $\delta_{\ell,pot}$ and phase shifts due to resonance scattering $\delta_{\ell,res}$ according to

$$\delta_{\ell,tot} = \delta_{\ell,pot} + \delta_{\ell,res} \tag{17}$$

The resonant part is described by

$$\delta_{\ell,res} = \frac{\pi}{2} + \Sigma \frac{\arctan \frac{1}{2} \Gamma_{\ell n}}{E_{\ell n} - E} \tag{18}$$

Taking theoretical values for the phase shifts and the positions $E_{\ell n}$ of the ^1S and ^3P resonances of atomic hydrogen and their energy width $\Gamma_{\ell n}$, a theoretical shape for the elastic cross section, as shown in fig.1, can be calculated. This method can be used to work out individual phase shifts from experimental data by curve fitting, resulting in an explanation of the configurations involved, as well as making an absolute measurement of the elastic cross section possible. This type of experiment has been carried out for He (Andrick D. and Ehrhardt H. 1966, Gibson J.R. and Dolder K.T. 1969). Similar experiments with atomic hydrogen have not yet been published.

The whole theoretical treatment has been described

Figure 1:

Computed resonance profile for the elastic
scattering resonance structure ^1S and ^3P in
atomic hydrogen.   The s-wave shifts used are
those of C. Schwartz (1961), p and d phases
are those of A. Temkin and J. C. Lamkin (1961).
Energies used are 9.571eV for the ^1S resonance
with a half width of 0.049eV, and 9.727eV for
^3P with a half width of 0.010eV.
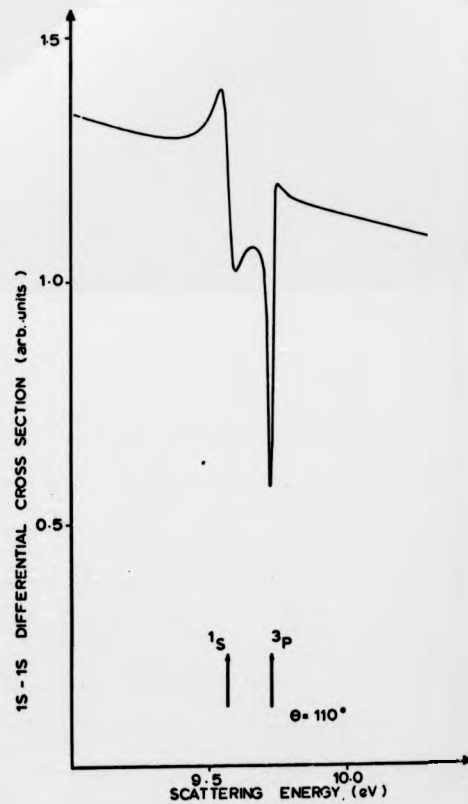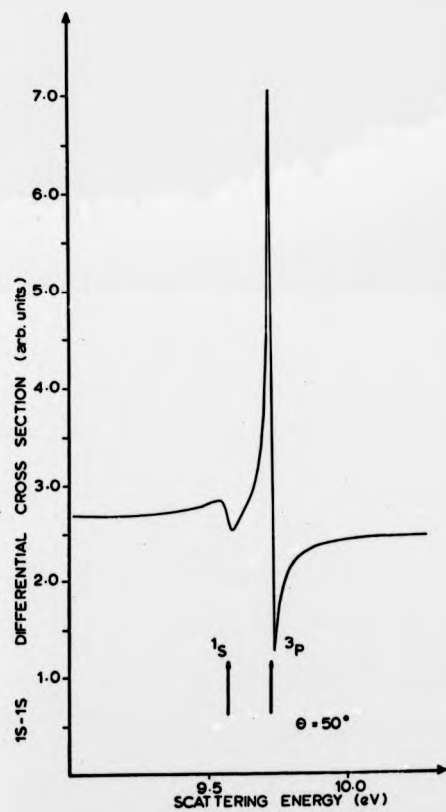
astic

^3P in

sed are

phases

in (1961).

resonance

27eV for

in great detail by a number of authors (e.g. Massey H.S.W. and
Burhop E.H.S. 1969, Smith K. 1966, etc.).

1.3 Previous experiments

Since the first resonance was observed in elastic
electron-He scattering by G. J. Schulz (1963), a number of
similar features have been discovered in a number of scattering
processes. A full description of these experiments can be
found in a recent review article by G. J. Schulz (1973).

The only e-H scattering experiments which studied
resonances in the elastic channel and which have been published
so far, have been carried out by G. J. Schulz (1964) a
transmission experiment, and by Kleinpoppen and Raible (1965) -
a crossed beam experiment, which was followed by another
crossed beam experiment by McGowan et al (1965). The results
were in agreement. An angular distribution measurement is
still outstanding. Recently the positions of hydrogen
resonances in the elastic channel have been thoroughly
investigated by Sanche and Burrow (1972). Their results
are shown in fig.2 and compared with theoretical results.
The same type of transmission experiment was used to locate
resonance structure in rare gases (Sanche L. and Schulz G.J.
1972). Some of these structures have been observed in total
metastable excitation experiments (Pichanick F.M.J. and
Simpson J.A. 1968), elastic scattering experiments and optical
excitation measurements (Kisker E. 1972). Figures 3 and 4 show
level diagrams of Neon and Argon with the experimental values
for resonances obtained in transmission experiments. The transi-
tions which have been observed in Neon and Argon during the

Figure 2:

Energy level diagram for compound states in
atomic hydrogen. The diagram is reproduced in
modified form from G. J. Schulz (1973) and
shows the theoretical values of Burke (1968).
Experimental values for the compound states
below n = 2 are those by L. Sanche and
P. D. Burrow (1972), values higher than n = 2
are from McGowan et al (1965, 1969).

ates in

oduced in

3) and

e (1968).

states

nd

han n = 2

H   H⁻(theoret. values)

RESONANCES
(McGOWAN et al 1965,1969
SANCHE & BURROW 1972[f]
experim. values)

^1S ^3S ^1P ^3P ^1D

ENERGY (eV)

13.0

n=4 —— 12.75

12.35
12.23
12.16 —— 12.06

12.0 n=3 —— 12.08   12.037   11.915   12.048
11.733   11.764   11.819   — 11.89
11.77
11.65 —

11.0

10.45
^1P — 10.29
^1D — 10.128[f]

n=2 —— 10.20   10.178   10.202 10.222 10.20 10.125
10.150 10.177 10.190

10.0

9.74 ^3F — 9.738[f]
^1S — 9.558[f]

9.56

9.0
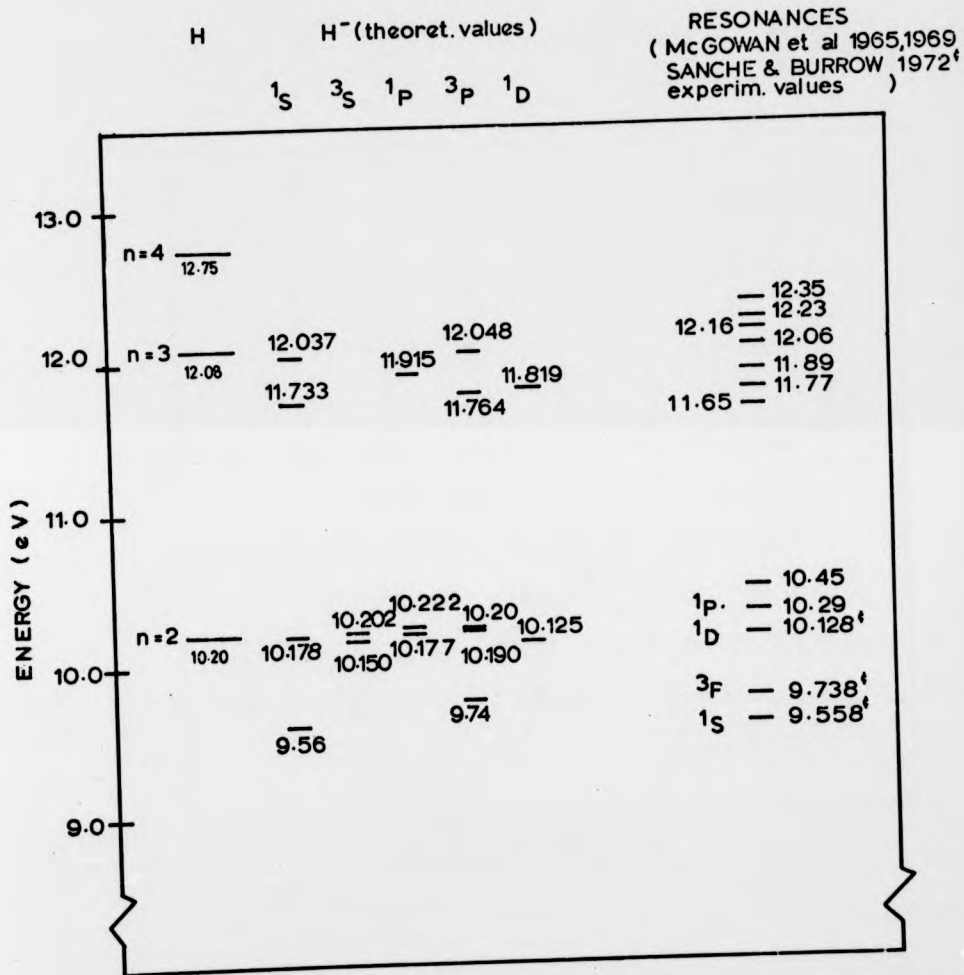
Figure 3:

Level diagram for argon. Reproduced, slightly
modified, from G. J. Schulz(1973).
Transitions described later on are indicated.
Experimental values as observed by L. Sanche
and G. J. Schulz (1972) in a transmission
experiment are shown on the right of the
diagram.
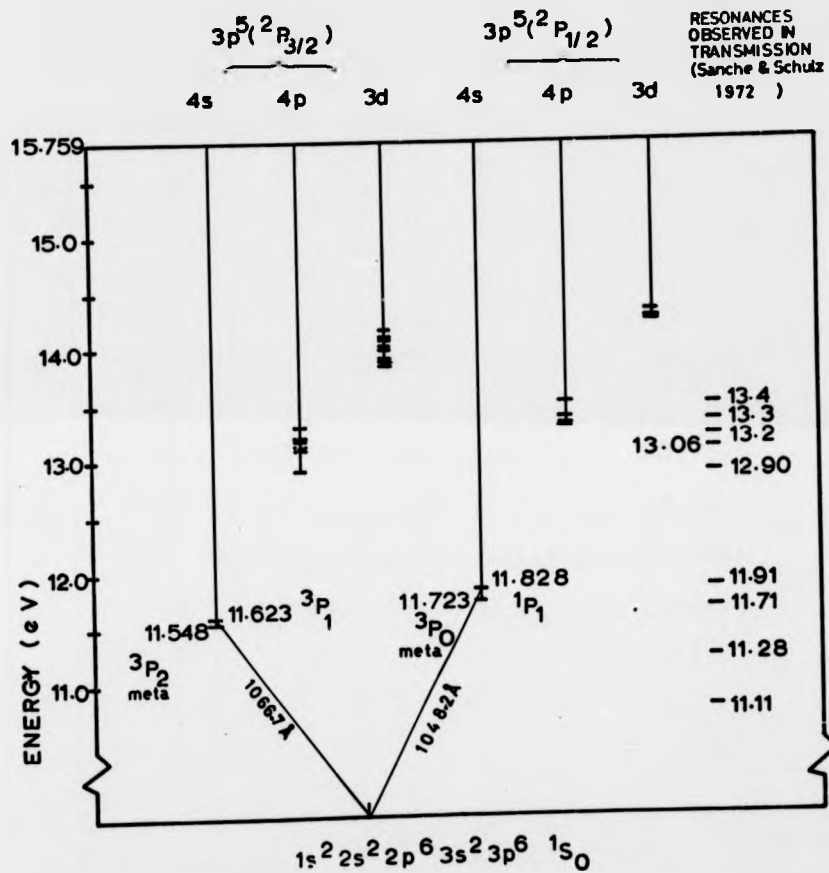
d, slightly

indicated.

. Sanche

ission

f the

Figure 4:

Energy level diagram for neon. Taken, in
a slightly modified form, from G. J. Schulz
(1973). The transitions discussed later on
are indicated. Energy values on the right
of the diagram are those observed in
transmission by L. Sanche and G. J. Schulz
(1972).

ENERGY (eV)

15.

RESONANCES
OBSERVED IN
TRANSMISSION
(Sanche and Schulz 1972)

experiments described here are also shown in these figures. Excitation measurements of the Ar resonance lines published recently (Lloyd C.R. et al 1972, McConkey J.W. et al 1973) showed no evidence of structure in the threshold region, owing to insufficient energy resolution.

2. The apparatus

In order to carry out resonance scattering experiments, some basic requirements have to be met, the most essential of which are
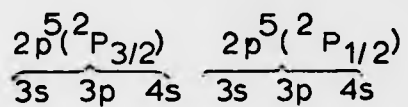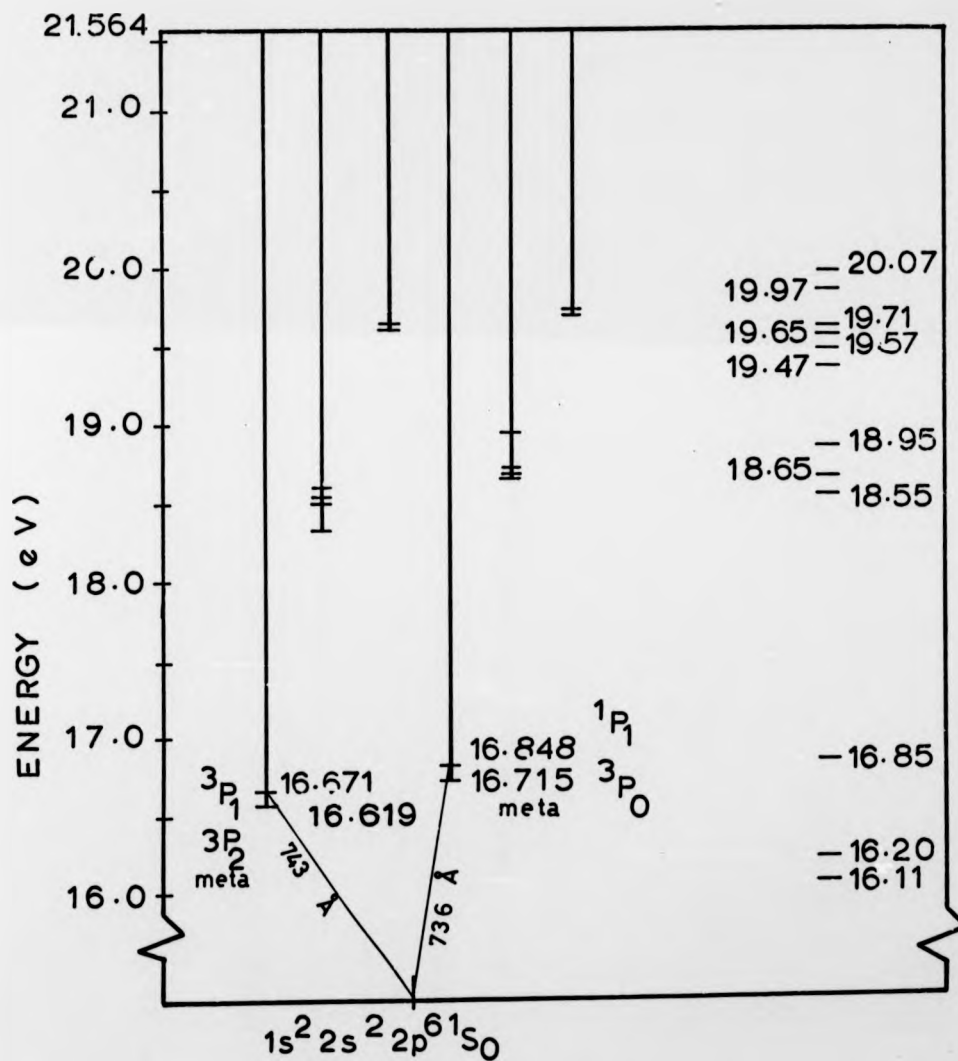
    (a)   intensive target beam source

    (b)   strong electron beam source

    (c)   electron beam of reduced energy distribution

    (d)   electron beam of defined energy

    (e)   low magnetic and electric fields in the scattering region

    (f)   clean system

    (g)   low basic pressure

    (h)   low contact potentials

2.1 The vacuum system

Since the apparatus is ultimately to be used for electron-atomic hydrogen scattering experiments, the actual design was based on requirements necessary for this case. Minor modifications for electron scattering from rare gases will be mentioned where necessary.
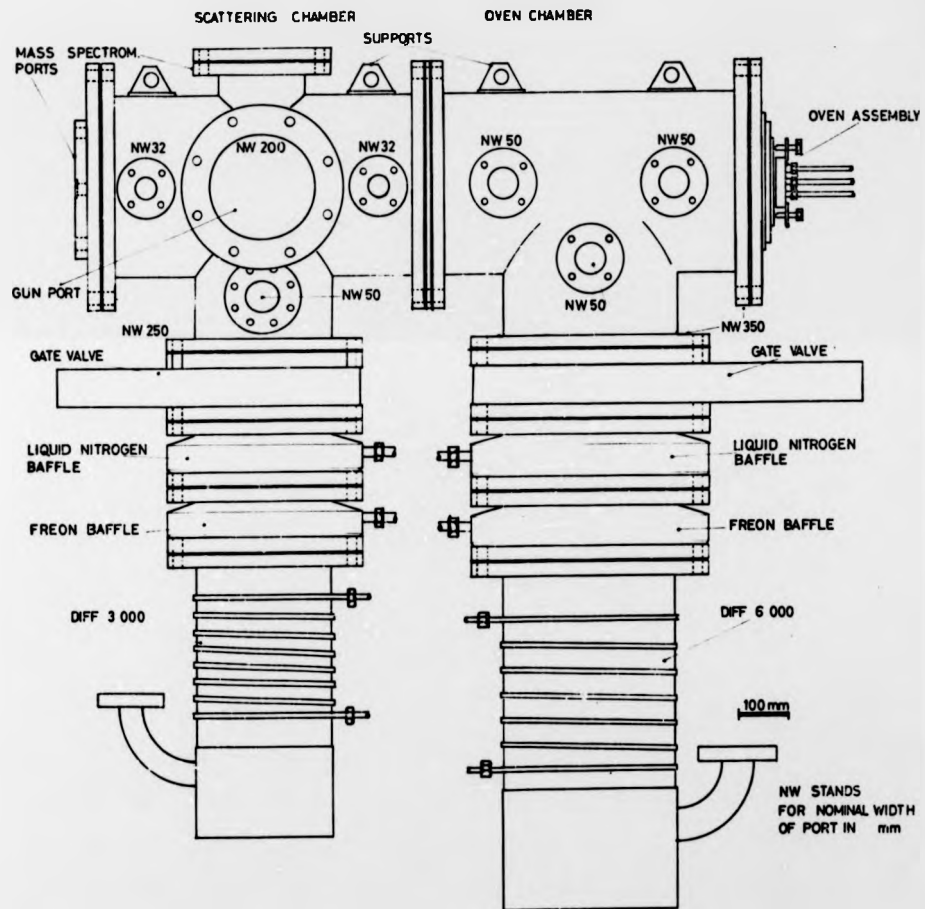
The vacuum system consists of two chambers - a target source chamber and a scattering chamber. Provisions exist for the use of a titanium sublimation pump in the scattering chamber. This additional pump was considered necessary, to reduce the molecular hydrogen background, a problem in hydrogen experiments, caused by recombination. This pump could not be used so far because its electric supplies create interfering pulses, which have not yet been suppressed.

The target source chamber is pumped by a four-stage oil diffusion pump. Pumping speed for air is 6000 l/sec. This pump is baffled by a liquid nitrogen chevron-type baffle and a freon cooled chevron baffle. The temperature of the freon baffle was kept at -30° to -50°C. The scattering chamber is evacuated by a 3000 l/sec four-stage oil diffusion pump, again baffled by liquid nitrogen and freon baffles. Both diffusion pumps are connected in parallel to a two stage rotary pump with a pumping speed of 100 m^3/h. The diffusion pumps can be separated from the main tanks by means of electro-pneumatically operated gate valves. There is a by-pass connecting each vacuum tank separately with the backing pump. This additional backing line is available through hand-operated right angle valves mounted on either tank. Figure 5 shows a schematic diagram of the vacuum system.

At the moment DC705 oil is used in the diffusion pumps and seals are of viton. An even better ultimate vacuum could be achieved using metal seals. This can be done when required. Four-stage diffusion pumps are used to prevent pressure fluctuations when large amounts of hydrogen have to be pumped (Franke H. and Bauer H. 1965). The first stage

Figure 5:

Side view of the vacuum system which was
used for the experiments described later
on. All dimensions are given according to
isometric standards. NW gives the nominal
width of the ports in mm.

SCATTERING CHAMBER   OVEN CHAMBER

MASS SPECTROM. PORTS

SUPPORTS

NW32   NW 200   NW32   NW 50   NW 50

OVEN ASSEMBLY

GUN PORT   NW 50

NW 250   NW 50   NW 350

GATE VALVE   GATE VALVE

LIQUID NITROGEN BAFFLE   LIQUID NITROGEN BAFFLE

FREON BAFFLE   FREON BAFFLE

DIFF 3 000   DIFF 6 000

100 mm

NW STANDS FOR NOMINAL WIDTH OF PORT IN mm

was

ater

ing to

ominal

of the pump acts as a booster pump.

The actual vacuum system consists of two tanks with a nominal bore 350 mm. The scattering chamber is separated from the source chamber by means of a helmet-shaped vacuum wall with provisions for mounting beam apertures of different diameter. There are sufficient ports in either tank to take components as required. Tanks and flanges have been machined from immaculate V stainless steel. Argon arc welding techniques were used to make sure that the magnetic properties of the material were not distorted. All components are held together by isometric screws and bolts made from 18/8 or 18/8/2 stainless steel.

The whole system was designed to isometric standards using metric components. This was done to allow a flexible interchange of this equipment or parts of it with other systems in the future. Sealing discs were again to isometric standards. This type of seal allows one to use a metal or non-metal vacuum seal by a simple exchange of duraluminium discs carrying the sealing material.

The main tanks of this vacuum system can be baked at moderate temperatures by heater coils wrapped around the vessels. The maximum temperature used so far was $150^{o}C$. This could be raised by using metal seals which are capable of standing up to higher temperatures. So far only viton and some Indium seals have been used.

Ultimate pressures of 2.10^{-7} torr can be achieved in both vacuum tanks after approximately two hours. The ultimate pressure after continuous running over several days is 10^{-8} torr. This pressure can be maintained with the

electron gun operating and a hot hydrogen dissociator. With
the hydrogen beam on, a hydrogen pressure of 7.10^{-5} torr in
the over chamber increases the pressure in the scattering
chamber to about 3.10^{-6} torr. This pressure increase is
almost entirely due to molecular hydrogen, which is created
by recombination of atoms hitting the metal parts of the
vacuum system. Some background pressure will also be caused
by diffusion between the two vessels of this differentially-
pumped system. This is one problem which could be reduced
by means of an intermediate chamber. This however would
certainly reduce the target beam intensity owing to the
longer beam path. It was this problem of high molecular
background which led to the consideration of using a titanium
sublimation pump as mentioned before.

One disadvantage of the vacuum system described
here could be the use of oil diffusion pumps, possibly resulting
in contamination of the electron monochromators. Although
great care was taken to reduce oil backstreaming into the system
by means of liquid nitrogen and freon baffles, it is not
possible to completely suppress it. To minimize the effect, the
electron gun system is bakeable. This should counteract an
extensive build-up of insulating oil layers on the electrodes.

2.2 The oven chamber

This part of the vacuum system consists of a
T-shaped vessel with a nominal internal diameter of 350 mm
(see fig.5) and a length of 652 mm. Six ports with nominal
widths of 50 mm are available to take auxiliary equipment.
One of these ports is used for a foreline by-pass which is

normally closed by means of a hand operated right angle
valve. Three other ports take bakeable ionisation gauge
heads, Balzers type IMR 5. One port contains an additional
Pirani gauge and a venting valve. The system can be vented
with air or other appropriate gas. The oven chamber extends into
the scattering chamber by means of a concentric water-cooled
vessel which has an overall length of 226 mm. This allows the
hydrogen dissociator to be positioned as close to the scattering
region as possible. The arrangement can be seen in figure 6.
The concentric vessel had interchangeable target beam apertures
up to a maximum of 20 mm ∅. The normal apertures used were
between 3 mm ∅ and 8 mm ∅, as required.

The pump column, which is suspended from a port
with nominal diameter of 350 mm, can be separated from the
oven chamber by means of an electro-pneumatically operated
gate valve (VAT). This chamber is evacuated by a four-stage
oil diffusion pump (Leybold Heraeus). The pump is baffled
with a liquid nitrogen cooled chevron baffle and a freon cooled
chevron baffle. The pumping speed of the diffusion pump is
6000 l/sec for air, according to the manufacturer.

A third port with nominal bore 350 mm is used to
introduce the hydrogen, or other beam source into the system.

2.3 The scattering chamber

Another T-shaped tank with nominal bore 350 mm
was used to accommodate the scattering section of the apparatus.
A port on top of the tank was used to take a quadrupole mass
spectrometer to investigate the fractional composition of the
atomic hydrogen target at the interaction region. The electron

Figure 6:

Longitudinal section of the apparatus showing
the electron spectrometer and the target beam
source in position. The concentric extension
of the source chamber into the interaction chamber
is also shown.
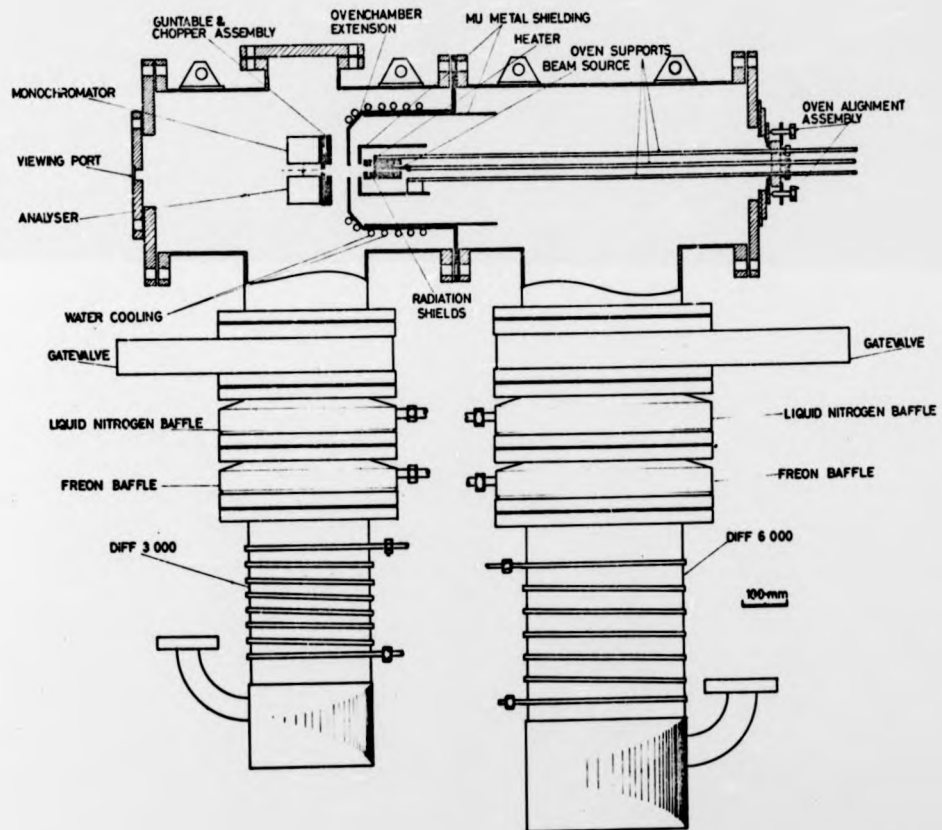
owing

beam

nsion

on chamber

spectrometer was introduced into the system through a port
of nominal internal diameter of 200 mm. The spectrometer
was mounted on a table which also supported a mechanical
chopper. This gun table was then suspended on two stainless
steel rods from an NW 200 mm flange. For the 2S excitation
experiment (Koschmieder H. 1974) there were two separate ports
on one side of the scattering tank to take components required
for this experiment.

Additional ports of internal diameter 32 mm and
50 mm were used to accommodate bakeable ionisation gauge heads,
a pirani gauge and a venting line. A separate foreline by-pass
was available through a hand-operated right angle valve. The
arrangement of vacuum ports and the internal arrangement of
important components can be seen in figures 5 and 6 respectively.

The pump column was suspended from a 250 mm diameter
flange and could be separated from the scattering chamber by means
of an electro-pneumatically operated gatevalve (VAT). The
scattering tank was pumped with a four stage oil diffusion pump
(Leybold Heraeus). This pump was baffled with a liquid nitrogen
cooled chevron baffle and a freon cooled chevron baffle. The
nominal pumping speed of the diffusion pump was 3000 1/sec for
air, according to the manufacturer.

The entire vacuum system was suspended from a
beam and could be moved with castor wheels running along the
beam. The steel beam itself was mounted on a scaffolding.
All parts of the system have been designed according to DIN
standards which have in the meantime been adopted almost
entirely as isometric standards. Only metric components
are used throughout.

2.4 Gas injection system

A schematic diagram of the gas injection system
is shown in figure 7. By means of several mechanical leak
valves it is possible to admit a number of pure gases or gas
mixtures into the system. Mixtures can be monitored either
by ionisation gauges or by means of a quadrupole mass
spectrometer. This gas handling system is pumped through
the main vacuum system. In the case of sudden leaks or of
breakdown, an electromagnetic safety valve is automatically
closed to safeguard the system. This is a necessary precaution,
especially for hydrogen operation.

Rare gases used in the system were from research
grade cylinders obtained from outside suppliers. Ultra-pure
hydrogen was generated by means of a palladium silver diffusion
cell. Heated to about $350^{\circ}C$, this cell transmits hydrogen but
is impermeable to any other gas. The hydrogen was extracted
from ordinary town gas which contains about 40% hydrogen. This
method avoids the use of high pressure hydrogen gas cylinders
and the dangers associated with them.

2.5 The interlock system

A system as expensive and elaborate as the one
described here, a system which can even be a severe safety risk
must be supplied with a fully automatic control system. This
is even more necessary, since some of the experiments might
require extended operation of the system, sometimes without
attention.

A complete shut down of the system involving all
equipment is caused by water failure, steep pressure rise or

Figure 7:

Schematic diagram of the gas handling system.
The electromagnetic valve is connected to an
interlock system to safeguard the apparatus.
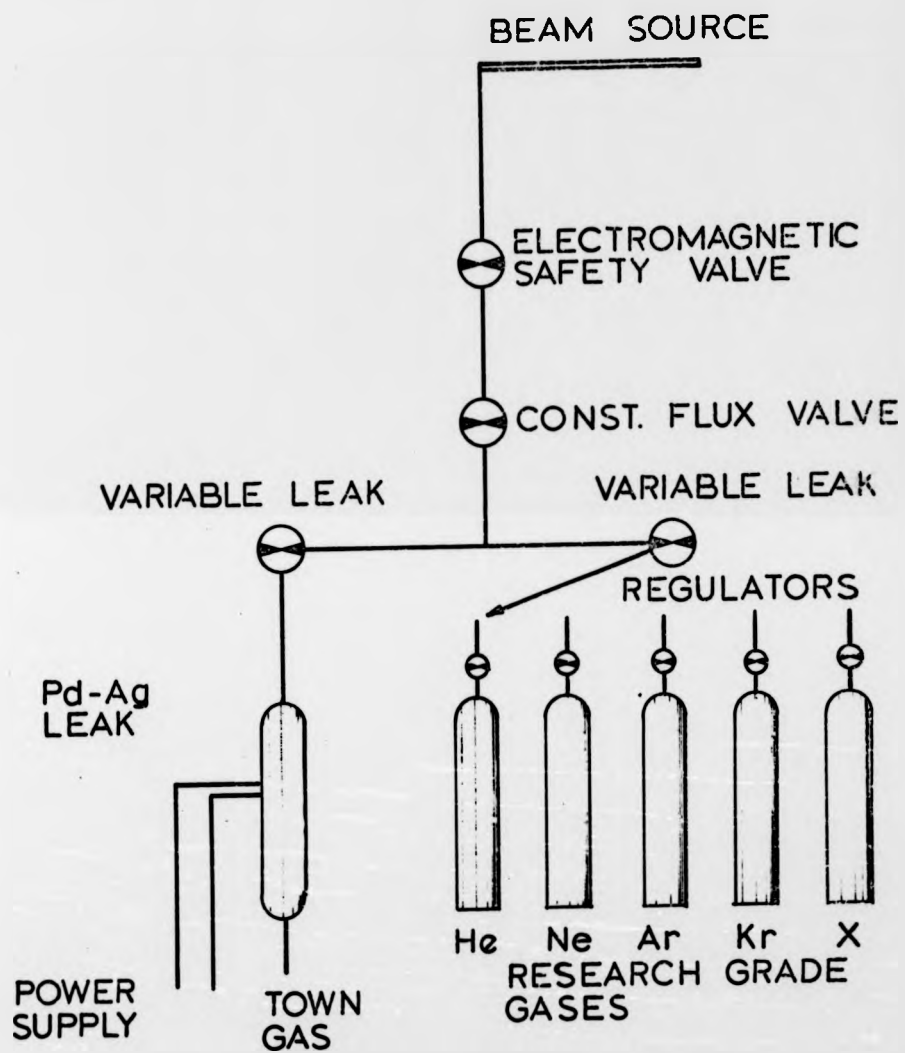
failure in the liquid nitrogen cooling system. The
control system designed works in two possible sequences.
In one sequence there is a 20 minute delay of this
procedure to carry out necessary adjustments. The other
sequence, which is used if the system is left unattended,
causes an immediate shut down including electric isolation
of the system. This shut down involves the isolation of
the vacuum system from pumps and gas intake. Disconnection
of all electric supplies to the system is caused after a
preset interval and the water supply to the apparatus is
closed. The cause of this failure has to be cured otherwise
it is not possible to restart the apparatus. These
precautions have proven to be valuable and have certainly
prevented expensive damage to the system on several occasions.

3.   The atomic beam source

In this chapter the production of an atomic
target beam and its properties, such as intensity and directivity
are discussed. The treatment is for the complicated case of
atomic hydrogen. In order to produce a significant proportion
of atomic hydrogen in a beam, temperatures in excess of $2500^{\circ}K$
are required. This creates technical problems, as will be
mentioned. The recombination of atoms into hydrogen molecules
results in background problems which have led to the design of
a modulated beam.

3.1 General considerations

Using atomic beams in a vacuum system is
equivalent to the artificial introduction of a leak into the

vacuum system. The leak rate and thus the intensity of the
beam will be limited by the maximum value of the background
pressure which can be tolerated in the system. This pressure
is mainly determined by the proper functioning of components
like detectors and, in this case, by the electron beam source.
In order to maintain this pressure in the system one has to
continuously pump the gas intake. This means, that the intensity
of the target beam is very much dependent on the pumping speed of
the vacuum system.

Pumping speeds given by manufacturers are normally
optimum values, reached with a particular pump when pumping air
of molecular weight 28. Since diffusion processes are involved,
one can work out the actual pumping speed of a diffusion pump
for different gases according to (Dennis N.T.M. and Heppel T.A.):

$$S_{GAS} = S_{AIR} \ (\frac{28}{m_{GAS}})^{\frac{1}{2}} \qquad\qquad (1)$$

S is given in $l.sec^{-1}$, and m_{GAS} is the molecular weight of the
gas being evacuated. Considering the conductance C_i of baffles,
which are in series with the diffusion pump, the effective
pumping speed at the vacuum system is

$$S_{eff_{GAS}} = \frac{S_{GAS}}{1 + S_{GAS} \cdot \sum_i C_i^{-1}} \qquad\qquad (2)$$

C_i is again in $l \cdot sec^{-1}$. in the case of the source chamber
described here, the pumping speed of the four stage diffusion
pump is 6000 $l \cdot sec^{-1}$ for air. Taking the total conductance
C as 4600 $l \cdot sec^{-1}$ one expects effective pumping speeds of

$$5200 \ l \cdot sec^{-1} \leqslant S_{H_2} \leqslant 6500 \ l \cdot sec^{-1}$$

A factor of between 2 and 2.5 (Leybold Heraeus) has been used as more realistic than the correction suggested by (1). This pumping speed drops, for the noble gases, to

$$S_{Ne} = 3000 \; l.sec^{-1}$$

$$S_{Ar} = 2200 \; l.sec^{-1}$$

These figures can be used to make estimates of the beam intensities which can be achieved with the present system. Gas leaking into a vacuum system will cause the pressure in the source chamber to rise to p Torr. If S l.sec^{-1} is the effective pumping speed for the particular gas leaked into the system, then it is possible to work out the total effusion rate of this source according to

$$N = 3.54 \cdot 10^{19} \cdot S.p. \; molec.sec^{-1} \tag{3}$$

This assumes that the apparatus is working in a stationary state and the pumping speed at the source chamber is known. For a source chamber pressure of 5.10^{-5} torr of hydrogen and using a pumping speed of $5.2 \cdot 10^3 \; l \cdot sec^{-1}$, the total effusion is $N = 9.2 \cdot 10^{18} \; molecules \cdot sec^{-1}$. The problem which arises is to get as many of these particles as possible into a limited target area, in order to make the target intensity as high as possible. The source configurations one has to consider are

  (a) simple aperture source

  (b) long channel source

  (c) multicapillary source

  (d) supersonic nozzle

Bearing the flexibility of the system in mind, only the first three possibilities were considered. Out of these the multicapillary source had to be ruled out for hydrogen, since a new type of heater was to be used for the dissociator. This heater was not efficient enough for this type of source. A multicapillary source has been used in previous experiments (Raible V, 1965) and has temporarily been used here for some rare gas experiments.

The use of long channel beam sources, that is sources with length L cm and radius a cm, where

$$L \gg a, \tag{4}$$

as compared to thin-walled aperture sources has proven to be advantageous. These long channel sources have a higher directivity and thus achieve higher target densities for the same gas intake. This has been investigated both experimentally and theoretically by several groups (Giordmaine J.A. and Wang T.C. 1960, Hanes G.R. 1960, Zugenmaier P. 1966). The intensity of a beam effusing from an ideal orifice source at a distance ℓ cm from the source is

$$I(\theta) = \frac{n\bar{v}A}{4\pi\ell^2} \cdot \cos\theta \quad molec.cm^{-2}.sec^{-1} \tag{5}$$

A is the area of the aperture, θ is the polar angle, n is the number density in the source. The mean velocity of the gas molecules in the source is given by

$$\bar{v} = (\frac{8kT}{\pi m})^{\frac{1}{2}} \tag{6}$$

and the particle density is given by

$$n = p/kT \tag{7}$$

where p is the source pressure, T the source temperature, k the Boltzmann constant and m the mass of the particle.

On the axis normal to the source, the beam intensity is described by

$$I(0) = \frac{n\bar{v}A}{4\pi\ell^2} \quad molec.cm^{-2}.sec^{-1} \tag{8}$$

The total number of molecules emerging from the source is given by

$$N = \int_0^{\pi/2} \frac{n\bar{v}A}{4\pi} \cdot \cos\theta d\omega \tag{9a}$$

Where dω is a solid angle at an angle θ with respect to the normal of the aperture, dω = 2πsinθdθ.

$$N = \frac{n\bar{v}A}{4} \tag{9}$$

The centre beam intensity (8) can therefore be expressed in terms of the total effusion

$$I(0) = \frac{N}{\pi\ell^2} \tag{10}$$

It becomes clear, that the maximum beam intensity is determined by the rate at which particles, which are no longer part of the beam, are pumped away.

In the case of long channels, these simple relations are no longer valid. Depending on the mean free path of the particles compared to the dimensions of the channel, several modes of flow have to be investigated. The importance of the source pressure plays a significant role in the beam intensity. The mean free path of molecules is given by

$$\lambda = (\sqrt{2}.\pi.n.\delta^2)^{-1} \tag{11}$$

where n is related to the source pressure according to (7).
δ is the hard sphere molecular diameter. Two important cases
are to be considered:

(a) Collisions between individual molecules can
be neglected, $\lambda \gg L$. The molecules pass through
the channel with collisions only with the walls
and this is described as transparent flow. Peak
intensities are < 10^{17} particles.sterad^{-1}.sec^{-1}.
The peak intensity is proportional to the pressure
behind the source.

(b) By increasing the source pressure, one reaches
conditions where $\lambda < L$ but $\lambda \gg a$. This is
referred to as intermediate flow conditions.
This region produces centre beam intensities of
(Giordmaine J.A. & Wang T.C. 1960)

$$I(0) = \frac{1}{2^{\frac{1}{4}}.8.\delta} \cdot (\frac{\bar{v}.a.N}{\pi})^{\frac{1}{2}} \text{ molec.sterad}^{-1} \cdot \text{sec}^{-1} \quad (12)$$

which means, that this intensity is no longer
proportional to the total flow as in (8) but to
the square root of the total flow (3). The half
width of the beam, that is, the angle $\theta_{1/2}$ for which
the intensity drops to half the centre beam intensity
at $\theta=0$ is given by (Giordmaine and Wang)

$$\theta_{\frac{1}{2}} = \frac{2^{7/4}.\delta}{1.78} \cdot (\frac{3.N}{a.\bar{v}})^{\frac{1}{2}} \quad (13)$$

The beam expands in proportion to the square root of the total
flow. The criterion for the validity of these equations to

within 1% is given (Giordmaine and Wang) by

$$L \geqslant \frac{2.5}{\delta} \cdot 2^{3/4} \cdot a^{3/2} (\frac{\bar{v}}{3N})^{\frac{1}{2}} \qquad (14)$$

In the present experiment, the radius of the 10 cm long tungsten tube used was 0.35 cm. Taking a pressure of 10^{-4} torr Hydrogen in the source chamber, the total effusion rate according to (3) is

$$N = 1.8 \cdot 10^{19} \text{ molec.sec}^{-1}$$

At an operating temperature of 2800°K the centre beam intensity according to (12) works out to be

$$I \tilde{=} 5.10^{18} \text{ molec.sterad}^{-1}.\text{sec}^{-1}$$

and drops at a distance of 10 cm from the source to

$$I \tilde{=} 5.10^{16} \text{ molec.cm}^{-2}.\text{sec}^{-1}$$

The corresponding values for a simple aperture source are

$$I \tilde{=} 2.10^{16} \text{ molec.cm}^{-2}.\text{sec}^{-1}$$

and a beam half-width of 60° compared to about 35° for the tube source. Thus a gain of about 2.5 in intensity is achieved by using a long channel source.

The beam density, at a source temperature of 2800°K, is now

$$n = \frac{I}{v} \tilde{=} 6.10^{10} \text{ molec.cm}^{-3}.$$

This is the actual target density at the scattering region which is about 10 cm from the source, in the case of hydrogen experiments.

In elastic scattering experiments, the limit of sensitivity for a measurement not only depends on the target

beam intensity - the signal is proportional to the intensity -
but also depends on the signal created by the background gas.
This of course assumes that no other signals arise for example
from electrons scattered off metal surfaces, which can be a very
important disadvantage. The signal to noise ratio is directly
proportional to the ratio of target beam intensity to background
intensity.

　　　　　With the hydrogen beam on, and a pressure of
$p_1 = 10^{-4}$ torr in the source chamber, the pressure in the
scattering chamber drops to $p_2 = 2.10^{-6}$ torr. This background
pressure corresponds to a background particle density of about
7.10^{10} molec.cm^{-3}. This background is caused by a direct
contribution of the target beam entering the scattering
chamber through an aperture of radius r which defines a
solid angle $\Delta\Omega$. This contribution is given by

$$N = I(0).\Delta\Omega$$

Due to the pressure difference between the two chambers,
particles diffuse through the partition aperture at a rate
given by

$$N = 3.5 \cdot 10^{22} \frac{(p_1 - p_2)}{\sqrt{MT}} . \pi r^2$$

where M is the molecular weight of the gas considered.
The background particle density is of the same magnitude
as the target beam itself. This creates the problem of
distinguishing between electrons scattered from the target
beam and those scattered from background particles.
The target beam in the present experiment was therefore
modulated.

In rare gas experiments, the situation is much more favourable. The major disadvantage in atomic hydrogen scattering experiments is the large distance between the beam source and the actual scattering centre. This distance is a consequence of the high temperatures required to dissociate hydrogen. The total effusion rate in the case of Argon, based on the effective pumping speed of 2200 $\ell.sec^{-1}$ is, according to (3)

$$N = 8 \cdot 10^{18} \text{ atoms} \cdot \sec^{-1}$$

This intensity can be fully utilised by moving the target beam source to within millimetres of the scattering centre. The normal distances used in the excitation measurements were between 1 cm and 2 cm.

As has been shown, the target intensity of a beam experiment strongly depends on the effective pumping speed of the pumps used and the source to interaction region distance which is to be as short as possible. Limitations on the latter are caused by the use of hot beam sources and auxiliary equipment such as mechanical choppers. In order to improve the ratio of target beam intensity to background intensity, the aperture used between source-chamber and scattering chamber should be as small as possible in order to reduce diffusion from the higher pressure vessel to the scattering chamber.

3.2 The atomic hydrogen source

Since hydrogen in its stable form is a diatomic molecule, one has to produce atomic hydrogen by dissociation. The energy required to split the molecule is 4.478 eV. Two

methods are generally used, namely electrical discharge and thermal dissociation. Atomic hydrogen, in high concentration was probably first produced in a discharge tube (R. W. Wood) which is now known as the Woods tube. The first successful thermal dissociation was achieved in 1950 (Lamb W.E. and Retherford R.C. 1950). The use of discharge methods, whether d.c. discharge or microwave was thought to be unsuitable, since the apparatus was to be used for ultraviolet excitation measurements (Koschmieder H. 1974) and discharges are strong sources of Ly_α-radiation. Only thermal dissociation has therefore been considered.

There are three methods to achieve thermal dissociation

     (a)   direct heated ovens (e.g. Fite W.L. et al 1958)

     (b)   heating by electron bombardment (e.g. Raible V. 1965)

     (c)   heating by radiation

The first type of dissociator is a tungsten cylinder which is heated in its central part by direct passage of current through its walls. A disadvantage of this type of furnace is mechanical instability leading to a short life-time. A further disadvantage is due to its beam properties. The oven acts like a simple aperture source which has poorer directivity compared to long channel sources. In the second type of oven this problem no longer exists. A massive tungsten pipe is bombarded by electrons with energies between 1 keV and 2 keV. This type has been used in previous experiments (Raible V. 1965). Merits of this type of furnace are high reliability, long lifetime and high stability. An electron-bombarded oven can easily be used as a multi-capillary source.

The reasons for not using this type of furnace were that, owing to the electron bombardment this type of source creates Ly_α photons, electrons and ions. They create a lot of experimental difficulties and were thought to be no longer present in a radiation heated dissociator.

3.3   Radiation heated atomic hydrogen beam source.

The hydrogen dissociator consists of a 10 cm long, thin tungsten tube. This tube is surrounded by a heater. The heat is transferred by radiation (see figure 8). This arrangement combines low ultraviolet background radiation emerging from the oven region into the scattering region with the collimation properties of a long tube. Since radiation heating is less efficient than direct heating or heating by electron bombardment, thorough provisions had to be made to prevent heat losses by radiation or conduction. Conduction was kept low by using a tube with walls as thin as possible. Radiation losses were reduced by a set of radiation shields which contain the heat in a confined volume.

The tungsten tube was rolled from 0.025 mm thick tungsten foil and has a diameter of 3.5 mm. One end of the tube was fitted around the molecular hydrogen intake and held by a ring. This sandwich arrangement produced a tight fit which prevented gas from leaking into the source chamber. The open end of the tungsten pipe was surrounded by a heater loop, which was made from tungsten sheet 0.15 mm thick and 15 mm wide. The total length of this heater ribbon was 80 mm. Both tungsten pipe and heater were heat treated at 700-1000°C in special jigs to get rid of mechanical stress.

Figure 8:

The top part shows a cross-section through
the hydrogen oven. The hydrogen source is
perpendicular to the plane of drawing. The
ribbon heater and its suspension is shown,
as well as the supports and radiation cylinders.
The bottom drawing shows a longitudinal section
of the hydrogen beam source.

HEATER SUPPORT

MICA

HEATER

WATERCOOLED
SUPPORTS

OVEN

RADIATION
SHIELDS

RADIATION
CYLINDER
WATERCOOLED

SUPPORT FOR
MU METAL CYLINDER

10mm

WATERCOOLING

OVEN SUPPORT

GASTIGHT FIT

THERMOCOUPLE

OVEN TUBE

RADIATION
SHIELDS

RADIATION
CYLINDER
WATERCOOLED

RETAINING
PIN

BEAM APERTURE

SUPPORTS
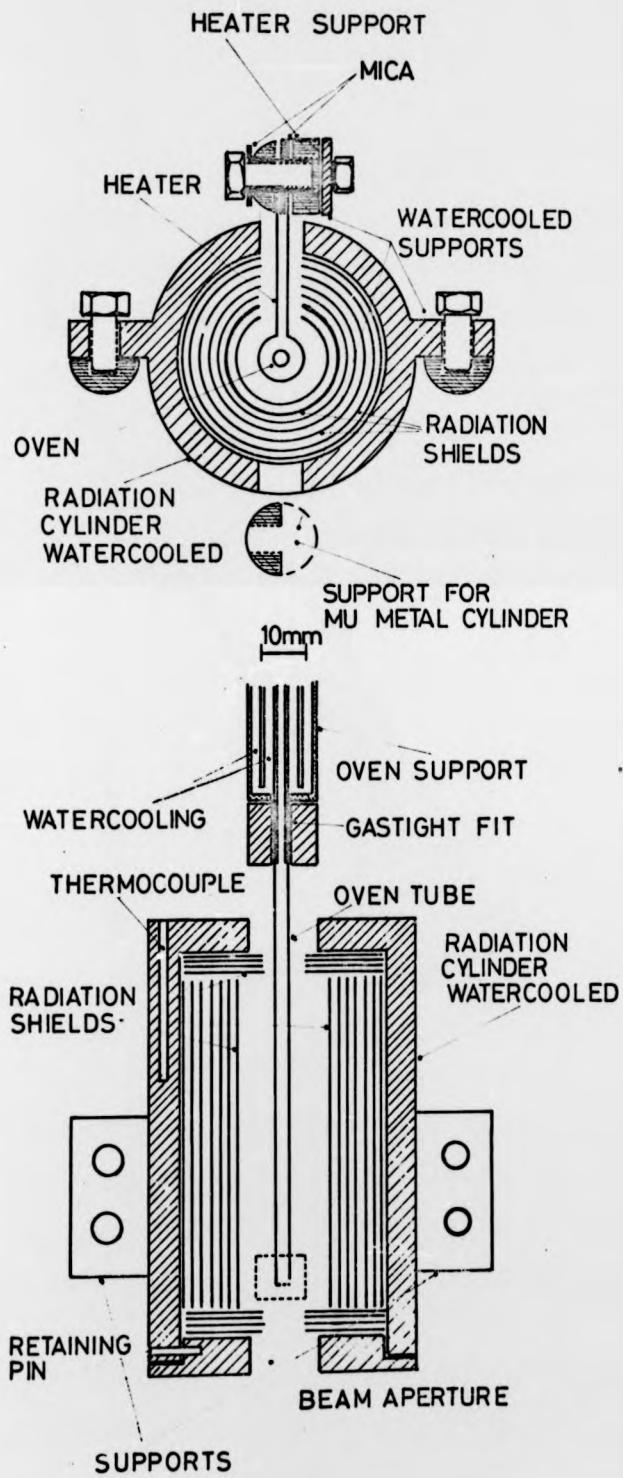
Figure 9:

The most critical part of the hydrogen
oven was the coaxial current supply line.

38.

WATER COOLING

COAXIAL FEEDTHROUGH

CURRENT LEAD (flexible)

LOW VAPOR PRESSURE RESIN

INSULATED JOINT

HEATER SUPPORT

MICA
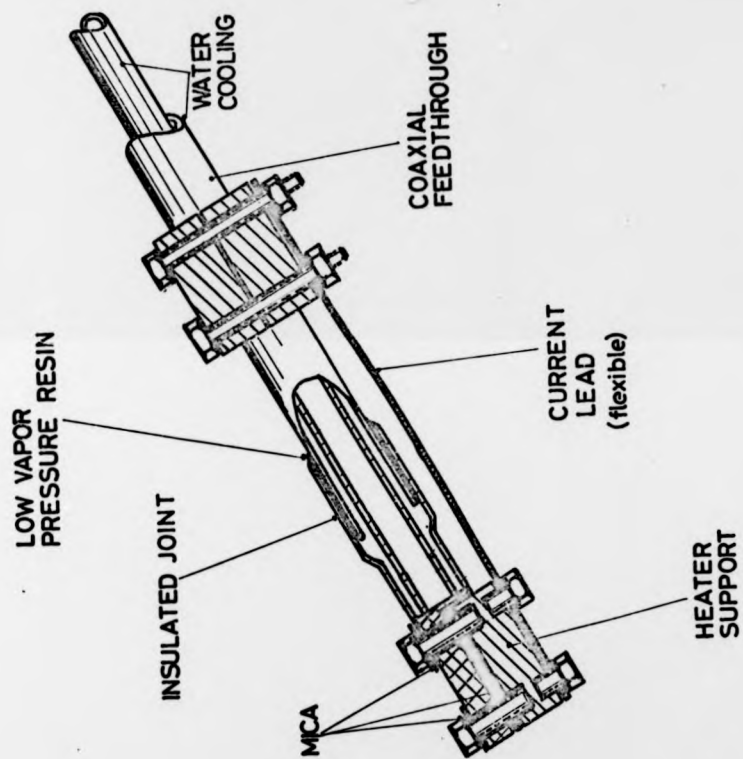
The part of the oven consisting of heater
and tungsten pipe were then surrounded by a set of six
concentric radiation cylinders made from molybdenum, and
two inner shield cylinders made from tungsten. These
radiation shields were separated from each other by small
punchmarks. The complete set of radiation shields was
contained in a stainless steel cylinder which was mounted
onto two watercooled stainless steel rods.

A further watercooled support was designed as
a coaxial current feedthrough. This was used to mount the
heater ribbon. Technically, the most difficult problem was
this heater arrangement. The final version was a circular
loop with the heater current flowing in opposite directions
along straight legs. Since under normal operation conditions
150A were passed through the heater, this design reduced the
magnetic field created by the heater current. In order to
maintain a low magnetic field along the current supply line,
a special water-cooled coaxial heater support was designed.
The final design of this is partly shown in fig.9. The outer
section of the coaxial current feedthrough was interrupted by
an insulated joint a few cm behind the connection to one side
of the heater ribbon. A connection to the other end of the
ribbon was made by means of a flexible lead. The two ends of
the heater are insulated from each other by a mica strip and
then clamped together by the two connectors in a sandwich.
The insulated joint in the current feedthrough was made with
low vapour pressure resin. Mechanical stability was achieved
by using a concentric joint. This final version of heater
and heater connector proved strong enough to withstand the

mechanical stress caused by thermal expansion when in operation and it was water- and leak-tight. Due to this assembly, the magnetic field caused by high heater currents was reduced considerably.

A fourth water-cooled support was used to mount a mu-metal shield around the oven assembly. Another mu-metal cylinder was fitted inside the oven chamber extension. This extensive mu-metal shielding in addition to the coaxial current supply reduced the magnetic field in the scattering region to less than 20 m Gauss.

The oven was a.c. heated, using a variable transformer to supply the primary side of a high power transformer. The latter had an 0-12V output with a maximum current of 300A. 1500 watt were dissipated by the 150A heater current.

One disadvantage of the present oven is the low heater efficiency. Despite the radiation shields, radiation losses are still too high. Temperatures of around 600°C have been measured at the stainless steel cylinder containing the radiation shields, even though this cylinder is water-cooled. Owing to these radiation losses it is very difficult to reach or exceed oven temperatures of 2800°K at the higher flow rates of hydrogen through the tungsten pipe. The final assembly of the hydrogen oven is shown in fig.10.

As soon as the oven was completed, an investigation of its background properties was carried out, since this was one of the reasons for designing this type of dissociator. It was found that the oven emitted a number of electrons which managed to get into the interaction region, thus interfering with electron

detection in the elastic scattering mode. These electrons can
be suppressed by means of biasing voltages applied to the oven
assembly, in such a way that electrons were collected by the
radiation cylinders. At heater voltages larger than 10V a.c.,
the creation of 2S hydrogen atoms in the oven region caused
some trouble with the 2S excitation measurements.

3.4   The hydrogen beam characteristics

The efficiency of a dissociation process of the
type

$$H_2 \rightleftharpoons 2H$$

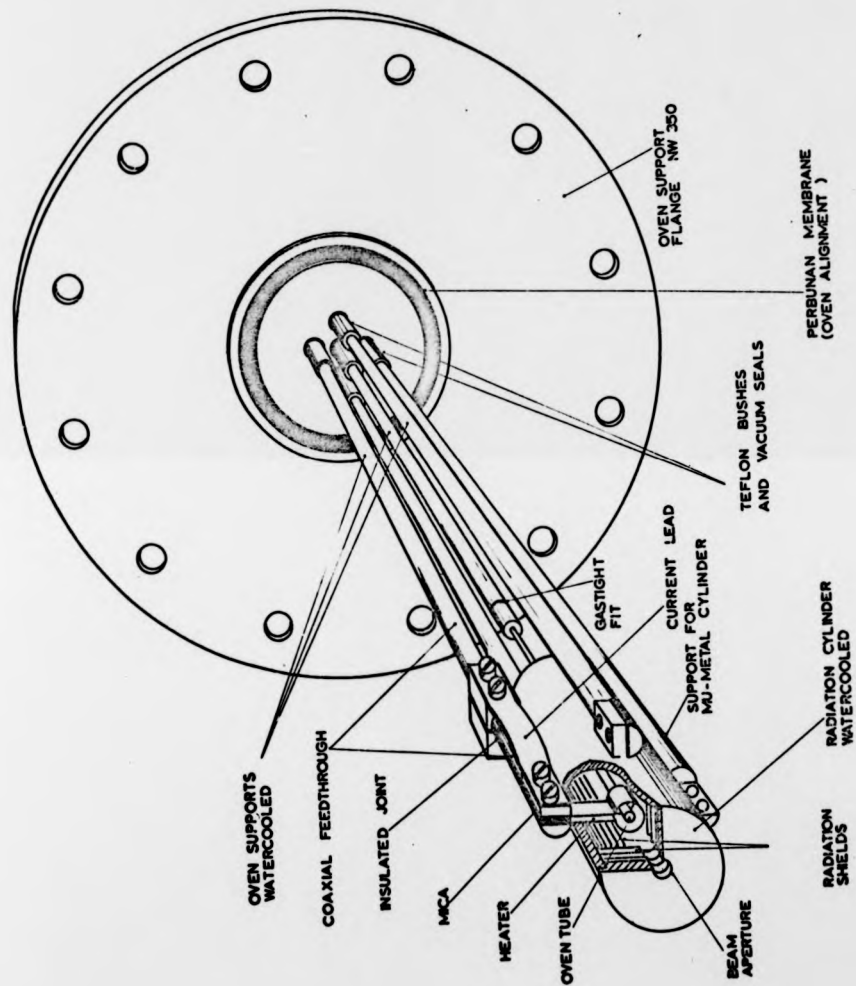can be described, assuming thermal equilibrium of the gases
concerned with the oven walls, by

$$\frac{[H]^2}{[H_2]} = K(T,p)$$

The equilibrium constant K is a function of the absolute
temperature T and the pressure. This method was used by
Lamb and Retherford (1950) to work out the degree of
dissociation in their hydrogen beam.

Since the actual dissociation process is not
yet well enough understood (chemisorption processes, which are
influenced by the surface properties of tungsten (G. Ehrlich
1959, Joe Smith and Wade L. Fite 1962), on hot surfaces followed
by evaporation are probably involved) this method was not
thought to be appropriate to describe a hydrogen oven which
has not been used before. It was considered essential to
actually measure the dissociation which can be achieved with
the furnace described in chapter 3.3. This can be done by
comparing the H_1 and H_2 particle fluxes in the beam using a
mass spectrometer.

Figure 10:

The hydrogen oven in its final version.
The radiation cylinders are cut open to give
a view of the dissociator arrangement. The
complete assembly can be lowered and raised
by means of a perbunane membrane. For rare
gas experiments, the tungsten tube is replaced
by a stainless steel tube and pushed through the
heater section to shorten the source interaction
region distance.

ion.

to give

t. The

raised

or rare

s replaced

through the

interaction

OVEN SUPPORT
FLANGE NW 350

PERBUNAN MEMBRANE
(OVEN ALIGNMENT)

TEFLON BUSHES
AND VACUUM SEALS

GASTIGHT
FIT

CURRENT LEAD

SUPPORT FOR
MU-METAL CYLINDER

RADIATION CYLINDER
WATERCOOLED

RADIATION
SHIELDS

OVEN SUPPORTS
WATERCOOLED

COAXIAL FEEDTHROUGH

INSULATED JOINT

MICA

HEATER

OVEN TUBE

BEAM
APERTURE

The dissociation fraction D of a beam of diatomic molecules can be defined as

$$D = \frac{\frac{n_1}{2}}{\frac{n_1}{2} + n_2} \qquad (1)$$

that is, by the ratio of the number of dissociated molecules $\frac{n_1}{2}$ to the total number of molecules. n_1 refers to atomic hydrogen and n_2 to molecular hydrogen. If Q_i is the ionisation cross section of beam particle i per unit electron current at a given electron energy, then the ion current observed is

$$S_i \sim Q_i \cdot \frac{n_i}{\bar{v}_i} \qquad (2)$$

If the gas comes to equilibrium in the hydrogen furnace, the mean speed in the beam is given by

$$\bar{v}_i = const. (\frac{T}{m_i})^{\frac{1}{2}} \qquad (3)$$

where m_i is the mass of the particle considered and T the absolute temperature of the oven. This leads to

$$S_i \sim const. Q_i n_i \cdot m_i^{\frac{1}{2}} T^{-\frac{1}{2}}$$

and

$$S_i = A \cdot Q_i n_i m_i^{\frac{1}{2}} \qquad (4)$$

A contains the beam geometry and other constants at a given temperature T. This can be used to express the fractional dissociation in the beam according to (1), remembering that $m_2 = 2 m_1$, as

$$D(T) = (1 + \sqrt{2} \cdot \frac{S_2}{S_1} \cdot \frac{Q_1}{Q_2})^{-1} \qquad (5)$$

Q_1/Q_2 is the known ratio of the ionisation cross sections of H_1 and H_2. This method of expressing the fractional dissociation of a hydrogen beam in terms of ion signals according to (5) has been used previously (i.e. Fite Wade L. and Brackmann R.T. 1958, Kauppila W.E. et al 1970).

Since the beam profile of a long channel source varies with the source temperature as described in chapter 3.3, another method of describing the beam is to define a fractional beam composition D* as the ratio of the particle number n_1 of species 1 to the total number of particles in the ion formation region of the mass spectrometer:

$$D* = \frac{n_1}{n_1 + n_2}$$

This leads to the following expression:

$$D*(T) = (1 + \frac{\sqrt{2}}{2} \cdot \frac{S_2}{S_1} \cdot \frac{Q_1}{Q_2})^{-1} \tag{6}$$

Equation (6) gives a better description of the beam composition available for scattering experiments, provided the beam is investigated at the actual scattering centre of the experiments. Both considerations (5) and (6) neglect contributions arising from dissociative ionisation of H_2 in the mass spectrometer. This process is very small (Massey H.S.W. and Burhop E.H.S. 1969) and certainly inside the uncertainty of this beam investigation.

A thorough investigation of the hydrogen beam was carried out before it was used in experiments. This presented the problem of measuring the H_1 and H_2 components of the beam against a background which mainly consisted of molecular hydrogen. A series of tests was carried out using a modulated beam. For this

purpose the electron spectrometer was removed from the gun table which remained in the system, since it carried the chopper facility and the final beam aperture. A commercial quadrupole mass spectrometer, Balzers QM 101, equipped with a cross beam electron gun was substituted for the electron spectrometer. The arrangement is shown in fig.11. This was done to measure the beam composition at the actual interaction region of the later hydrogen experiments. The cross beam ionizer used was suitable for the analysis of a beam. A mechanical chopper, which will be described in more detail in the following chapter, interrupted the hydrogen beam with a frequency of 62 Hz. This chopper was positioned inside the scattering tank in order to prevent modulated background hydrogen from reaching the scattering tank by simple diffusion from the source chamber. A photocell (later on a photomultiplier), observing the hydrogen furnace through the scattering region and chopper wheel, supplied a reference signal for the chopper frequency and phase. A lock-in phase sensitive detector PAR type HR8 was used to analyse the mass spectrometer signals. Repetitive sweeps of the mass range 1 and 2 supplied signals proportional to the actual partial densities of H_1 and H_2 in the beam, according to (2). Typical signal traces are shown in fig.12. Since the electron energy in the ionizer is fixed at 95eV, the signals observed have to be corrected for their respective ionisation cross sections, the ratio being taken to be $Q_1/Q_2 = 0.67$ (Fite Wade L. and Brackmann R.T. 1958).

The source temperature was measured by means cf an optical pyrometer which looked along the beam axis through a viewing point in the scattering tank. Source chamber pressure as well as the pressure in the scattering tank were monitored

Figure 11:

This schematic diagram shows the quadrupole
mass spectrometer in position for measurements
of the hydrogen beam composition in a modulated
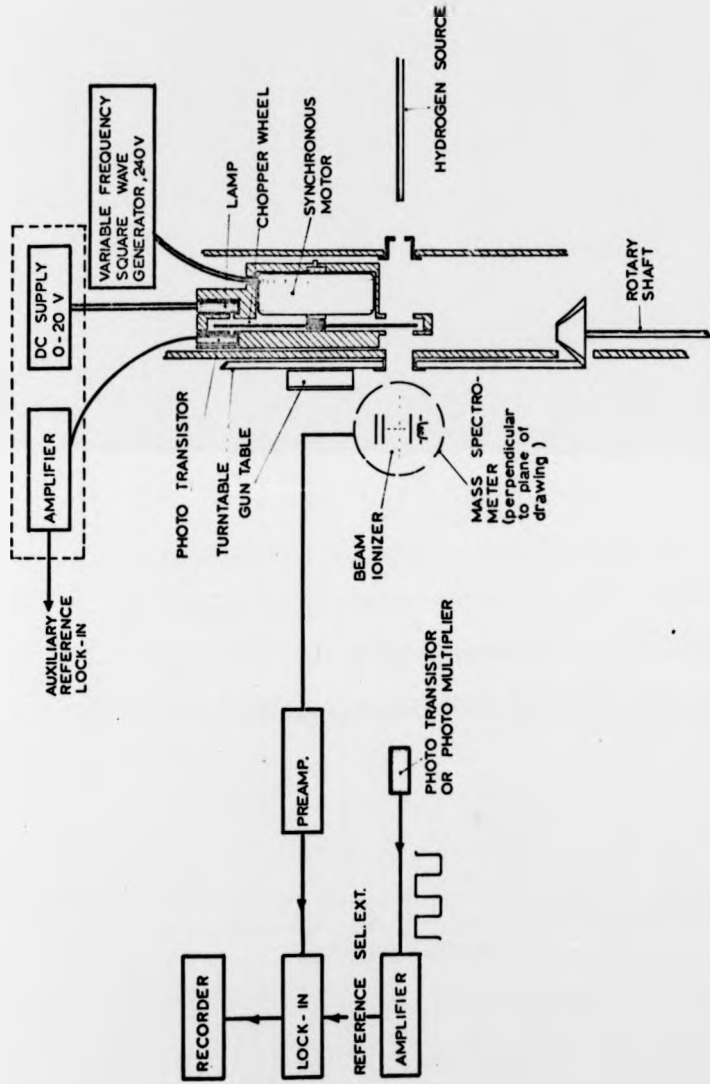beam experiment.
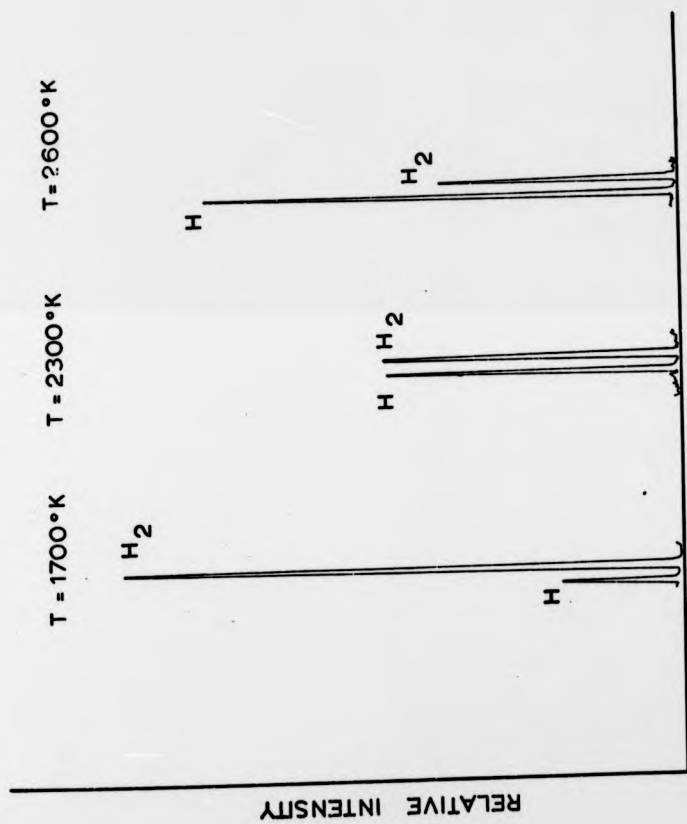
ble

ements

dulated

Figure 12:

Relative intensities of atomic and molecular
hydrogen.   The recorder traces were taken at
different source temperatures as indicated.
The source chamber pressure was $7 \cdot 10^{-5}$ torr.

olecular

taken at

icated.

$^{-5}$ torr.

T = 1700°K   T = 2300°K   T = 2600°K

H_2 H_2 H

H H_2

H

RELATIVE INTENSITY

using ionisation gauges. The peak heights of signals S_1 and S_2 were used to work out the beam composition.

Typical values of the fractional dissociation of the beam are shown in fig.13. An extended series of dissociation measurements was carried out, at different source pressures and with new tungsten tubes and heaters, until a reliable reproducible set of the beam values was found. Then the mass spectrometer was removed from its position and kept at a different position in the beam for occasional monitoring purposes. At pressures of $7 \cdot 10^{-5}$ torr in the source chamber, the beam contained more than 80% atomic hydrogen at source temperatures of $2500^{\circ}K$.

The same arrangement can be used, to inject mixed gas beams as for example in rare gas experiments, although this possibility has not been used so far. The beam composition could again be worked out.

3.5 Target beam modulation

One of the main problems in electron-atomic hydrogen scattering is the recombination of atomic hydrogen into molecules, producing a background of molecular hydrogen. Scattering signals therefore contain a component due to electron scattering from molecular hydrogen. An additional signal component, especially in the elastic scattering mode, is caused by scattering of electrons from metal surfaces. This contribution to the elastic scattering signal can be significant.

To overcome problems of that kind the target beam is modulated. It is periodically interrupted by means of a rotating wheel with ten blades. This wheel, which is

Figure 13:

Composition of the hydrogen target beam as
measured in a modulated beam experiment,
using a commercial quadrupole mass-spectrometer.
These measurements were repeated to establish
that the performance of the hydrogen beam source
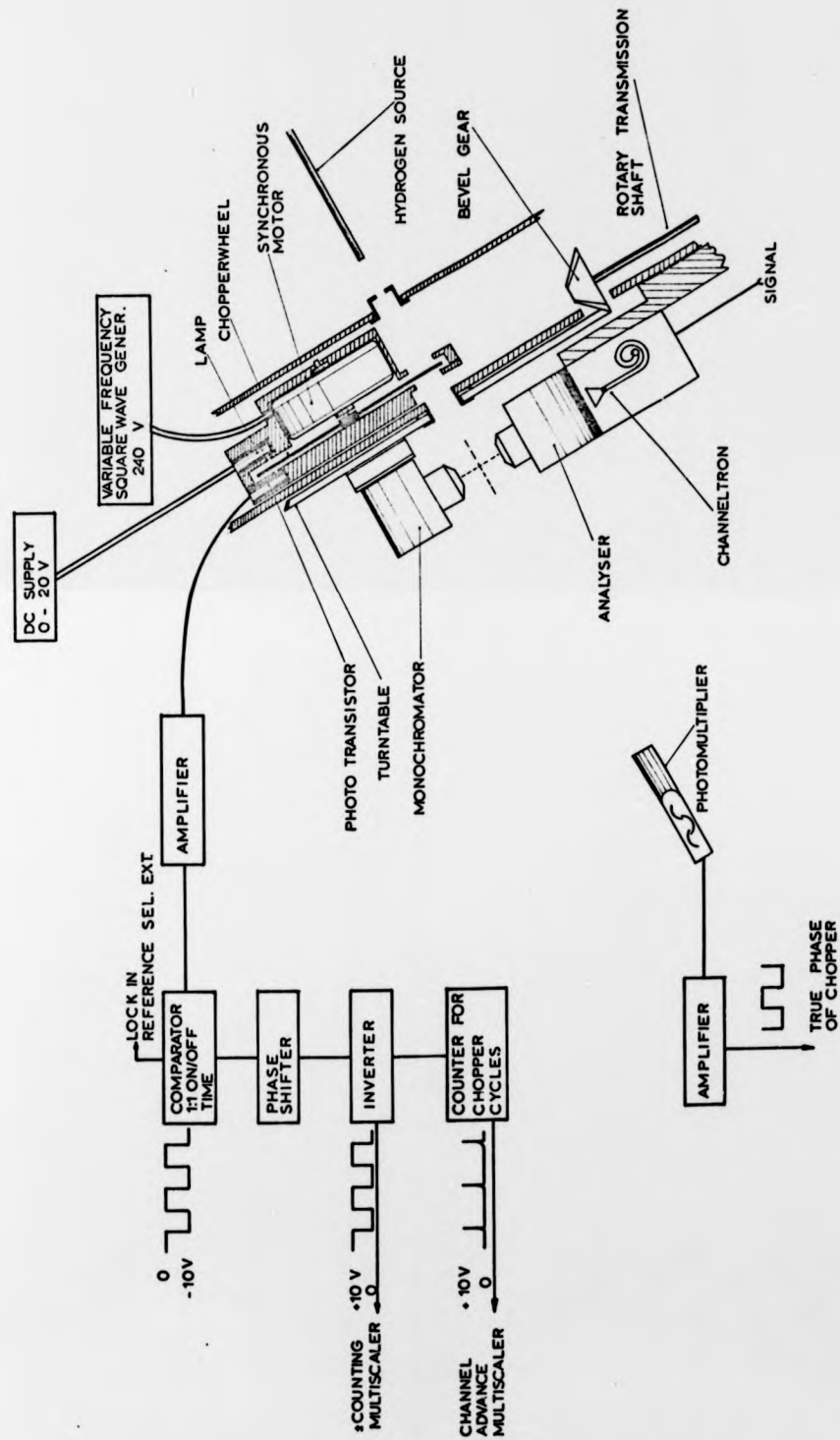was reproducible.
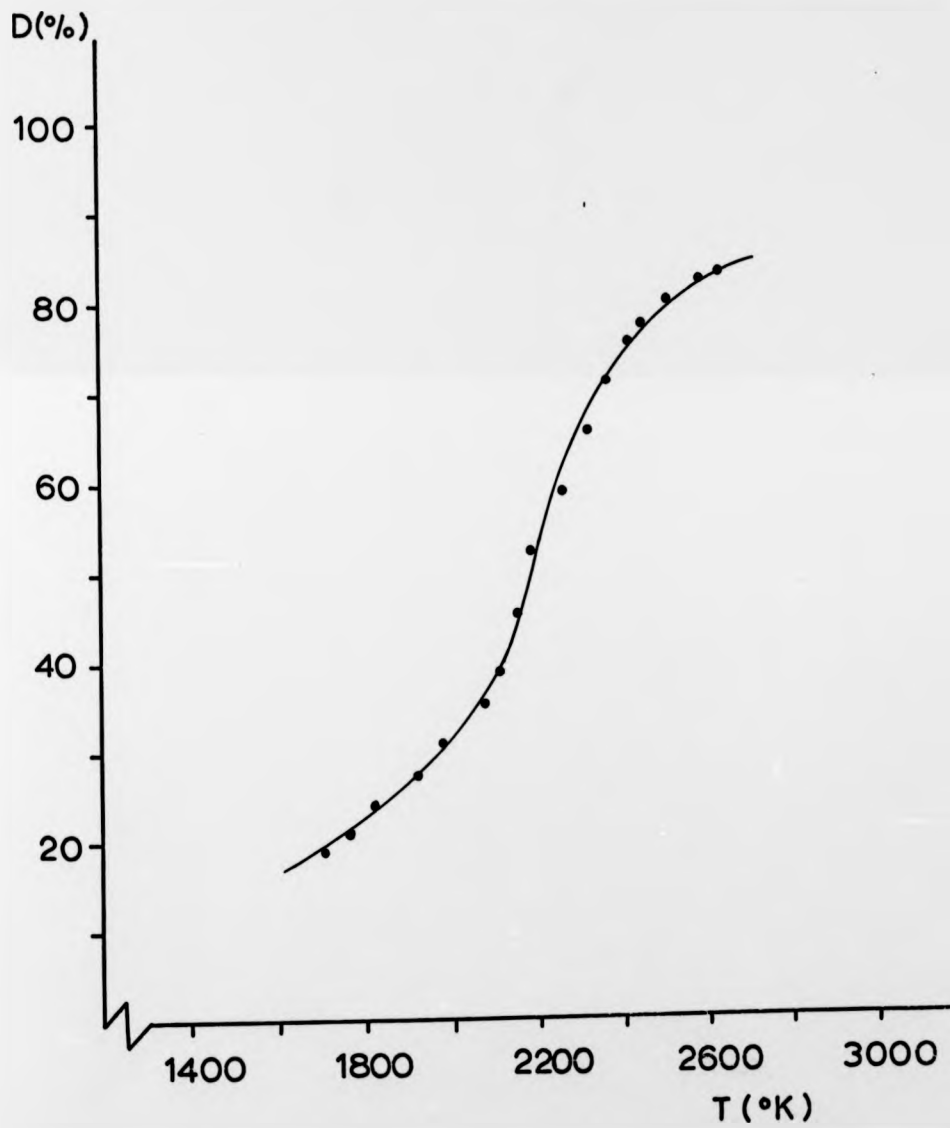
beam as

ment,

spectrometer.

establish

n beam source

made from duraluminium, is driven by a synchronous
motor (AEG) which is powered by a variable frequency
square wave oscillator capable of supplying 240V.
This mechanical chopper arrangement is an integral part
of the gun table and is therefore inside the scattering
tank.   The assembly is shown in fig.14 with the electron
spectrometer mounted on the gun table.   This position of
the beam chopper was chosen to make sure that the actual
target-beam which reaches the interaction centre is modulated,
whereas the background gas is unmodulated.   Background
modulation would take place if the chopper was located in
the sourcechamber or even in an intermediate chamber.   One
further advantage of this chopper arrangement is, that during
the off period the background gas pressure is not influenced,
since the beam is only dispersed during that time and the
total gas load in the chamber remains constant.   The physical
layout of the modulation part of the apparatus including a
schematic description of the electronics is shown in fig.14.

The correct chopper frequency is observed by
interrupting a light beam which is monitored by means of a
phototransistor.   The light source is a normal 6.3V miniature
light bulb.   Power to the lamp comes from a d.c. power supply.
Both lamp and transistor have been stripped of insulation
in order to prevent vacuum problems arising from outgassing.
The modulation signal derived in this way is then amplified
and adjusted to a 1:1 mark to space ratio by means of a time
comparator.   To ensure that the target modulation is in phase
with this modulation detector circuit, the light from the
hydrogen dissociator oven is monitored by means of a photo-
multiplier.   By comparing the two signals, phase discrepancies

Figure 14:

Beam modulation system. The electron
spectrometer is shown in its final position.
Parts of the rotary drive of the turntable
are shown, as well as a section through the
integrated gun table-chopper assembly.
Electronic circuits used to derive the
modulation signals are shown schematically.

VARIABLE FREQUENCY SQUARE WAVE GENER. 240 V

DC SUPPLY 0 - 20 V

LAMP

CHOPPERWHEEL

SYNCHRONOUS MOTOR

HYDROGEN SOURCE

BEVEL GEAR

ROTARY TRANSMISSION SHAFT

SIGNAL

PHOTO TRANSISTOR

TURNTABLE

MONOCHROMATOR

ANALYSER

CHANNELTRON

AMPLIFIER

LOCK IN REFERENCE SEL. EXT

COMPARATOR 1:1 ON/OFF TIME

PHASE SHIFTER

INVERTER

COUNTER FOR CHOPPER CYCLES

0

-10V

+10 V

0

CHANNEL ADVANCE MULTISCALER

+10V

0

COUNTING MULTISCALER

PHOTOMULTIPLIER

AMPLIFIER

TRUE PHASE OF CHOPPER

ition.

able

h the

ally.

can be adjusted with a phase shifter.

The modulation signal is then converted to a
square wave with positive polarity for switching the external
± counting input of a multiscaler. After completion of every
beam on-off-cycle a + 10V pulse is derived to advance the
channel of the multiscaler. These pulses can be accumulated
to advance the storage channels after 1,2,4,8 or 16 complete
on-off cycles of the chopper. Since the channel advance is
related to the electron beam energy, the modulation also
controls the electron beam energy. This will be described
in more detail later on.

The detection of the oven light with a photo-
multiplier also monitors the oven temperature and indicates
temperature fluctuations. This facility might prove to be
very valuable for future experiments. In the case of hydrogen
dissociation measurements, the phase adjustments were made with
a phase shifter incorporated in the lock-in detector, while for
modulated counting an additional phase shifter was used.

4. The electron gun

In this chapter the design and operation of
the electron spectrometer is discussed. Its characteristics,
including energy distribution and energy calibration will also
be considered.

4.1 Introduction

The energy properties of an electron beam can
be described by the most probable energy E and the energy spread
around this mean energy. The energy spread ΔE can be defined as
the energy between the half-maxima of the electron beam current

distribution. Conventional types of electron sources do
not produce electron beams having uniform energy. Furthermore
the mean energy of electrons in the beam usually differs from
the applied accelerating voltages. The main contribution to
the energy distribution of electrons is given by the thermal
energy of electrons emitted from a thermionic cathode. The
current distribution of such an emitter can be described by
the Maxwell distribution

$$\frac{I(E)}{I}dE = \frac{E}{kT} \cdot e^{-E/kT} \cdot d(\frac{E}{kT})$$

normalized to the total current I. This leads to an energy-
spread

$$\Delta E \cong 2.5 \ kT.$$

One therefore expects energy spreads of between 0.2eV to
0.6eV according to the type of cathode used. The energy
at high current densities in the electron beam broadens
owing to space charge effects and the distribution function
is no longer Maxwellian. Differences between applied
voltages and actual energies can be of the order of several
volts and are a result of cathode surface conditions plus
contact potentials arising from surface conditions in the
electron gun.

Since this apparatus described here was to be
used to investigate structures with an energy width of 0.1eV
or less, one requires an electron beam with an energy spread
of the same order. Devices for reducing the thermal energy
spread of electron beams are reasonably well known. A
description of such electron monochromators can be found in
a number of articles (i.e. Simpson J.A. 1967).

In atomic beam experiments, especially in the case of atomic hydrogen scattering experiments, where the target beam source is distant from the interaction region, it seems to be advantageous to use a ribbon-type electron beam. This should make better use of the already divergent target beam. The 127° electrostatic electron monochromator was therefore considered to be the most suitable electron source for this apparatus.

4.2   The 127° electron monochromator

This device was suggested by Hughes and Rojanski (1929), who worked out the focussing and energy selection properties of an inverse first power electrostatic field. The first selector was built by Hughes and McMillen (1929), but had a rather poor resolution owing to the use of sheet metal for the cylindrical electrodes. This original design has been improved meantime (Marmet P. et al 1961) and gives good energy resolution with reasonable current throughputs.

The electric field between two concentric cylinders of radii r_1 and r_2 ($r_1 < r_2$) and which are at potentials V_1 and V_2 respectively is given by (see fig.15)

$$E(r) = \frac{1}{r} \cdot \frac{V_2 - V_1}{\ln r_1/r_2} \qquad (1)$$

Electrons injected into that field only remain on a centre trajectory $R = 1/2 (r_1 + r_2)$ if
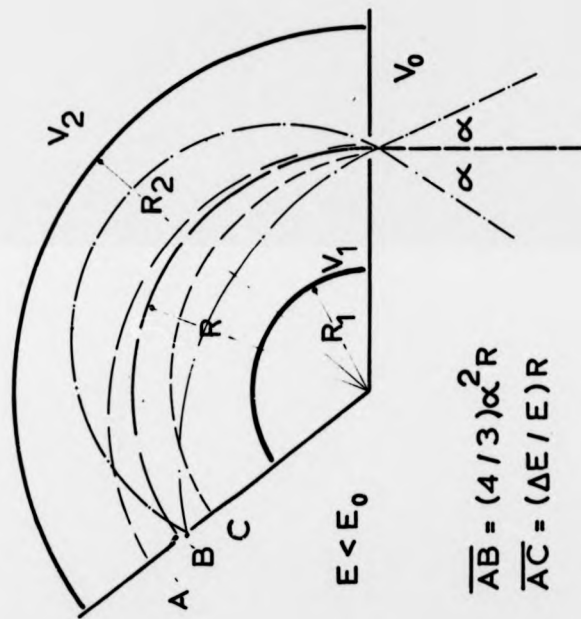
$$\frac{m_e \cdot v^2}{R} = E(R) \cdot e$$

and their kinetic energy will be

$$E_{kin} = 2^{-1} e \cdot \frac{V_2 - V_1}{\ln r_1/r_2} \qquad (2)$$

Figure 15:

Schematic description of the 127° selector
field showing the centre trajectory as well
as a typical trajectory for electrons with
$E < E_o$.

$$R = \frac{R_1 + R_2}{2}$$

$E < E_0$

$$\overline{AB} = (4/3)\alpha^2 R$$

$$\overline{AC} = (\Delta E/E)R$$

This is one of the operating conditions of the system.
It is found that a beam entering the cylindrical field
through a slit and having a small beam divergence α with
respect to the slit normal, is focussed at an angle of
$\pi/\sqrt{2} = 127^{\circ}17'$. This can be seen by solving the equation
of motion of an electron in this field which, in cylindrical
polar coordinates, is given by

$$m(\ddot{r} - r\dot{\theta}^2) = \frac{e}{r} \frac{V_2 - V_1}{\ln r_1/r_2} \tag{3}$$

This differential equation can be solved in first order
approximation for the case of the entrance slit positioned
on the mean trajectory, and for small angular divergence of
the electron beam. In a recent calculation (Delage Y. and
Carette J.D. 1971) the assumption of small α was dropped
and this leads to an energy resolution

$$\frac{\Delta E}{E} = \frac{\Delta R}{R} + \frac{4}{3}\alpha^2 + \beta^2 + \ldots \tag{4}$$

ΔE is the full energy width at the half maximum of the
distribution curve, E is the mean energy of the electrons
entering the monochromator. ΔR is the width of two identical
slits positioned at either end of the 127° field on the mean
radius R. α is the aperture angle of the electron beam. The
expression (4) suggests operation of the monochromator at as
low energies as possible and small values of ΔR. However the
influence of α will increasingly dominate the energy resolution
of the device. In order to reduce α, the electron beam should
be formed in a conventional electron gun before injecting it

into the selector. Another adverse effect on the resolution
of this type of monochromator is caused by the length of
the slits. This introduces a beam divergence β perpendicular
to the plane of selection. The effect can be lowered by a
pre-selector injection system.

The reason the first 127° selector (Hughes A.L.
and McMillen J.H. 1929) did not succeed was the neglect of
space charge in the selector. The space charge is built up
by electrons which are not transmitted because they have an
unsuitable energy, as well as by the main electron beam.
The maximum current one can put through a 127° monochromator
is given by (Simpson J.A. 1968)

$$I_{max} = 38.5.E^{3/2}(\frac{\sqrt{2}}{\pi} \cdot \frac{\Delta R}{R})^2 \ \mu A \qquad (5)$$

The space charge problem was solved by Marmet and Kerwin.
They replaced the sheet metal cylindrical plates by high
transparency grids. Behind these grids are collector plates.
The effect of this modification is, that electrons not
transmitted through the device owing to having an unsuitable
energy or too large a beam divergence, leave the selector
field and are collected by the outer collector plates.
This counteracts the build up of a high space charge and
leads to a higher current throughput. Furthermore it
reduces the possibility that the undesired electrons could
pass through the exit slit after metal reflections, thus
decreasing the energy resolution.

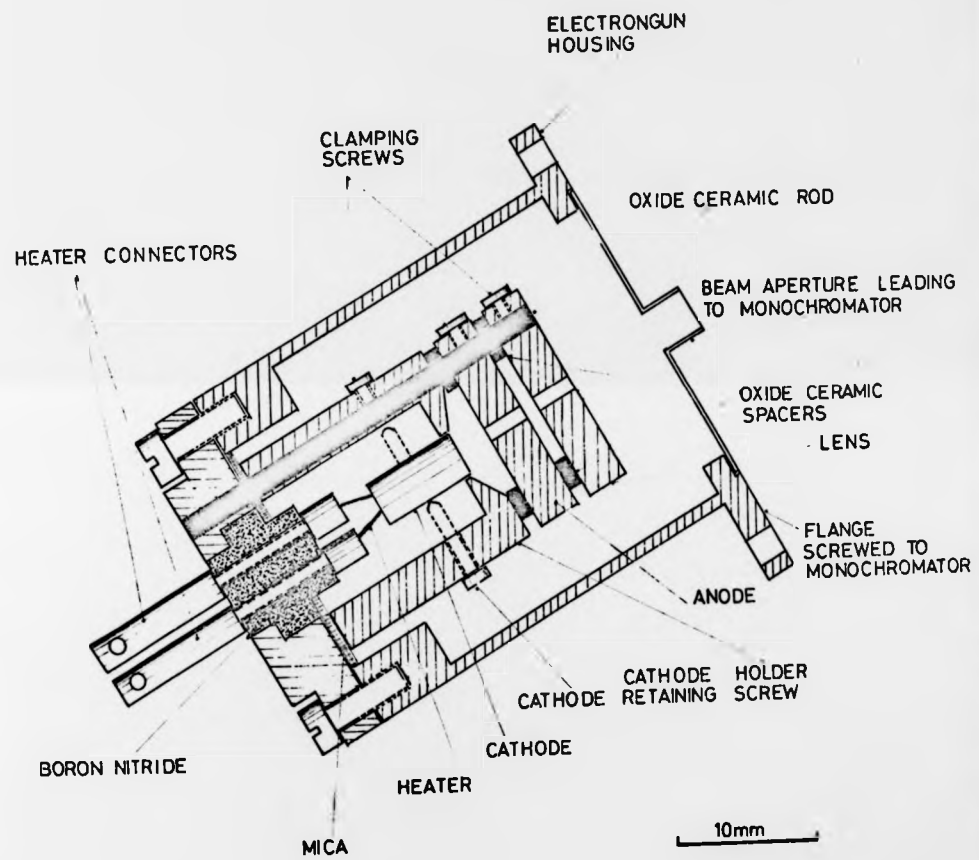4.3 Mechanical design of the monochromator system

The electron monochromator used in the present apparatus was designed to achieve a resolution of the order of 0.1eV and give a well-collimated beam. The system consists of three parts, an electron gun, the 127° selector field and a lens system to accelerate, align and focus the beam emerging from the selector.

4.3.1 Electron gun

A three-electrode system was used as electron gun-cathode, anode and a final thick lens which could alternatively be used as a deflector. This facility allowed the beam to be aligned with respect to the entrance of the selector. The cathode used was a dispenser type cathode BP1A supplied by Philips. It was mounted by means of three pointed screws in the centre of a Pierce-type cathode holder. All the electrodes were mounted on three oxide ceramic rods 1.5 mm Ø and separated by means of oxide ceramic washers. The aligned system was then mounted on a small flange and inserted into a metal tube. The assembly is shown in fig.16. The metal housing used for the electron gun is necessary to prevent stray electrons from leaving this injector system. One difficulty arising here is the trapped volume inside the injector assembly. To enable a reasonable evacuation of this tube, the injector assembly ends in a baffle which leads right up to the entrance slit of the monochromator.

Figure 16:

A standard electron gun is used as injector
into the selector field to reduce the beam
divergence. The third electrode can
alternatively be used as a split electrode
to align the beam.

ELECTRONGUN HOUSING

CLAMPING SCREWS

HEATER CONNECTORS

OXIDE CERAMIC ROD

BEAM APERTURE LEADING TO MONOCHROMATOR

OXIDE CERAMIC SPACERS

LENS

FLANGE SCREWED TO MONOCHROMATOR

ANODE

CATHODE HOLDER RETAINING SCREW

CATHODE

HEATER

BORON NITRIDE

MICA

10mm

4.3.2   The monochromator section

The 127° monochromator section was a modified
version of Marmet and Kerwin's design.   The dimensions of
the system are

$r_{outer\ grid}$ = 18.00 mm ; $r_{inner\ grid}$ = 12.00 mm

$r_{outer\ plate}$ = 22.00 mm ; $r_{inner\ plate}$ = 8.00 mm

mean radius   R = 15.00 mm;   height of slits = 5.0 mm
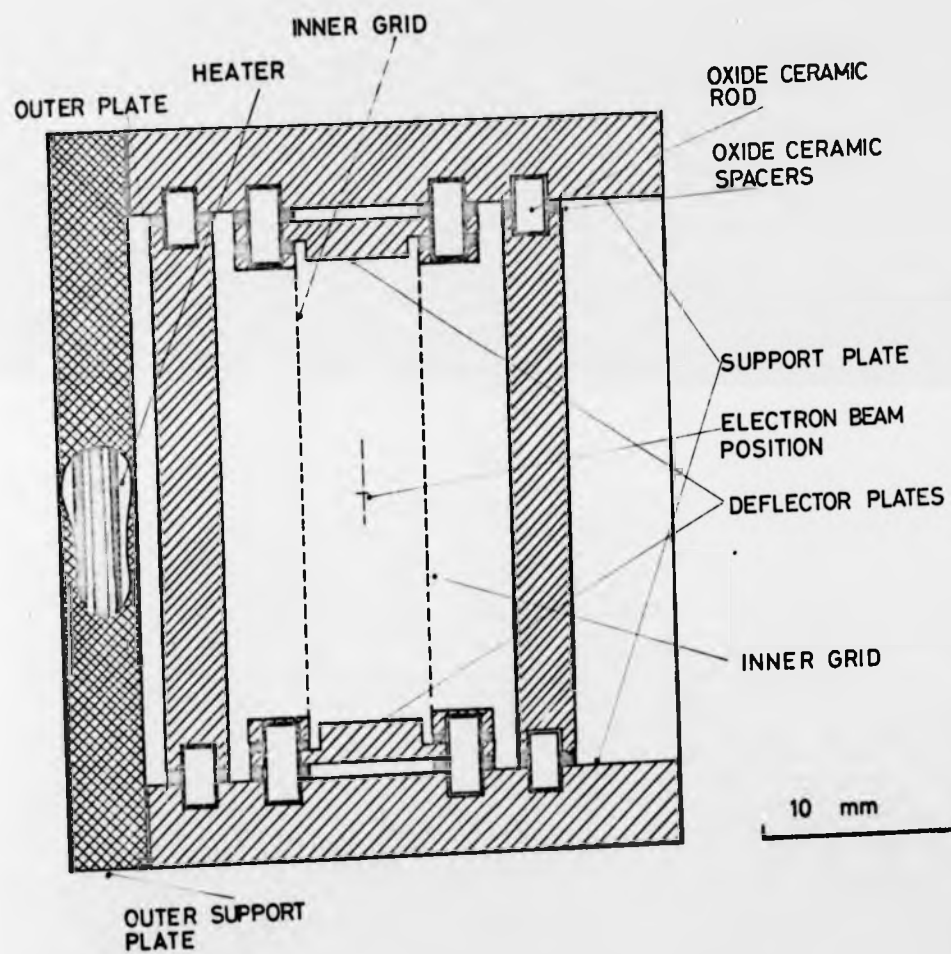
The width of the slits ΔR could be varied.

The grids had a transparency of 87% and were made from
tungsten mesh.   The mesh was woven from 0.018 mm Ø tungsten
wire.   The mesh size was 0.245 mm.   The grids were spot welded
onto frames.   All electrodes were mounted onto 120° segments
using 1.5 mm Ø oxide ceramic rods.   The correct spacing
between electrodes was achieved using oxide ceramic washers
which slipped over the mounting rods.   This arrangement is
shown in fig.17.   This sandwich arrangement was then held
together by an outside shield which was built as a heater so
that the system could be baked at temperatures up to 200°C.
The entrance and exit slits of the 120° field section were
screwed onto frames which were mounted on brackets using
oxide ceramic supports and spacers.   These brackets were
screwed to the 120° field section.   Electrical connections
to individual electrodes were made to pins which protruded
from the top of the monochromator.

Two identical monochromators were built, one
made from Immacculate V stainless steel and the second, which
was gold plated, from oxygen-free copper.   There were no
differences in performance.   All slits used in the system

Figure 17:

Vertical section through the 127° selector, showing the insulation of individual electrodes. The heater section used to bake this part of the system is cut open to show the oxide ceramic capillaries used to take the heater wire. One of these is used for a thermocouple. All insulators are hidden from the electron beam by the metal electrodes.

OUTER PLATE · HEATER · INNER GRID · OXIDE CERAMIC ROD · OXIDE CERAMIC SPACERS · SUPPORT PLATE · ELECTRON BEAM POSITION · DEFLECTOR PLATES · INNER GRID · 10 mm · OUTER SUPPORT PLATE

were made of molybdenum and spark-eroded to a knife-edge finish in order to minimize electron scattering from the edges. The complete monochromator is shown in fig.18.

4.3.3 Output lens system

The electron beam emerging the monochromator section was focussed and aligned by two thick lenses L_1 and L_2, a method first used by Andrick and Ehrhardt (1966). L_1 is a split lens, which could be used as a deflector to align the beam. In addition to the deflecting voltage the lens potential was adjusted to focus the beam. L_2 was also used to focus the beam. These two thick lenses were located in a nozzle-type housing, held in position and aligned by insulated screws as shown in fig.19. The insulating material used was either boron nitride or oxide ceramic. The electron beam emerged from the nozzle through a rectangular aperture 1.5 mm wide. There were provisions for a second aperture behind the main exit aperture.

Using this lens system, the transmitted current was a smooth function of energy. The voltages necessary to handle the beam varied according to the energy range. Typical voltages for one particular case will be given later.

4.3.4 Main beam collector

The electron beam leaving the monochromator passed through the target beam and primary electrons not undergoing scattering processes were collected. The collector allowed the intensity of the primary beam to be monitored. A 2mm Ø copper wire inside a copper tube acted as collector.

Figure 18:

Electron beam source, horizontal section,
showing the electron gun, monochromator section
and thick lenses L_1 and L_2. L_1 is a split lens
and acts as deflector. P_o and P_i are the outer
and inner collector plates. G_o and G_i are the
selector field electrodes made from high
transparency grids. H is the heater element
used to bake this part of the system.

63.

ection

lens

outer

the

ent

OUTER COLLECTOR PLATE P_o

OUTER GRID G_o

INNER GRID G_i

SPLIT LENS L_1

LENS L_2

MONOCHROMATOR
HEATER SECTION

SLIT

INNER COLLECTOR
PLATE P_i
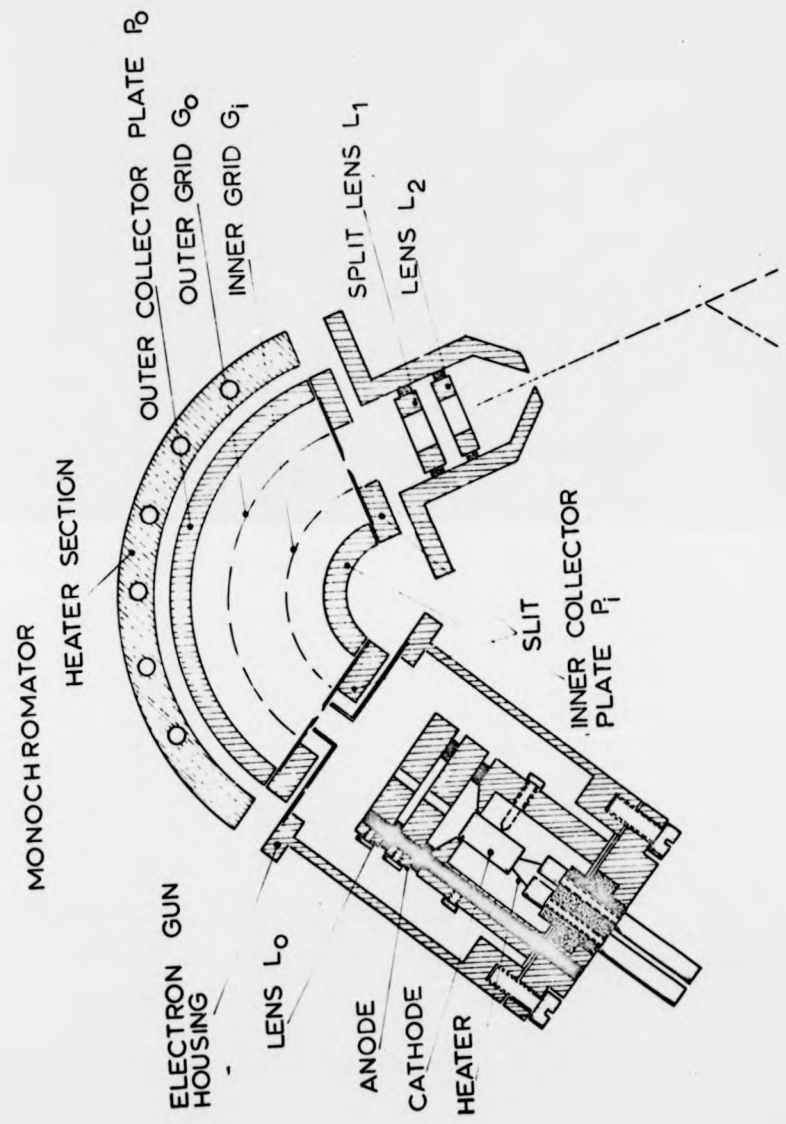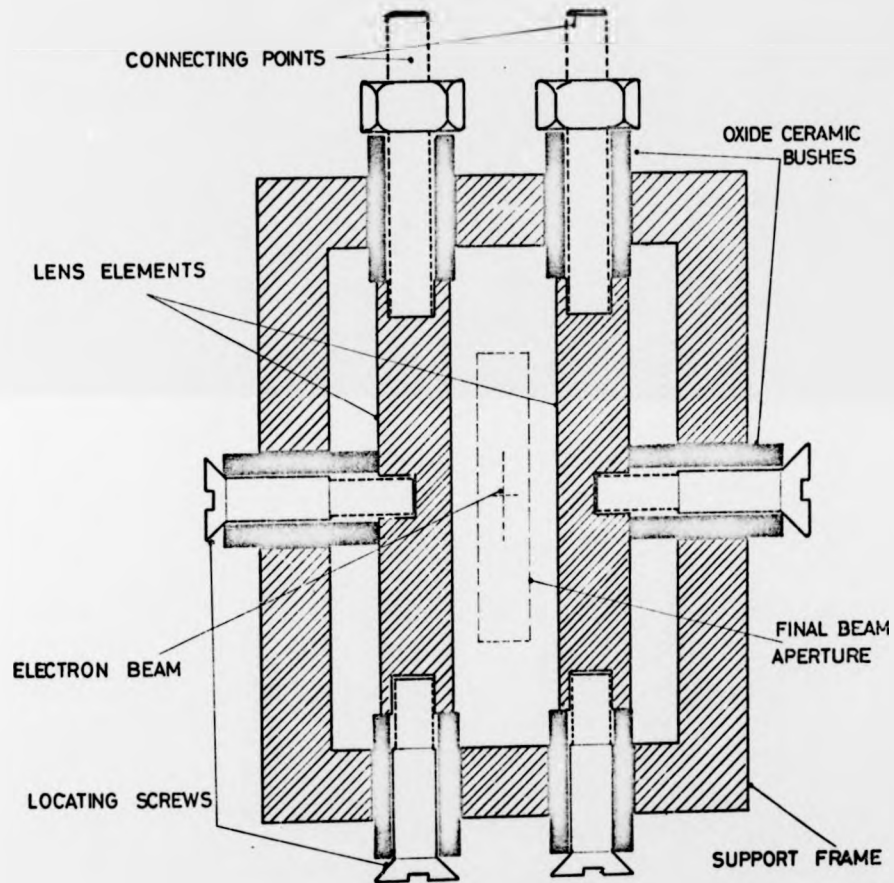
ELECTRON GUN
HOUSING

LENS L_o

ANODE

CATHODE

HEATER

Figure 19:

A vertical section through the split lens L_1,
showing how it is assembled and the method
of insulation from the housing which is kept
at earth potential.

ns L₁,

hod

kept

CONNECTING POINTS

OXIDE CERAMIC BUSHES

LENS ELEMENTS

ELECTRON BEAM

FINAL BEAM APERTURE

LOCATING SCREWS

SUPPORT FRAME

10 mm

Electrons reached the collector through a slit aperture.
The collector was permanently attached to the monochromator
by means of a metal bar, to ensure its proper location when
the scattering angle was being altered. The efficiency of
this main beam collector was poor. A more sophisticated
collector could not be accommodated owing to space limitations.

4.4   Analyser or scattered beam collector

A 127° system identical to the monochromator
was used to energy analyse electrons scattered from the
atomic beam. These electrons entered the analysing system
through a slit aperture 1.5 mm wide and were decellerated
and focussed onto the entrance slit of the analyser by
means of two thick lenses L_4 and L_3. L_3 again was a split
lens which enabled the electron beam to be deflected and
hence aligned. Electrons transmitted through the analyser
were detected by a channeltron electron multiplier.
Figure 20 shows the analyser section of the electron
beam system.

This arrangement of monochromator and analyser
permitted measurements of electron energy distributions in
both primary and scattered electron beams. Since the
analyser was tunable to transmit only electrons with a
defined energy, the device could be used for elastic
scattering experiments as well as for energy loss spectra.

4.5   The electron spectrometer assembly

All parts of the electron beam system described
so far are shown assembled in fig.21, which is drawn to scale.
The components are mounted on a gun table made from

Figure 20:

A horizontal section through the analyser.
P_i and P_o are the inner and outer collector
plates. G_i and G_o are the selector field
electrodes. L_3 is a split lens to align the
scattered electrons relative to the entrance
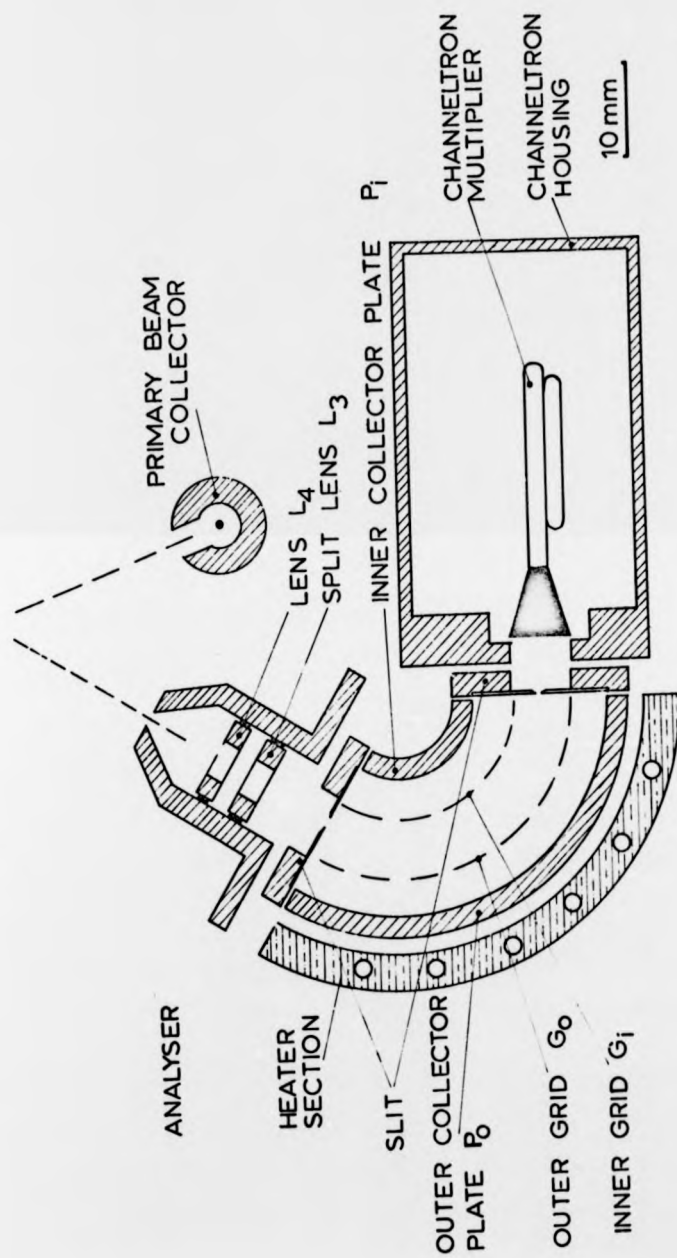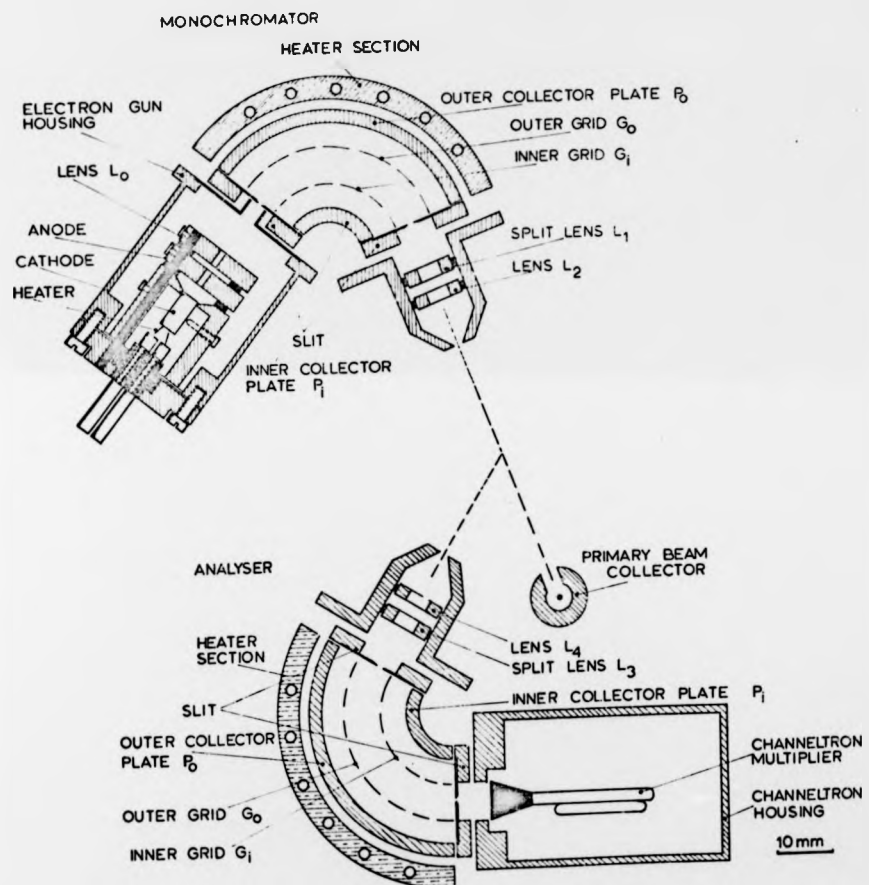slit of the analyser.

PRIMARY BEAM
COLLECTOR

LENS L_4
SPLIT LENS L_3

INNER COLLECTOR PLATE P_i

CHANNELTRON
MULTIPLIER

CHANNELTRON
HOUSING

10 mm

ANALYSER

HEATER
SECTION

SLIT

OUTER COLLECTOR
PLATE P_0

OUTER GRID G_0

INNER GRID G_i

Figure 21:

Electron spectrometer assembly, horizontal
section.   The target beam emerges perpendicular
to the plane of drawing.

ntal

endicular

MONOCHROMATOR

HEATER SECTION

ELECTRON GUN
HOUSING

OUTER COLLECTOR PLATE P_o

OUTER GRID G_o

INNER GRID G_i

LENS L_o

ANODE

CATHODE

HEATER

SPLIT LENS L_1

LENS L_2

SLIT

INNER COLLECTOR
PLATE P_i

ANALYSER

PRIMARY BEAM
COLLECTOR

HEATER
SECTION

LENS L_4

SPLIT LENS L_3

SLIT

INNER COLLECTOR PLATE P_i

OUTER COLLECTOR
PLATE P_o

CHANNELTRON
MULTIPLIER

CHANNELTRON
HOUSING

OUTER GRID G_o

INNER GRID G_i

10 mm

Immaculate V stainless steel and supported by two stainless
steel rods. These rods are screwed into the NW200 flange
(see fig.5) which accommodates all the feedthroughs
necessary for the electrical supply of the electron beam
system. The flange also supports a universal rotary drive.
A cross section through the gun table has already been shown
in fig.14, which also shows the electron beam system in
position.

The monochromator section is fixed to a double
T-shaped bench. This bench slides on a rail fixed to a
turntable which can rotate around the target beam. A bevelled
gearwheel of 100mm diameter is used as turntable and is rotated
by means of a precision universal rotary drive from outside the
vacuum system. The angular movement of the monochromator covers
the range $-90^{\circ} \leq \theta \leq 130^{\circ}$ with the analyser in position.

The analyser section is supported by a duraluminium
platform which is screwed to the gun table. This platform can
be moved in two directions perpendicular to one another to
permit alignment of the analyser with respect to the primary
electron beam direction and the atomic beam. Alignment of the
monochromator-analyser system is performed with a jig which can
be inserted into the final target-beam aperture which is at the
centre of the gun turntable.

The entire assembly can be moved perpencidular
to the target beam, since the gun table slides on its support
rods which move in PTFE bushes fitted to the gun table. This
alignment of the electron beam system relative to the target
beam can be performed from outside the vacuum chamber with the
same universal rotary drive which rotates the gun.

All connections to the electron spectrometer are made with copper wire covered in fibre glass sleeving. The leads are then screened and led to nine-pin feedthroughs which have been designed for this purpose.

4.5.1 Suppression of stray electrons

A serious problem in all experiments which monitor scattered electrons, either in the elastic or inelastic channels, is presented by electrons leaving the beam forming system before passing the final aperture. These electrons may reach the detector, thus creating a background signal. The most likely source contributing to this background is the electron gun itself. This stage of the electron beam system carries currents of up to 0.5mA. In order to reduce the escape of electrons from this stage, the electron gun is concealed in a tube as has already been mentioned in chapter 4.3.1. This arrangement has proved to be very effective.

The monochromator section is accommodated in a box which is pumped through the bottom and top support plates. The same design is used for the analyser. Electrons can only reach the detector if they pass through the exit slit of the analyser, since the channeltron multiplier is again in an earthed box leading right up to the exit slit. The number of electrons reaching the detector by completely by-passing the monochromator and analyser gives a background of the order of 10 counts per second.

A much more serious source of stray electrons is the small fraction of the primary electron beam which is not

completely suppressed by a collector. These electrons, especially in the elastic mode, reach the analyser after metal reflections and are transmitted, thus creating a significant contribution to the background signal. This was especially serious at the lower electron energies which were necessary in the case of elastic electron-hydrogen scattering. Some improvement has been achieved by coating all the metal components surrounding the target region with aquadag which in turn was covered with soot, but further improvements ought to be possible by modifying the primary beam collector. The electron count rate with the target beam switched off, is of the order of 100 counts per second in the elastic scattering mode, at a scattering angle of 90°. This count rate increases considerably for small angles.

4.6 Electrical supply of electron spectrometer

All voltages required to run the electron beam system are derived from individual power supplies. These d.c. power supplies were built by the electronic workshop to our specifications and have a high stability and low noise performance. The outputs are fully floating and screened. Fine adjustments are made possible by means of multi-turn helipots. A schematic diagram of the circuit used is shown in fig.22. The electrical supply lines to the electron spectrometer are fully screened.

Signal connections to the channeltron and primary beam collector are also fully screened. The same precaution applies to the high voltage supply to the channeltron detector.

All electrical supplies of the apparatus are earthed

Figure 22:

Schematic circuit of the electron spectrometer.
All potentials are relative to one reference
point in each monochromator and analyser. This
reference point is biassed relative to earth
potential to define the electron beam energy.

REFERENCE POTENTIAL ANALYSER

REFERENCE POTENTIAL MONOCHROMATOR
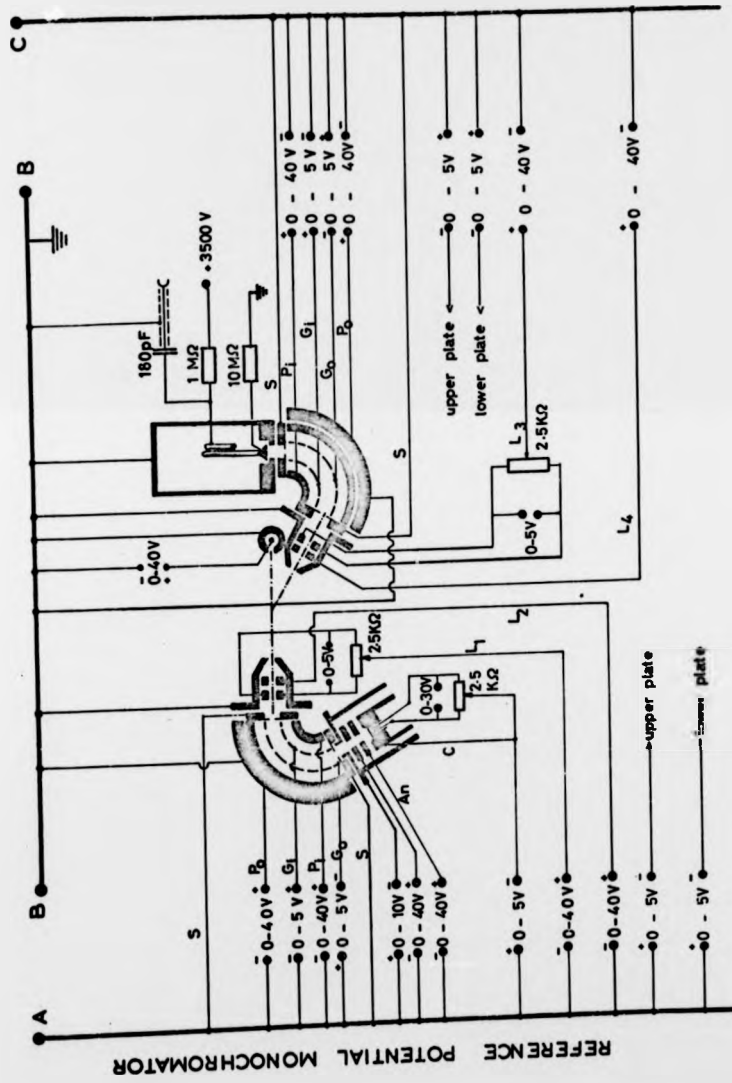
tromometer.

ference

er. This

earth

energy.

at one common point to prevent spurious signals due to earth loops. This central earth point is connected to a galvanic earth outside the laboratory.

If the spectrometer is to be used in the elastic channel, the scattering energy is determined by a staircase voltage relative to earth, derived from a multichannel analyser. This will be described in more detail in a later chapter. The same method is used for optical observations. In the energy loss mode, a fixed voltage applied to the monochromator relative to earth determines the incident energy in the primary beam, whereas the staircase voltage is used to scan the energy loss, i.e. the analyser.

4.7 Cancellation of magnetic and electric fields

In electron scattering experiments involving low energy electrons, stray magnetic or electric fields can disturb the electron beam considerably. The Lorentz force acting on the electrons simply deflects the electron beam. It is therefore necessary to suppress these fields.

The electric fields were minimized by keeping all outside parts of the electron beam system at earth potential as well as all the other components of the system which can be seen by the electron beam in the interaction region. All electrical supplies are fully screened and installed as far from the electron beam as possible. Insulators are shielded from the electron beam throughout the system in order to prevent electric fields, created by charging up of the insulators, from interfering with the electron beam.

Magnetic fields in the interaction region arise from various sources. Static magnetic fields result from the earth's field and from the residual magnetisation of steel components used in the system. Dynamic fields are caused by the a.c. supplies of the apparatus, by the motor powering the chopper wheel and, in the case of hydrogen experiments by the heavy a.c. current necessary to heat the oven.

The static magnetic field in the interaction region was reduced by a constant field of equal magnitude but of opposite direction. This field was obtained by surrounding the scattering tank with three mutually perpendicular pairs of Helmholtz coils. The scattering centre is the centre of all three sets of coils, which consisted of 50 turns of insulated copper wire wound on duraluminium formers. All Helmholtz coils were firmly attached to the scattering tank. The current for these coils was supplied by three independent constant current supplies. The static field was thereby reduced to less than 10 mGauss. A Hewlett Packard magnetic probe was used to check the field cancellation. For this purpose the system was opened and the probe positioned at the interaction centre.

Alternating magnetic fields created by the oven and chopper motor were reduced by extensive mu-metal shielding of the oven and of the chopper motor housing. The chopper motor was contained in a mild steel box to contain its magnetic field.

4.8 Performance of the electron spectrometer

The energy resolution of the electron spectrometer described was then tested and possible means of calibrating the energy scale were investigated. When studying resonance features

one must not only have an idea of the actual energy width
of the electron beam used, but it is also important to
position the features observed on an absolute energy scale.
Calibration should be made easy, for example by the observation
of some reproducible feature, since the energy scale might alter
owing to variations of contact potentials.

4.8.1 Energy distribution measurements

There are several methods one could use to
determine the energy distribution of an electron beam.
A retarding field in front of the primary beam collector
could be used, or one could observe a feature of known energy
width. However a monochromator-analyser arrangement offers
methods of observing energy distributions which are quicker
and easier to evaluate.

If V_o is the potential corresponding to a
circular trajectory of radius R through the monochromator,
the equation (2) chapter 4.2 can be rewritten as

$$V_o = \frac{V_2 - V_1}{2 \ln r_1/r_2} \qquad (1)$$

This offers the first method of observing the energy resolution
of a monochromator using an analyser. The monochromator is
tuned to transmit electrons with an energy equivalent to a
potential V_o. The analyser is then tuned to the same energy
and its potential difference $(V_2 - V_1)$ is scanned symmetrically
with respect to V_o. This method has been used in transmission
to display the energy distribution on an oscilloscope so that
coarse adjustments of the distribution curve could be made.

The method normally used is to scan the analyser against the monochromator which is set to transmit electrons having a certain energy. Assuming the transmission function $\sigma_m(E)$ of the monochromator is Gaussian with a width at half maximum of ΔE_m eV, where E_m is the mean energy transmitted by the monochromator, then

$$\sigma_m(E) = \frac{1}{\sqrt{2\pi\Delta E_m{}^2}} \cdot \exp\left(-\frac{(E-E_m)^2}{2\Delta E_m{}^2}\right) \tag{2}$$

A similar profile applies to the analyser

$$\sigma_a(E) = \frac{1}{\sqrt{2\pi\Delta E_a{}^2}} \cdot \exp\left(-\frac{(E-E_m)^2}{2\Delta E_a{}^2}\right) \tag{3}$$

If the analyser scans the monochromator profile the resultant observed profile is given by

$$\sigma_{tot} = \frac{1}{2\pi\Delta E_m\Delta E_a} \int_{-\infty}^{+\infty} \exp\left(-\frac{(E-E_m)^2}{2\Delta E_m{}^2}\right) \cdot \exp\left(-\frac{(E-E_a)^2}{2\Delta E_a{}^2}\right) dE \tag{4}$$

$$\sigma_{tot} = Const. \cdot \exp\left[-\frac{(E_m-E_a)^2}{2(\Delta E_a{}^2+\Delta E_m{}^2)}\right] \tag{5}$$

This is a Gaussian distribution with a half width

$$\Delta E_{tot} = (\Delta E_m{}^2 + \Delta E_a{}^2)^{\frac{1}{2}} \tag{6}$$

If both analyser and monochromator are identical then

$$\Delta E_m = \frac{\Delta E_{tot}}{\sqrt{2}} \tag{7}$$

Since the set up described here uses mechanically identical
selectors which operate with almost identical potentials,
this assumption should be good enough to obtain a reasonable
idea of the actual resolution of the monochromator. Using
the methods described, energy distribution curves as shown
in fig.23 are observed. The second method described,
scanning the analyser relative to the monochromator, has
been used for measurements in transmission as well as at
scattering angles other than 0° and was repeated frequently
to observe possible changes in the distribution. The best
resolution achieved with the present system was 50 meV with
currents of the order of 10^{-10} A. So far the system has
normally been run with resolutions of the order of 100 meV and
primary currents of around 3.10^{-8} A, depending on the energy
range. A set of typical figures for the system is given in
Table I.

4.8.2 Energy calibration

The energy of an electron beam should be given
by the potential difference between the cathode and the last
element of the electron gun. The channel address of a
multiscaler is used to derive this energy, as will be described
in chapter 5. The voltage reading of every tenth channel is
recorded using a digital voltmeter. This gives relative
energy values, but the absolute values can be considerably
different. The source of this discrepancy is the effective
potential difference between the target region and the nominal
energy zero and is caused by a combination of

TABLE I

Electrode	Monochromator		Analyser	
	Dimension mm	Voltage referred to slit	Dimension mm	Voltage referred to slit
ΔR (slit)	variable, but in experiments descr. 0.4 x 5.0	0.0	variable, but in experiments descr. 0.4 x 5.0	0.0
mean radius R	15.00		15.00	
r_{in} grid	12.00	+ 1.2	12.00	+ 1.17
r_{out} grid	18.00	- 0.5	18.00	- 0.26
r_{in} plate	8.00	+ 50	8.00	+ 40
r_{out} plate	22.00	+ 50	22.00	+ 40
top deflector	-	- 0.10	-	- 0.12
bottom deflector	-	- 0.10	-	- 0.12
cathode	-	- 2.5	-	-
anode	-	+ 55.2	-	-
lens	-	+ 17.7	-	-

Figure 23:

Energy distribution in the electron beam
scattered elastically through 34°.
Incident beam energy 19.00 eV.
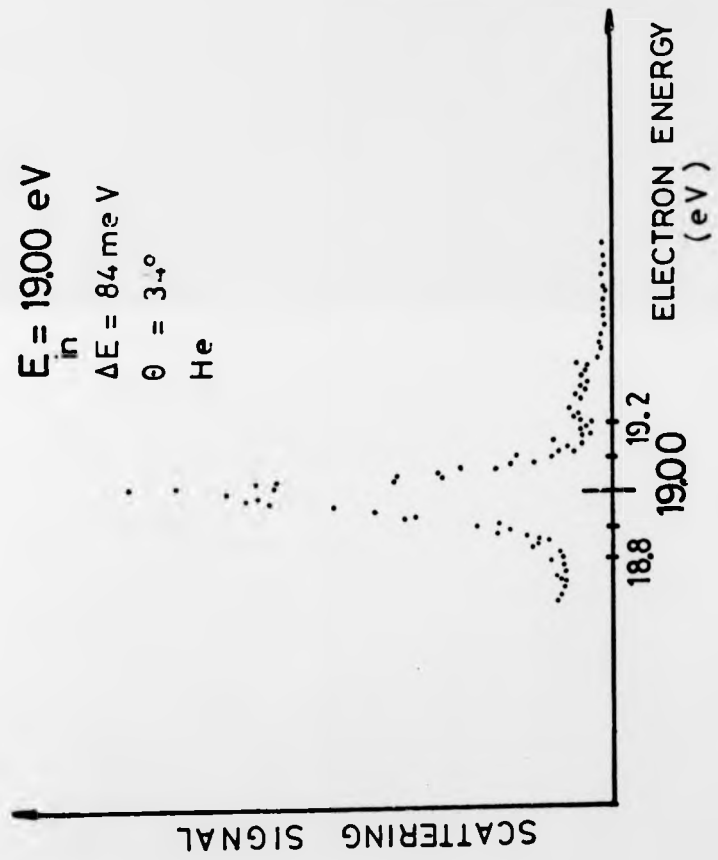
(a)   contact potentials, which depend on the
        surfaces involved, surface conditions, etc.
(b)   finite energy of electrons leaving the cathode
(c)   space charge effects

Introducing gases into the system can change
the contact potentials. Space charge effects can be
compensated for in those parts of the electron beam system
where the electron energy might exceed the ionisation
potential of the gas. These effects make it impossible
to determine the electron energy simply by measuring the
voltage between the cathode and the last element of the
electron beam source. A correction must be applied which
must be determined experimentally. Primary standards
normally used to calibrate energy scales are known ionisation
or excitation potentials. Well established resonances, which
have been calibrated against these primary standards can be
used as secondary calibration standards. This means that
the reliability of energy calibrations is limited by the
accuracy of a previous experiment. Two methods are available
in the present apparatus. Energy loss spectra of electrons
scattered from Helium give a calibration against the
spectroscopic levels of the He-atom. This possibility has
been used to check the position of the elastic He resonance.
The method generally used in all of the experiments was the
observation of the elastic He resonance at $19.35 \pm 0.008eV$
(Schulz G.J. 1973).
            The accuracy of the energy calibration is
limited by the precision with which the position of the
observed features can be positioned on the calibration curves.

Another limitation is imposed by energy drifts occurring in the time necessary to obtain calibration curves. Errors caused by the non-linearity of the ramp voltage used to scan the energy and by voltage measurements are negligible. It must however be emphasized that, since calibration was carried out with respect to a secondary standard, a recalibration of the standard could very well lead to better energy values for the features presented later on.

Having obtained an absolute energy scale there are two methods of transferring it to the energy region of interest. One is to observe the feature to be calibrated and the calibration signal in a mixture of calibrating gas and gas to be investigated. This method should be used if possible since the experimental conditions for observation of both calibration standard and feature to be calibrated are identical. The second method is to make successive runs using the different gases involved. Both methods have been described previously (i.e. Schulz G.J. (1964), Kuyatt C.E. (1965)).

5. Data collection system

As can be seen from fig.24, there are two detection channels available. Both can be used to detect scattered electrons and one can be used to detect uv-photons. The particle detector is, in either case, a channel-electron multiplier Mullard B312 BL. For photon observation one channeltron is positioned behind two high transparency grids S_1 and S_2, which can be used to suppress charged particles. The entrance cone of this detector is at earth potential and

Figure 24:

Geometry of the electron spectrometer showing
the photon detector in position. S_1 and S_2
are suppressor grids to keep charged particles
from entering the channeltron during uv-photon
observations. The electronics used is
indicated schematically.

owing

S_2
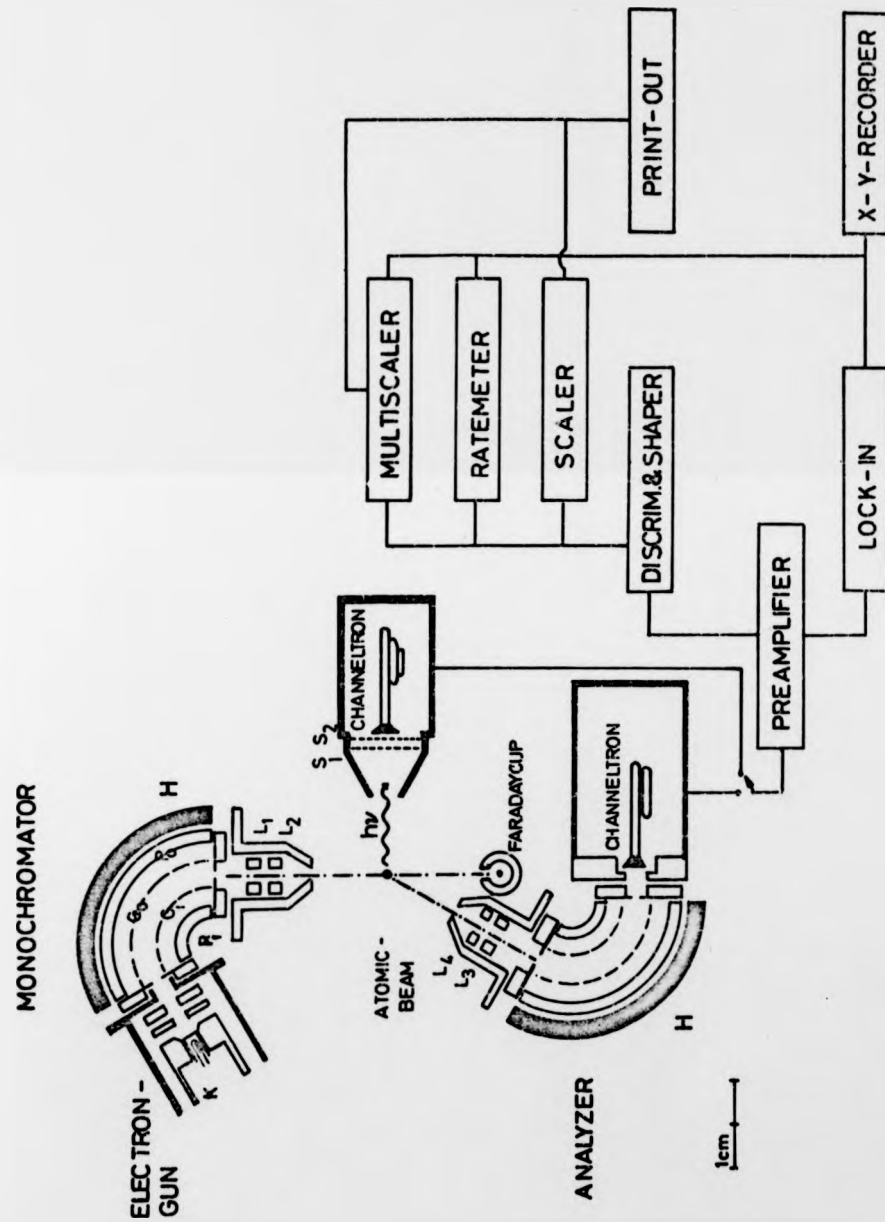
ticles

photon

the voltage across the channeltron is 3400V. A second
channeltron is positioned behind the analyser and is used
for electron detection only. The entrance cone of this
detector is kept at + 10V with respect to the analyser
exit. The total voltage across this channeltron is again
3400V. Individual particles are observed as discrete pulses
and are transmitted through a 180 pF high voltage capacitor
from the high voltage end of the channeltrons. The load
resistor used was 1 MΩ in both channeltrons.

The pulses are then passed through an emitter
follower, which is battery operated. This reduces the output
impedance of the channeltron circuit. The pulses are then
amplified by an NE4603 amplifier and an integral discriminator
is used to cut off noise without affecting the actual signal.
Standard pulses from the discriminator are counted by a timed
scaler, or displayed on a pen recorder which records the
analogue output of a ratemeter, or stored in the memory of
a multiscaler. The number of pulses accumulated in a preset
counting time or in a preset number of sweeps can be printed
out on an electric typewriter. A schematic diagram of the
main electronic components is shown in fig.25.

For cross section measurements a multichannel
analyser was used in the multiscaling mode. The system available
is an 800-channel analyser (Didac 800, Intertechnique).
This instrument operates in a continuous sweep mode for
a preset number of sweeps. Pulses are stored in individual
channels of a memory and the counting time per channel can
be varied. At the end of each complete sweep, the instrument
automatically restarts at the first channel.

Figure 25:

Schematic diagram of the electronics
circuit. The detector can be either the
electron detector or the photon detector.
In case of modulated beam experiments,
additional information from the chopper
circuit is used to control the counting
system as indicated by the sub-section.

the
tor.
,
r
ng
n
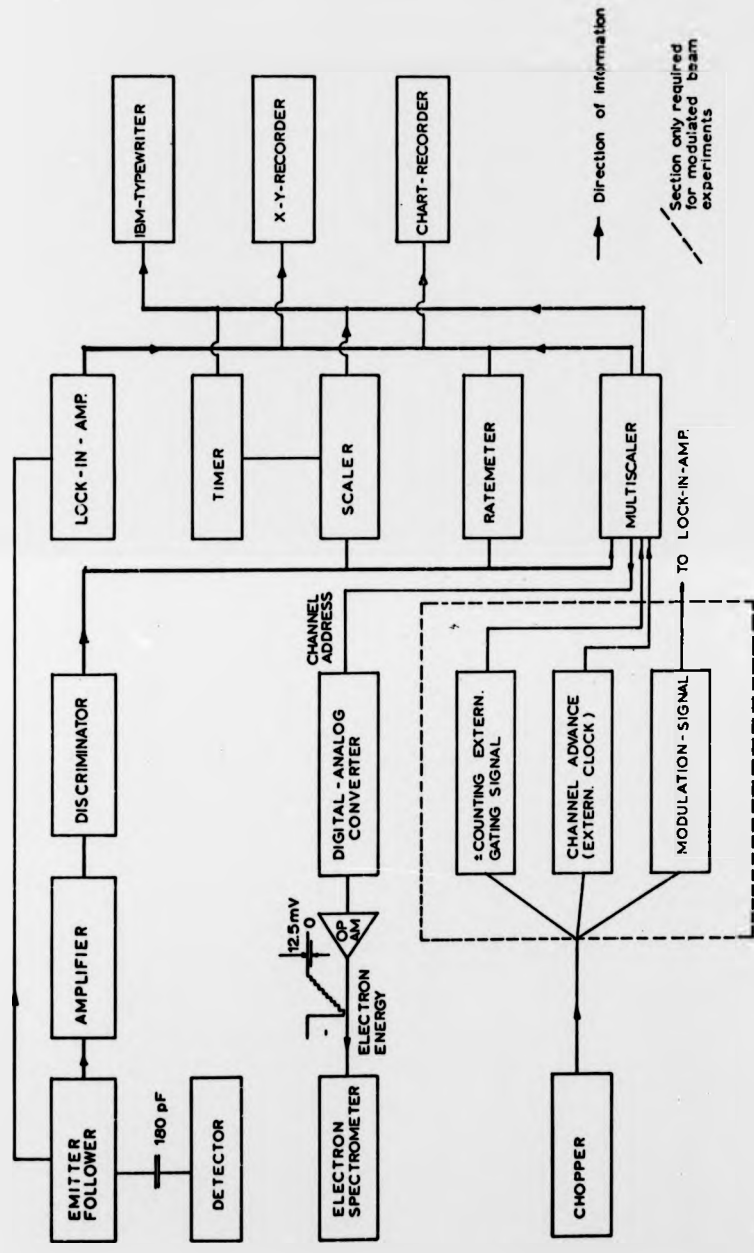
The channel number is used to synchronise
the electron beam energy with individual channels of the
memory unit. For this purpose, the channel address is
converted into a step function by means of a digital-to-
analogue converter. This step function which has an
overall amplitude of 8.0V corresponding to the full range
of the 800 channels is fed into an operational amplifier.
The operational amplifier outputs a negative ramp which
controls the energy of the electron beam. A normal step
width of 12.5 meV was used throughout the experiments to
be described later. This means that a maximum energy
interval of 10eV can be covered by the full range of the
800 channels. It is however possible to select small
sub-groups out of the total number of channels available.

Experiments of the type described here are
very sensitive to pressure fluctuations, electron beam
current fluctuations and other variations of the experimental
conditions. The effect of these fluctuations can be kept low
by signal averaging which is achieved by continuous scanning
of the signal and summing up of individual scans, hence the
use of the multiscaler.

In the case of background signals created by
electron scattering from targets other than the beam, the
multiscaler can be used to automatically subtract the background
signal. For this purpose, the beam modulation facility as
described in 3.5 is used to gate the multiscaler. The circuit
is indicated in fig.25. The square wave signal derived from
the chopper frequency monitoring circuit is used to supply a
0 to + 10V square wave necessary for switching the memory unit

from + counting to - counting. A schematic of the signals
derived from the chopper circuit is shown in fig.26. An
additional pulse sequence derived from the modulation signal
takes over the function of the internal clock and adjusts the
dwell-time per channel in multiples of the chopper open-closed
sequences. Dwell-times equivalent to one chopper cycle and up
to 16 complete chopper cycles can be preset.

6.   Results

In this chapter the measurements carried out
are presented and discussed. The first part shows the helium
energy loss spectra which were taken to test the performance
of the electron spectrometer. This is followed by the elastic
scattering of electrons from Helium observing the helium
resonance which was to be used as energy calibration standard.
These measurements are followed by results obtained for Neon
and Argon. Preliminary results for the elastic scattering of
electrons from atomic hydrogen are shown at the end of this
chapter.

6.1 Helium

Helium energy loss spectra were taken in order
to obtain an indication of the energy shift of the electron
beam. One typical curve is shown in fig.27. The energy shift
varied for different measurements but the drifts were similar
to those measured against the elastic resonance in Helium.
The experimental conditions are given in the caption to fig.27.

The 19.35eV $1s(2s)^2$ ^2S resonance occurring in the
elastic scattering of electrons from Helium has been studied

Figure 26:

Time sequence of the modulation circuit.
The chopper position as indicated by the
photo-transistor is converted into a
suitable square wave to gate the $\pm$ counting
modes of the multiscaler. A pulse derived
from the modulation signal is used to drive
the channel advance of the multiscaler. A
counter enables the 2^n-th pulse received,
$n = 0,1,..,4$,to be used for channel advance.

CHOPPER POSITION

OV

OPEN | CLOSED

- 10 V

COUNTING MODE

+10 V

PLUS | MINUS

OV

CHANNEL ADVANCE[T]
(EXT. CLOCK)

+10 V

OV

ELECTRON BEAM ENERGY[T]
(800 Steps max.)

eV

12.5 mV

TIME
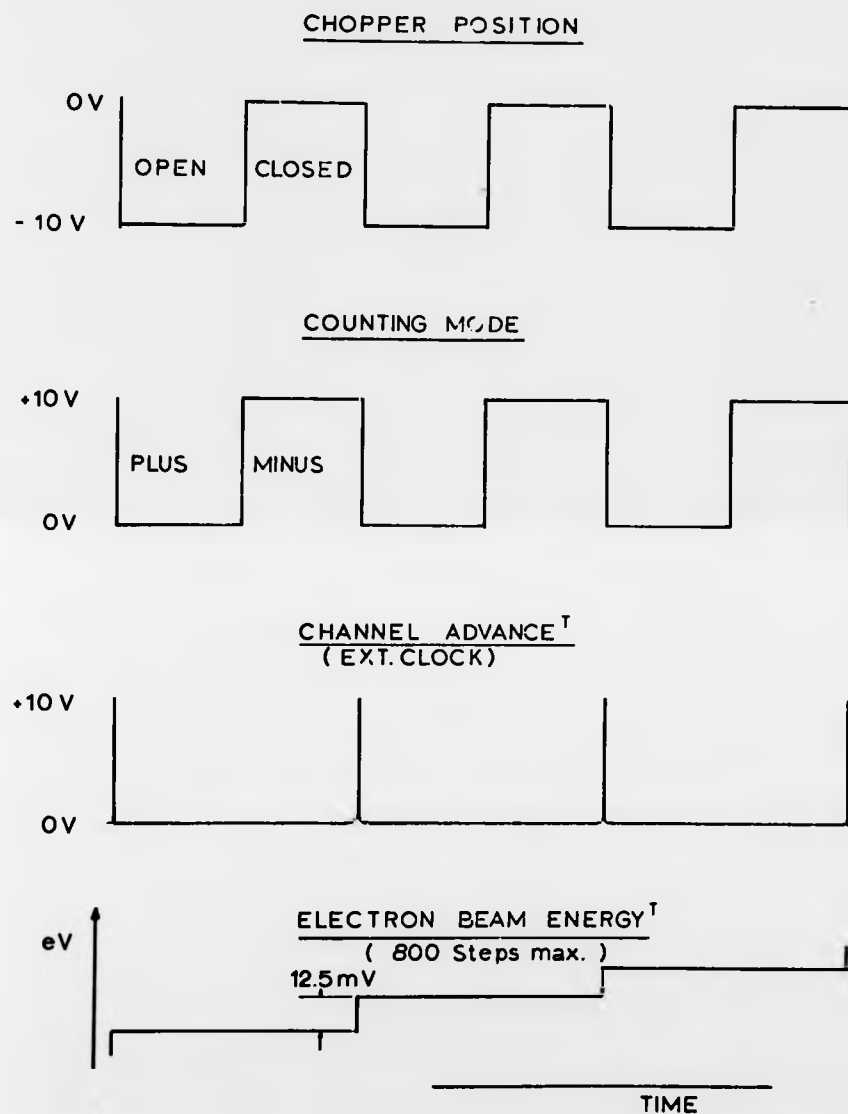
[T] THE MODULATION CIRCUIT PERMITS TO ADVANCE ONE
CHANNEL AFTER COMPLETION OF 1,2,4,8,16
CHOPPER CYCLES

Figure 27:

Typical energy loss spectrum in helium.
Incident energy 40.00eV, source chamber
pressure $1 \cdot 10^{-4}$ Torr. Scattering angle
45°. 2^1P appears at 21.22eV compared to the
spectroscopic value of 21.24eV. The 2^3P
level is not resolved and only indicated
as a slight shoulder of the 2^1P. For n=3
and n=4 energy values for the ^1P levels only
are shown in the diagram.

r

e

the

^3P

ed

n = 3

s only
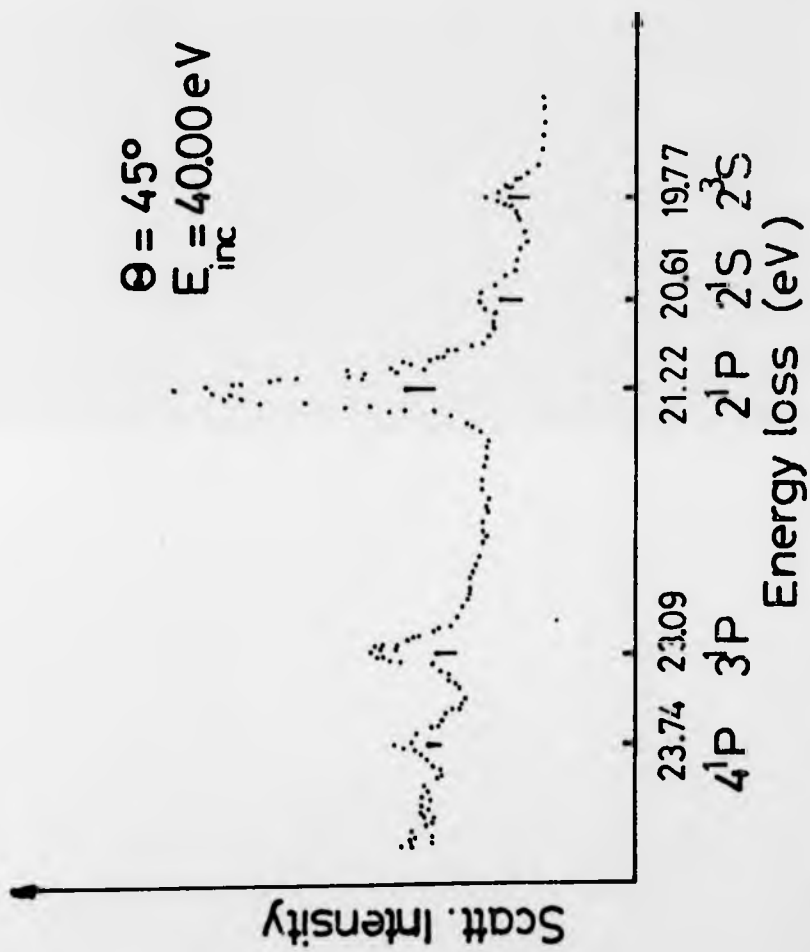
in great detail (Schulz G.J. 1973). It was studied with
the present apparatus at various angles. One typical curve
is shown in fig.28. The observation of this structure was
used as a calibration standard and is available as such in
future observations using the apparatus.

This structure can be seen after about 20 minutes
sampling time and can thus be easily repeated between different
observations in order to calibrate the energy-scale. The
repeated observation of this structure showed energy drifts
of the electron beam system over periods of 4 tc 5 hours
and this led to the restriction of the sampling time before
recalibration of the energy scale became necessary. These
relatively short integration times for individual runs were
the main contributions to the difficulties encountered with
the elastic scattering of electrons from atomic hydrogen in
the present set up.

6.2 Neon

The excitation of Neon was observed in the energy
region 15.0eV to 21.0eV. This leads to the excitation of the
neon states $(2p^5 3s)$ $^3P_1$ with a threshold at 16.671eV and
$(2p^5 3s)$ $^1P_1$ with threshold at 16.848eV. These excited states
decay to the $(2p^6)$ $^1S_0$ groundstate by emission of two lines
743 $\overset{o}{A}$ and 736 $\overset{o}{A}$. The combined excitation function of the two
lines was observed using an open channeltron multiplier
positioned at 90° to the incident beam direction. The detection
of scattered electrons was suppressed by means of biased grids
in front of the detector. Background count rates were of the
order of 1/sec. The counting rate depended linearly on the

Figure 28:

He elastic resonance, observed at 34°.
Helium pressure $1.5 \cdot 10^{-4}$ Torr in source
chamber.
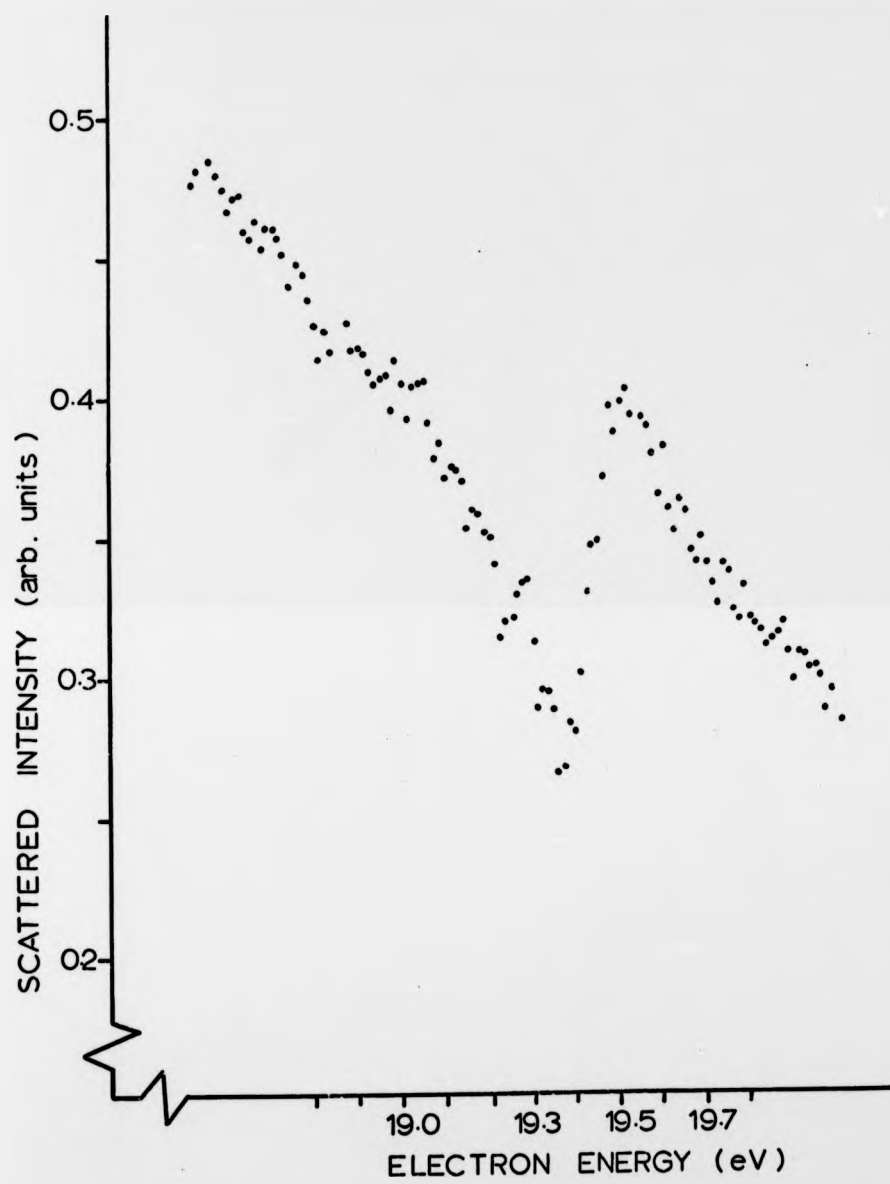
pressure in the interaction region as shown in fig.29.
The linear dependence of the excitation signal on the electron
beam current is shown in fig.30. This indicates single
collision conditions and ensures that resonance trapping is
negligible.

Structure in the combined excitation function
was observed and it is shown for one individual experimental
run in fig.31. Electron beam current variations over the
energy interval considered were smooth and showed a slight
increase at higher beam energies. This is caused by the
lens properties of the accelerating and beam forming elements
in the electron beam system. Figure 32 shows one typical
example of this change of transmission current versus energy.
An excitation curve resulting from the addition of the data
from several experimental runs is shown in fig..33. The
observed structure has been energy calibrated in two ways.
The first calibration was carried out by measuring the elastic
Helium resonance and the Neon structures in successive runs,
whereas the second calibration was carried out in a Neon-Helium
gas mixture. In the latter case the structures observed for
Helium and Neon could be directly compared under the same
conditions. The energy positions of the structures observed
by the two methods differed slightly. The values are listed
in Table II where they are compared with structures observed
in transmission experiments (Sanche, L. and Schulz G.J. 1972).
The error assigned to the energy scale for either calibration
is $\pm$ 0.06eV, which consists of the uncertainty in positioning
the points of individual curves and of the differences between
individual calibration runs.

Figure 29:

Linearity of signal versus pressure over
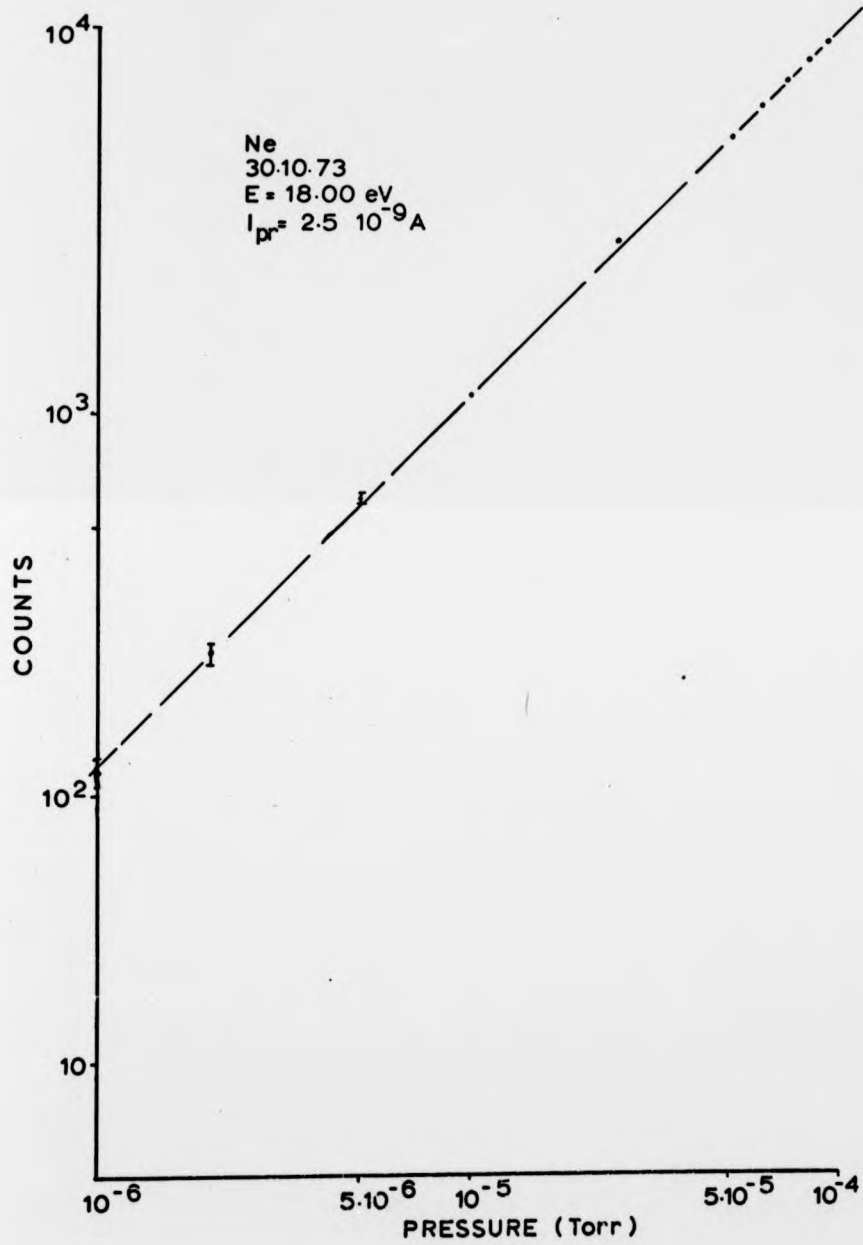a wide range. Beam energy 18.00eV, primary
beam current $2.5 \cdot 10^{-9}$A.

Ne
30·10·73
E = 18·00 eV
$I_{pr} = 2.5 \ 10^{-9} A$

Figure 30:

Linearity of signal versus beam current.
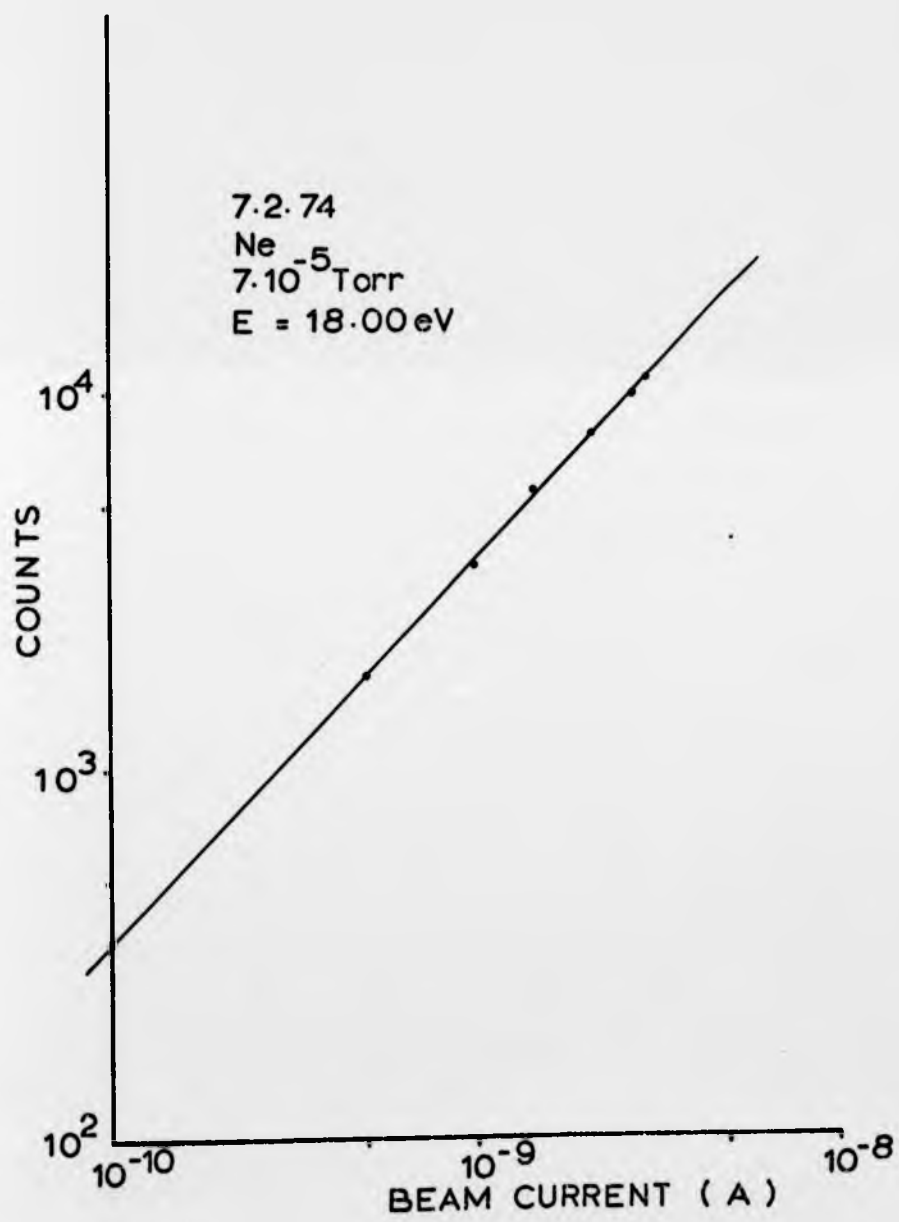Pressure was kept at $7 \cdot 10^{-5}$ Torr, incident
beam energy at 18.00eV.

7.2.74
Ne
7.10^{-5} Torr
E = 18.00 eV

Figure 31:

One individual run, showing structure in
the neon excitation.   Pressure $1 \cdot 10^{-5}$ Torr.
100 sweeps.
Approximate collection time 2 hours.

orr.

30.10.73
RUN 1
Ne

CHANNELNUMBER

COUNTS

2000

1500

1000

500

10   50   100   150   200   250   300   350
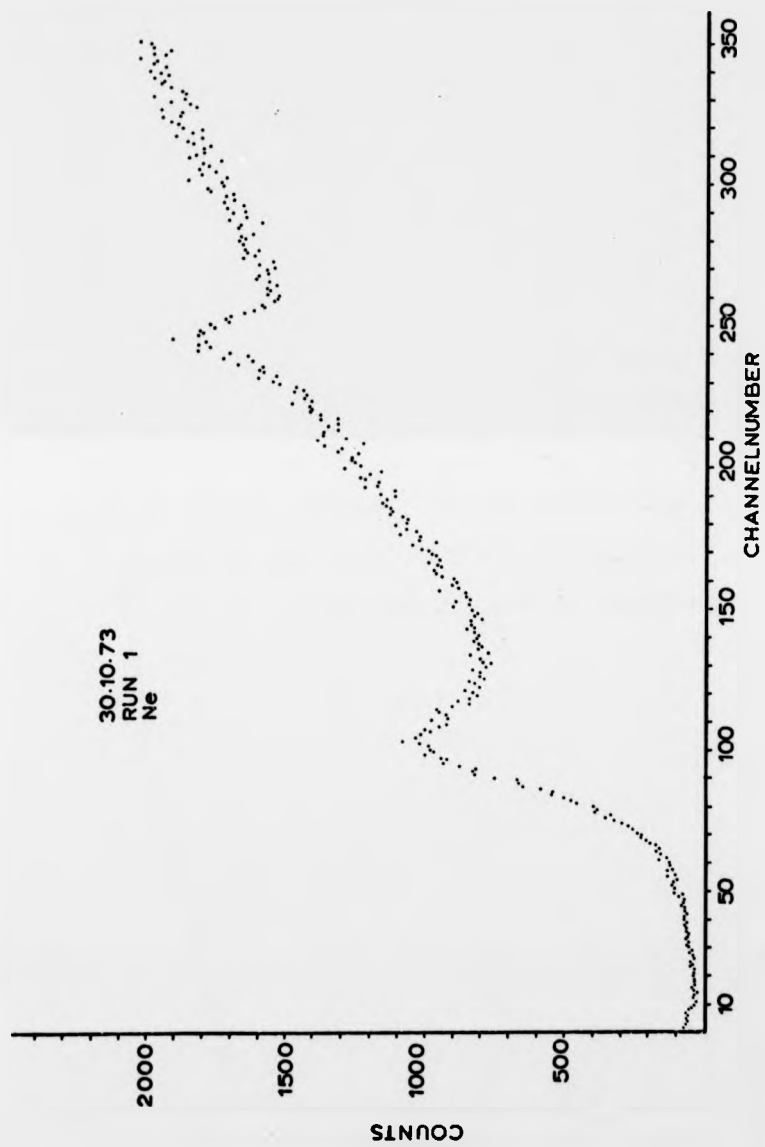
Figure 32:

Primary beam current recorder trace, showing
a smooth transmission curve which slightly
increases at higher energies.
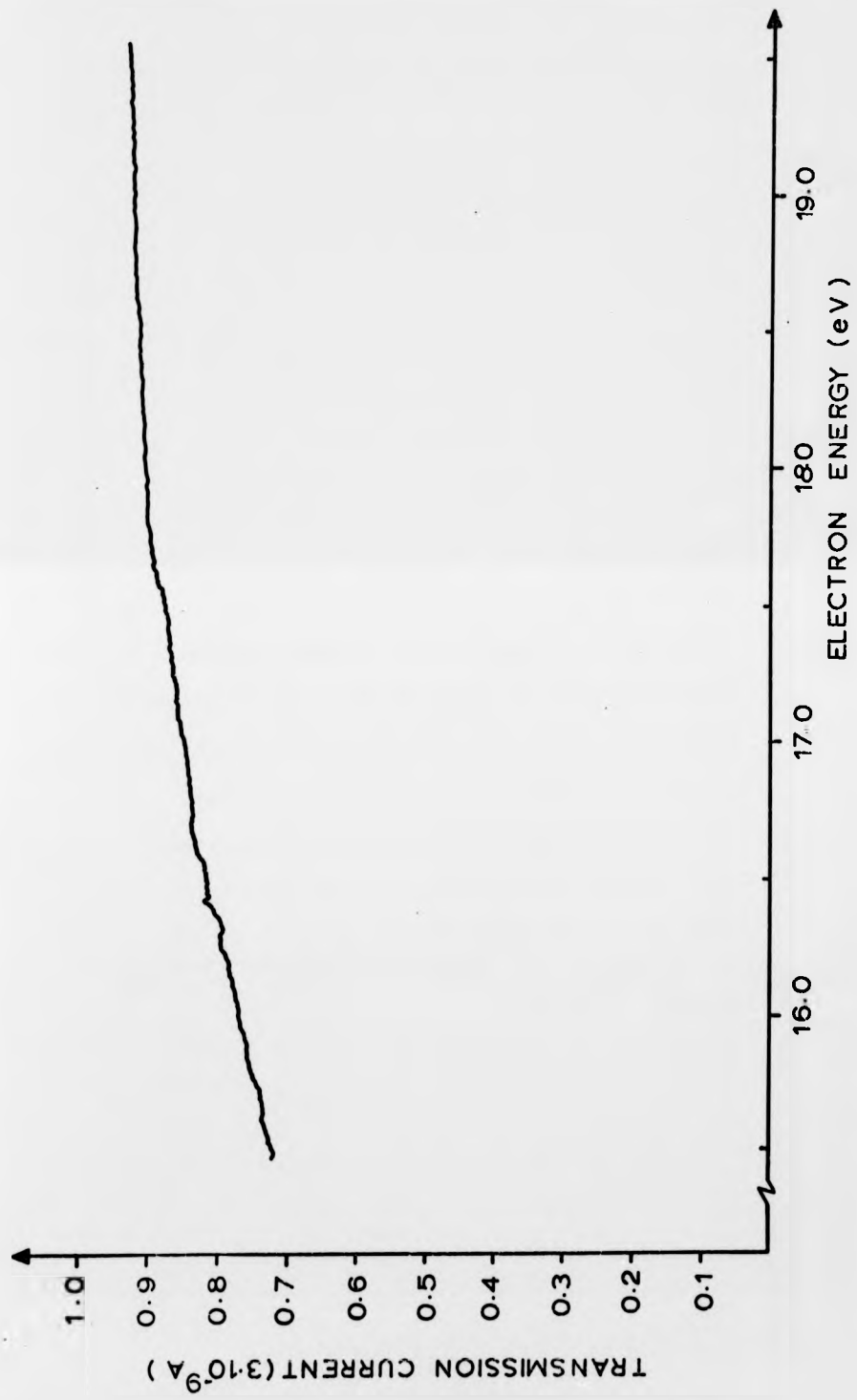
Figure 33:

Excitation cross-section of the combined
736 $\mathring{A}$ and 743 $\mathring{A}$ lines of neon near threshold.
The error bars show one standard deviation.
Clear structure A, C and D can be seen.
B shows a slight peak followed by a dip.
The energy values obtained for the structures
are listed in Table II.

ed

eshold.

tion.

o.
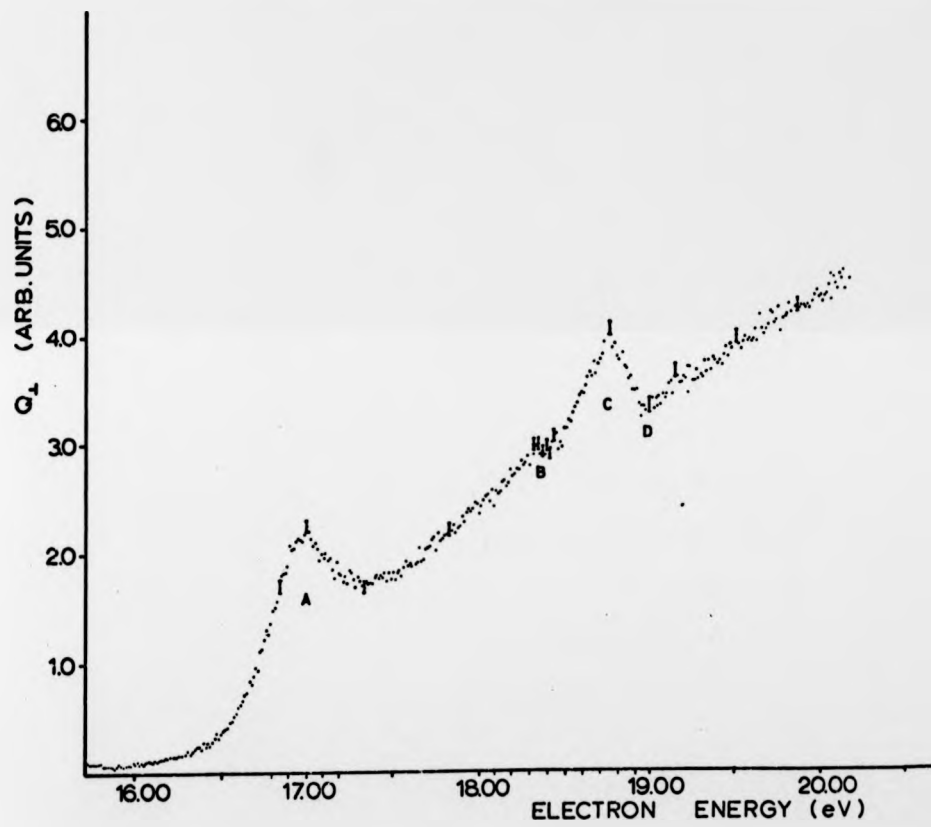
uctures

A clear description of the Ne$^-$ state causing the structure cannot be made, although it has been suggested that more information can be obtained by comparing the structures with isoelectronic systems (Swanson, N. et al 1973) as has been done for a similar case in Krypton.

TABLE II

Position of resonances in neon (eV)

Structure	Present Experiment		Transmission Experiment Sanche L. & Schulz G.J.
	He-calibr. §	He-Ne calibr. §§	
A	16.99+0.06	16.90+0.06	16.85-16.91
B	18.32 18.40	18.24 18.30	18.55
C	18.76	18.69	18.65-18.70
D	19.06	18.90	18.95

Position of structures observed in the combined excitation of the 736 Å and 743 Å lines of neon. Structure A has been used as sub-standard for energy calibration in He(§) and in a He-Ne mixture (§§). Structure B shows a slight peak followed by a dip. All values are given in eV.

6.3 Argon

The excitation of the two lowest states of Argon has been observed in the energy range 11.0eV to 14.00eV. These are levels with configuration $(3p^5 4s)$ $^3P_1$, with a threshold at 11.623eV and $(3p^5 4s)$ $^1P_1$ with a threshold at 11.828. They decay to the $(3p^6)$ $^1S_0$ groundstate by emission of two lines, 1066 $\mathring{A}$ and 1048 $\mathring{A}$. The combined excitation of these two lines was observed using the open channeltron multiplier positioned at 90° to the incident electron beam direction. Structure can be seen, as shown in fig.34. The signal depends linearily on the target gas pressure as well as on the electron beam current as can be seen in fig.35 and fig.36. The primary beam current over the whole energy region considered is a smooth curve, slightly increasing at higher energies as shown in fig.37. Data from different experiments have been accumulated and are shown in fig.38. The energy calibration was again carried out in the two ways already described for Neon. This again resulted in two sets of slightly different energy values. The structures observed are listed in Table III, where they are compared with results of transmission experiments (Sanche L. and Schulz G.J. 1972). The calibration error again consists of the uncertainty of positioning points on individual curves and of the energy differences of individual calibration runs. A clear assignment of the structures observed cannot be made and should be left until more detailed information is available.

Figure 34:

An individual experimental run, showing
structure in the argon excitation.
Pressure $2.5 \cdot 10^{-5}$ Torr.   140 sweeps.
Approximate collection time 2 hours.
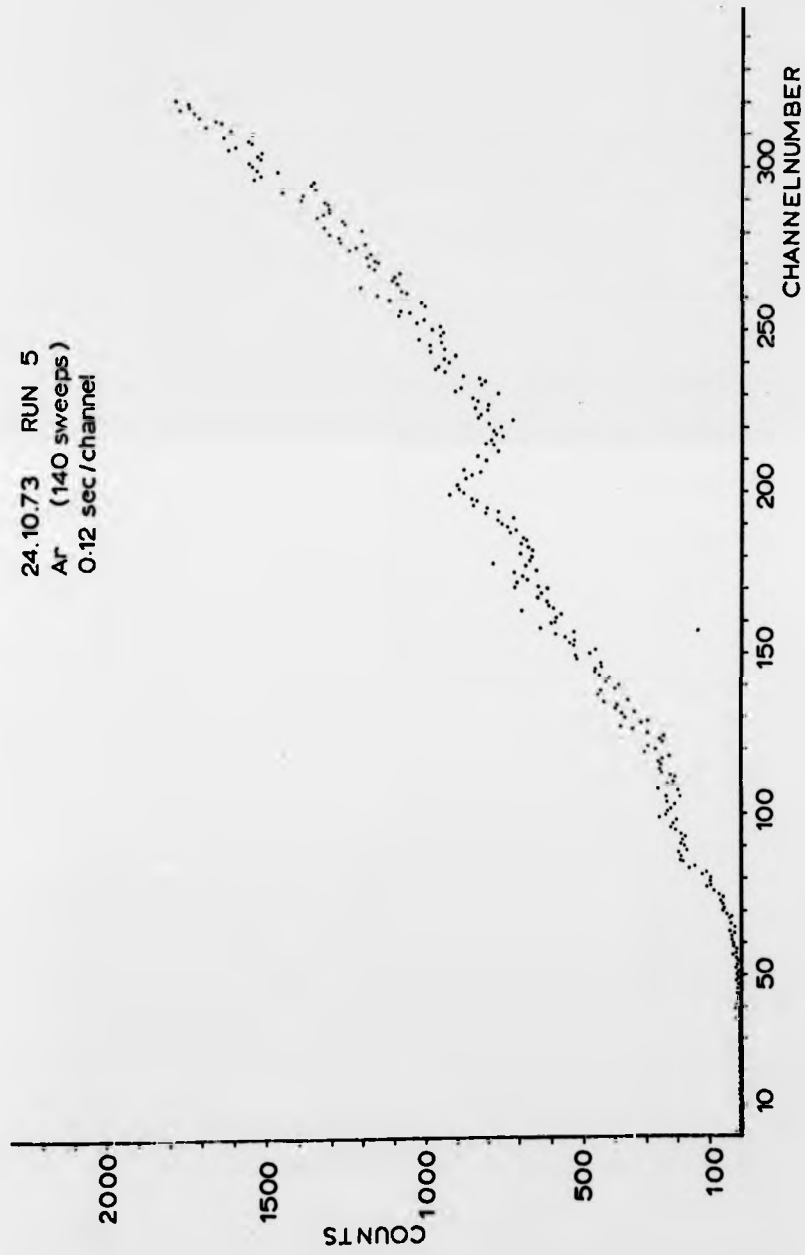
24.10.73   RUN 5
Ar   (140 sweeps)
0·12 sec /channel

Figure 35:

Linearity of argon signal with pressure.
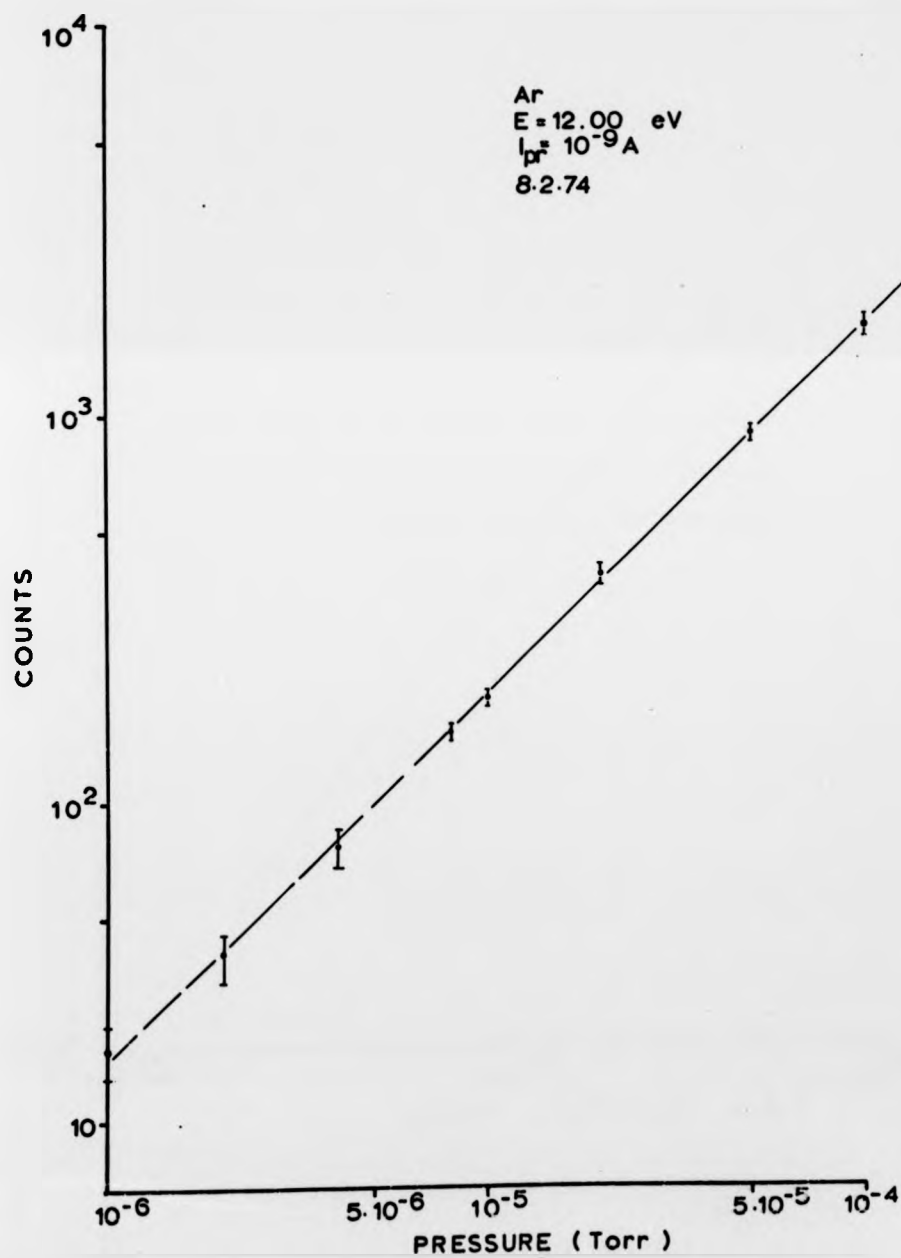Incident beam energy 12.00eV, primary beam
current 10^{-9}A.

COUNTS

Ar
E = 12.00 eV
$I_{pr} = 10^{-9} A$
8.2.74

Figure 36:

Linearity of argon signal with primary beam
current.   Argon pressure $7 \cdot 10^{-5}$ Torr.
Incident beam energy 12.00eV.

8·2·74
Ar
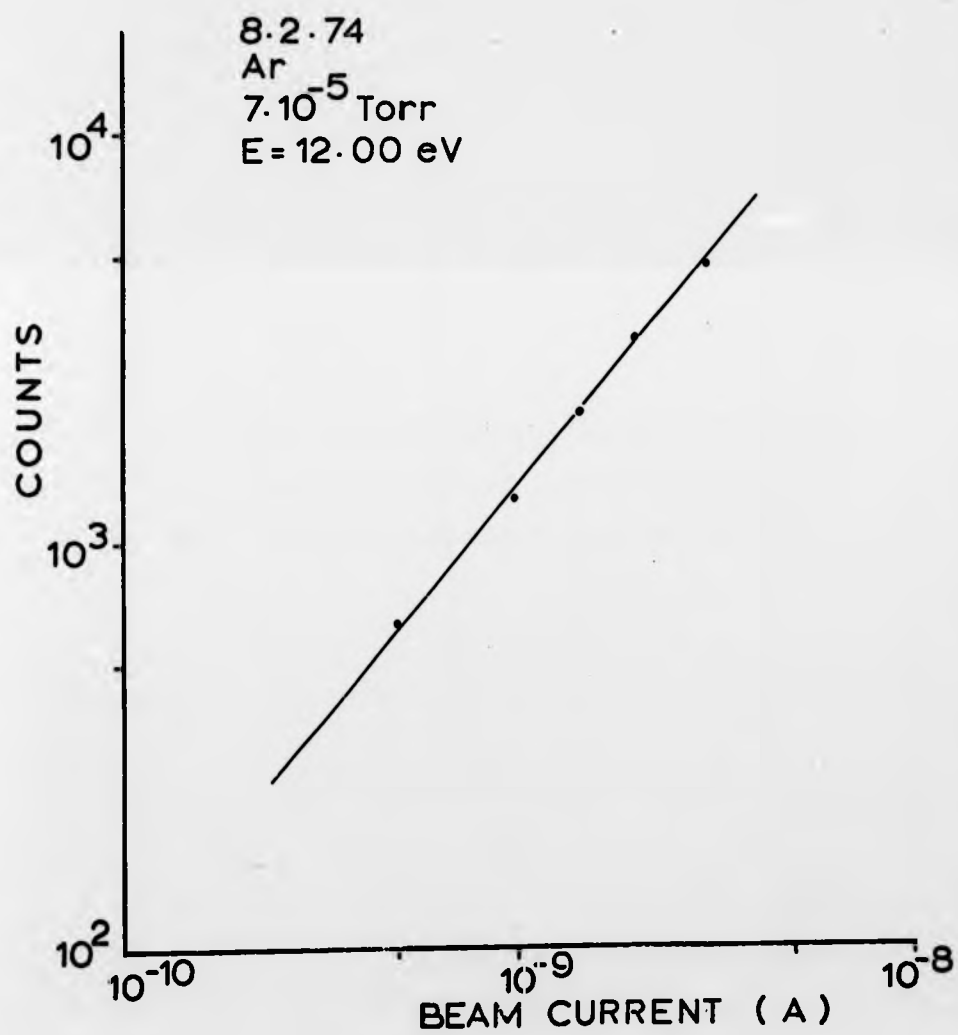7·10^{-5} Torr
E = 12·00 eV

COUNTS

10^4

10^3

10^2

10^{-10} 10^{-9} 10^{-8}

BEAM CURRENT (A)

beam

Figure 37:

Smooth transmission curve, slightly increasing.
at higher energies. The recorder trace is typical
of those that have been taken during all experiments.
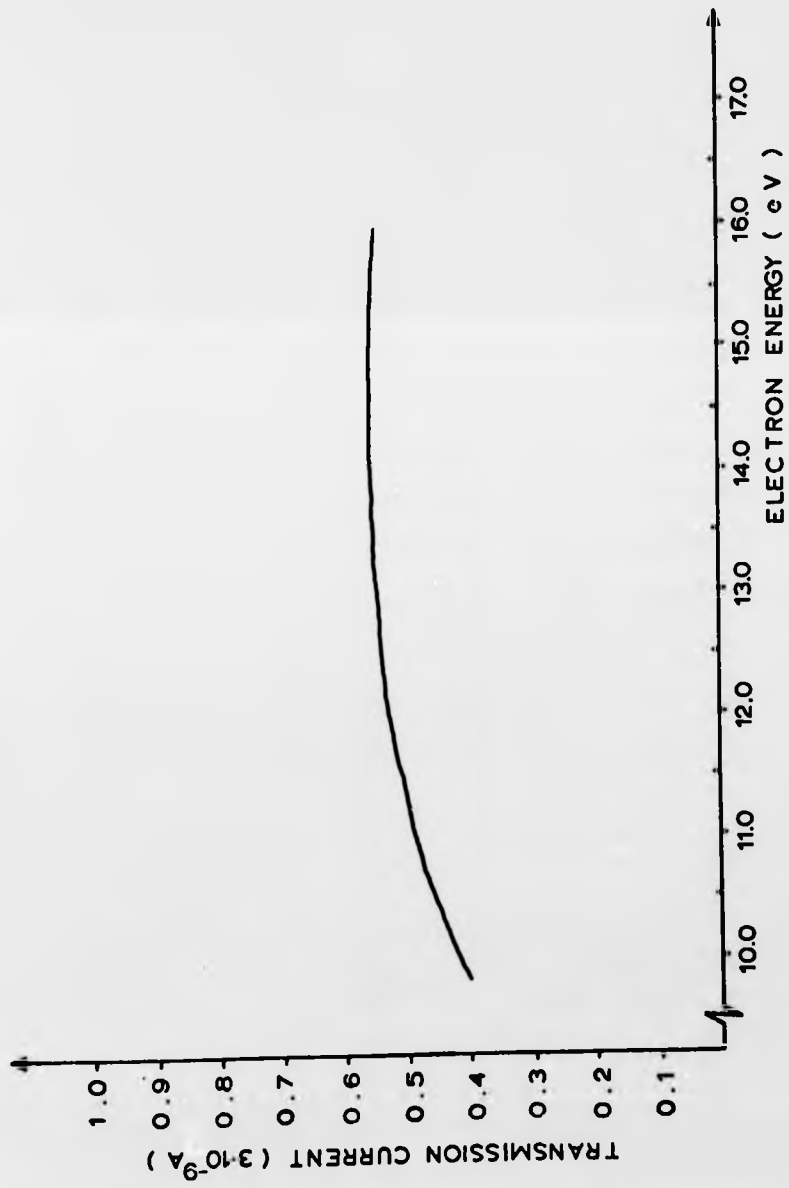
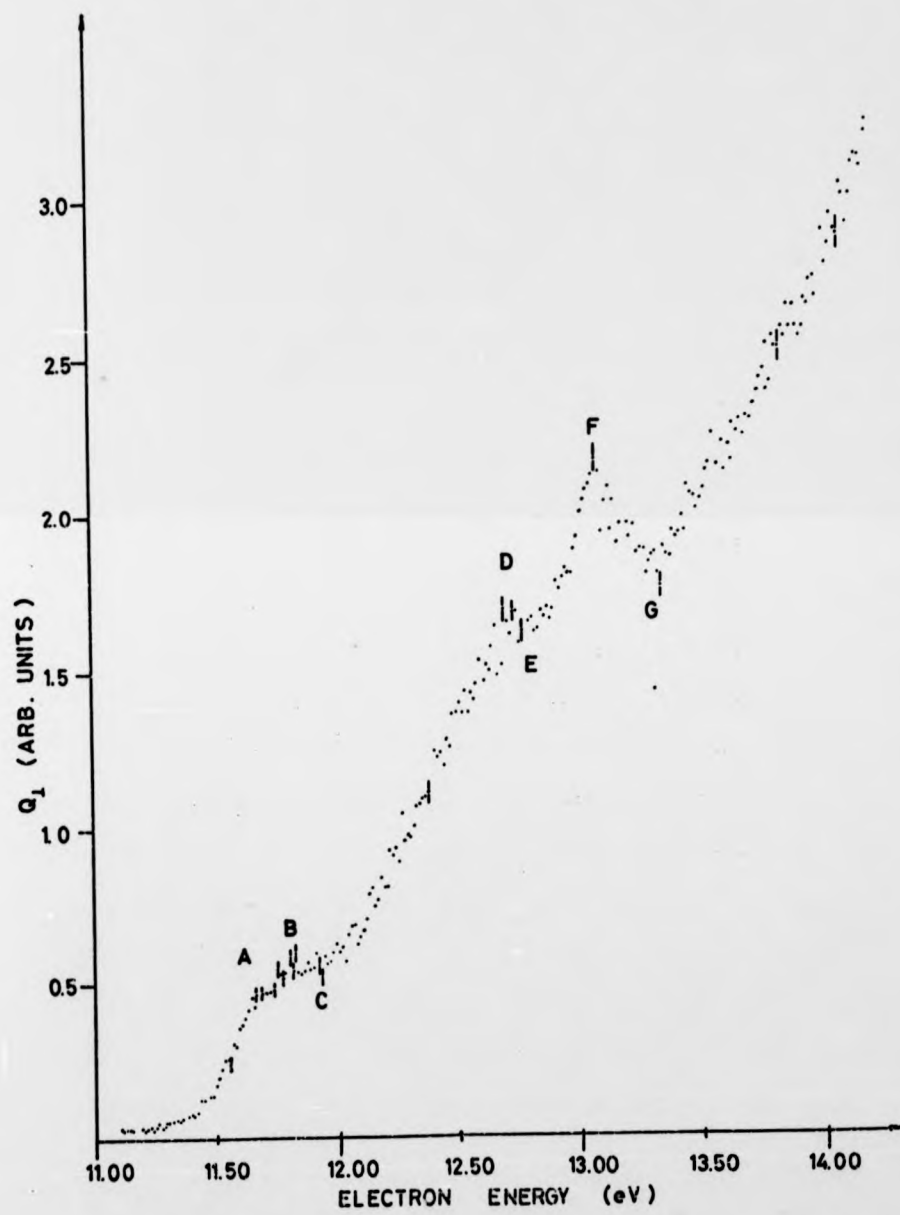creasing .

e is typical

ll experiments.

Figure 38:

Excitation cross-section of the combined
1048 $\mathring{A}$ and 1067 $\mathring{A}$ lines in argon near
threshold.   The error bars show one standard
deviation. Apart from clear structure D,E,F
and G, there is indication of structure around
A,B, and C.   The values obtained for the energy
positions are listed in Table III.

TABLE III

Position of resonances in argon (eV)

| Structure | Present Experiment | | Transmission experiment Sanche L. & Schulz G.J. |
	He-calibr. §	He-Ar calibr. §§	
A	11.68	11.72	11.71
B	11.80	11.84	11.91
C	11.93	11.97	
D	12.68	12.72	12.89-12.92
E	12.74	12.78	
F	13.05+0.06	13.09+0.06	12.95 13.06- 13.11
G	13.30	13.34	13.33

The position of strutures observed in the excitation of the combined 1048 $\mathring{A}$ and 1067 $\mathring{A}$ lines of argon. Sub-standard for calibration was structure F.

§   Values obtained by calibration in helium.

§§   Values obtained by calibration in a helium argon mixture.

6.4 Atomic hydrogen

The elastic scattering of electrons from atomic hydrogen close to the n=2 threshold presented problems which have only allowed preliminary results to be obtained so far. An accumulated curve resulting from the data of several experimental runs is shown in fig.39. There is an indication of structure, which is due to the formation of a hydrogen compound state having the configuration $(2s^2)$ ^1S, as has been reported in the few previous experiments which have already been mentioned in chapter 1.2.

Several difficulties have arisen which resulted in a very bad signal to background ratio which was of the order of 1:10. Although the atomic beam density is of the order of 10^{10} atoms cm^{-3}, the molecular background is of the same order, thus creating a background signal which interfered with the elastic scattering signal from atomic hydrogen. Furthermore there was a high background of electrons scattered from metallic surfaces. This is a problem which is well known for slow electrons. At scattering angles of 90°, this electron background dropped to a minimum which is the reason that the preliminary results were taken at this scattering angle.

Using the modulation facility available, there are two signal channels. With the chopper open, the signal detected is

$$S_1 = S + B$$

where S is the scattering signal caused by the atomic beam itself, and B describes scattering caused by background gas and metal surfaces. This latter contribution is detected with the chopper closed. The actual signal is the difference between

6.4 Atomic hydrogen

The elastic scattering of electrons from atomic hydrogen close to the n=2 threshold presented problems which have only allowed preliminary results to be obtained so far. An accumulated curve resulting from the data of several experimental runs is shown in fig.39. There is an indication of structure, which is due to the formation of a hydrogen compound state having the configuration $(2s^2)$ ^1S, as has been reported in the few previous experiments which have already been mentioned in chapter 1.2.

Several difficulties have arisen which resulted in a very bad signal to background ratio which was of the order of 1:10. Although the atomic beam density is of the order of 10^{10} atoms·cm^{-3}, the molecular background is of the same order, thus creating a background signal which interfered with the elastic scattering signal from atomic hydrogen. Furthermore there was a high background of electrons scattered from metallic surfaces. This is a problem which is well known for slow electrons. At scattering angles of 90°, this electron background dropped to a minimum which is the reason that the preliminary results were taken at this scattering angle.

Using the modulation facility available, there are two signal channels. With the chopper open, the signal detected is

$$S_1 = S + B$$

where S is the scattering signal caused by the atomic beam itself, and B describes scattering caused by background gas and metal surfaces. This latter contribution is detected with the chopper closed. The actual signal is the difference between

Figure 39:

Preliminary results for the elastic scattering
of electrons from atomic hydrogen. Scattering
angle θ = 90°.   This curve has been obtained by
accumulating several runs.   An indication of
structure can be seen.
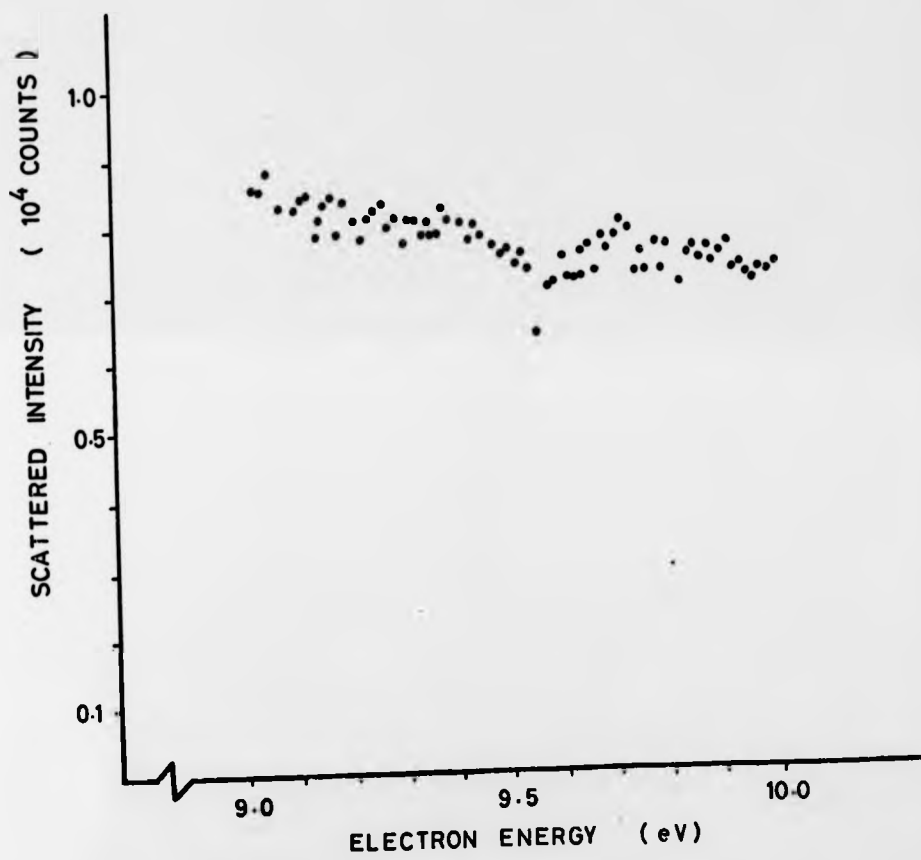
the two signal channels. The statistical error of such
a modulated signal is given by

$$\Delta S = ((\Delta S_1)^2 + (\Delta S_2)^2)^{1/2}$$

and therefore by

$$\Delta S = (S + 2B)^{1/2}$$

which means that the statistical fluctuations are mainly
caused by the background contribution. In order to achieve
better statistics, long integration times are required.
This, in turn, requires a good long-term stability of
the system. The main reason this has not yet been achieved
is that the energy of the electron spectrometer fluctuates
within a time period which is short compared to the time
necessary to get reasonable counting statistics. These
energy fluctuations smear out structure and the preliminary
results had to be accumulated from several short runs.
The structure indicated was positioned, according to the
transmission experiment of L. Sanche and P. D. Burrow (1972),
at 9.558eV. Initial calibration runs in pure helium placed
the structure at somewhat higher values, around 9.6 to 9.7eV,
which is not unexpected when compared with the energy
discrepancies encountered for the rare gas results presented
earlier. Future results will again have to be calibrated
in a gas mixture.

7.   Conclusions and suggestions for further experiments

The apparatus described can be used for a wide range of investigations for example the observation of electrons that have undergone collisions as well as photons originating from decay of excitation processes caused by these collisions. The final arrangement of two independent information circuits could be coupled in a coincidence experiment to give more detailed information about the actual collision processes. However the next step should be to remeasure the rare gas excitation functions with even higher resolution and to perform angular distribution measurements. This should give information on the polarisation of the lines involved as well as more information about the structures observed.

As far as atomic hydrogen is concerned, several improvements will have to be made before satisfactory results for the elastic scattering resonances can be obtained. The most urgent improvements should be to remove the hydrogen background in the interaction region by additional pumps. This could be done by cryo-pumping the hydrogen beam, or by means of an intermediate tank between source and interaction chamber. Although the latter modification involves longer distances between target beam source and scattering region, it should result in a much better signal to noise ratio. The electron beam system requires a much improved primary beam collector. An extended collector area surrounding the whole electron beam system together with a more sophisticated collector in the primary beam direction should reduce the problem of stray electrons considerably. This should result in a much better suppression of electrons which undergo reflections from various metal surfaces.

8. Acknowledgements

I wish to thank Professor H. Kleinpoppen
for supporting this work and for his encouragement and
continuous interest in its progress.

One of the pleasures throughout the
planning, building and running of the system described,
was to work with Mr. H. Koschmieder. I should like to
thank him for his co-operation in overcoming various
difficulties which both of us had to experience.

Technical advice was always available from
Mr. R. R. Harrison. I also thank for technical assistance
from the technical staff of the Physics Department.

The University's Shared Technical Service
constructed skilfully machined components and electronic
circuits. Two names have to be mentioned in this connection,
Mr. C. Chesterman built the first 127° monochromator-analyser
system in this University to metric standards, in which he had
had no previous experience. Mr. Bill Stirling never got tired
of supplying or repairing urgently needed electronic equipment.

In connection with the writing of this thesis,
I should like to thank Mrs. J. Weber for the typing and
Dr. J. M. Woolsey for reading the manuscript.

9. References

Andrick D., and Ehrhardt H., Z.Phys. 192, 99 (1966)

Bally Y., Rev.Phys.Appl. 3, 46 (1968)

Burke P.G., and Schey H.M., Phys.Rev. 126, 147 (1962)

Delage Y., and Carette J.D., Canad.Journ.Phys. 49, 2118 (1971)

Dennis N.T.M., Heppel T.A., Vacuum System Design,
   Chapman and Hall Ltd. (1968)

Ehrlich G., Journ.Chem.Phys. 31, 1111 (1959)

Fite W.L., and Brackmann R.T., Phys.Rev. 112, 1141 (1958)

Franke H., and Bauer H., Vakuum Technik. 7, 185 (1965)

Gibson J.R., and Dolder K.T., J.Phys. B2, 741 (1969)

Giordmaine J.A., and Wang T.C., Journ.Appl.Phys. 31, 463 (1960)

Hanes G.R., Journ.Appl.Phys. 31, 2171 (1960)

Heidemann H.G.M., Kuyatt C.E., and Chamberlain G.E.,
   Journ.Chem.Phys. 44, 355 (1966)

Hughes A.L., and McMillan J.H., Phys.Rev. 34, 291 (1929)

Hughes A.L., and Rojanski V., Phys.Rev. 34, 284 (1929)

Kauppila W.E., Ott W.R., and Fite W.L., Phys.Rev. A1, 1099 (1970)

Kisker E., Z.Phys. 256, 121 (1972)

Kisker E., Z.Phys. 257, 51 (1972)

Kleinpoppen H., and Raible V., Phys.Lett. 18, 24 (1965)

Kuyatt C.E., Simpson J.A., and Mielczarek S.R.,
   Phys.Rev. 138, A 385 (1965)

Koschmieder H., Ph.D. Thesis, University of Stirling 1974

Lamb W.E., and Retherford R.C., Phys.Rev. 79, 549 (1950)

Lloyd C.R., Teubner P.J.O., Weigold E., and Hood S.T.,
   Journ.Phys. B5, L 44 (1972)

Marmet P., Clark E.M., and Kerwin L., Canad.Journ.Phys. 39,
   1240 (1961)

Massey H.S.W., and Burhop E.H.S., Electronic and Ionic Impact
   Phenomena, Oxford 1969

McConkey J.W., and Donaldson F.G., Canad.Journ.Phys.
   51, 914 (1973)

McGowan J.W., Clark E.M., and Curley E.K., Phys.Rev.Lett.
   15, 917 (1965)

McGowan J.W., Clark E.M., and Curley E.M., Phys.Rev.Lett.
   17, 66(E), (1966)

McGowan J.W., Williams J.F., and Curley E.K., Phys.Rev.
   180, 132 (1969)

Mott N.F., and Massey H.S.W., Theory of Atomic Collisions,
    Oxford, Clarendon Press, 1965

Pichanick F.M.J., and Simpson J.A., Phys.Rev. 168, 64 (1967)

Raible V., Diplomarbeit, Universität Tübingen 1965

Ramsey F., Molecular Beams, Oxford 1956

Sanche L., and Burrow P.D., Phys.Rev.Lett. 29, 1639 (1972)

Sanche L., and Schulz G.J., Phys.Rev. A5, 1672 (1972)

Sawada T., Purcell J.E., and Green A.E.S., Phys.Rev.
    A4, 193 (1971)

Schulz G.J., Phys.Rev. 136, A650 (1964)

Schulz G.J., Rev.Mod.Phys., 45, 3, 378 (1973)

Schwartz C., Phys.Rev. 124, 1468 (1961)

Sharpton F.A., John R.M.St., Lin C.C., Fajen F.E.,
    Phys.Rev. A2, 1305 (1970)

Simpson J.A., Methods in Experimental Phys., Vol.4a,
    Academic Press 1967

Simpson J.A., Rev.Sc.Instr. 35, 1698 (1964)

Smith K., McEachran R.P., and Fraser P.A., Phys.Rev.
    125, 553 (1962)

Smith K., Rep.Prog.Phys. 29, 373 (1966)

Swanson N., Cooper J.W., and Kuyatt C.E., Phys.Rev. A8, 1825 (1973)

Taylor H.S., Nazaroff G.V., and Golebiewski A., J.Chem.Phys.
    45, 2872 (1966)

Temkin A., and Lamkin J.C., Phys.Rev. 121, 788 (1961)

Wood R.W., Proc.Roy.Soc. 97, 455 (1920)

Zugenmaier P., Z.Angew.Phys. 20, 184 (1966)